MATHEMATICAL MODELLING OF WAVE IMPACT ON LANDWARD-INCLINED AND SEAWARD-INCLINED SEAWALLS

MOHD SHAHRIDWAN BIN RAMLI

MASTER OF SCIENCE

UNIVERSITI MALAYSIA PAHANG

UNIVERSITI MALAYSIA PAHANG

DECLARATION OF THESIS AND COPYRIGHT

Author's Full Name : MOHD SHAHRIDWAN BIN RAMLI

Date of Birth : 11 JANUARY 1988

Title : MATHEMATICAL MODELLING OF WAVE IMPACT ON LANDWARD-INCLINED AND SEAWARD-INCLINED SEAWALLS

Academic Session : SEM 1 2019/2020

I declare that this thesis is classified as:

- ☐ CONFIDENTIAL (Contains confidential information under the Official Secret Act 1997)*
- ☐ RESTRICTED (Contains restricted information as specified by the organization where research was done)*
- ☑ OPEN ACCESS I agree that my thesis to be published as online open access (Full Text)

I acknowledge that Universiti Malaysia Pahang reserves the following rights:

1. The Thesis is the Property of Universiti Malaysia Pahang
2. The Library of Universiti Malaysia Pahang has the right to make copies of the thesis for the purpose of research only.
3. The Library has the right to make copies of the thesis for academic exchange.

Certified by:

(Student's Signature)	(Supervisor's Signature)
880111-11-5117	DR NOR AIDA ZURAIMI MD NOAR
New IC/Passport Number	Name of Supervisor
Date:	Date:

NOTE : * If the thesis is CONFIDENTIAL or RESTRICTED, please attach a thesis declaration letter.

SUPERVISOR’S DECLARATION

We hereby declare that we have checked this thesis and in our opinion, this thesis is adequate in terms of scope and quality for the award of the degree of Master of Science.

____

(Supervisor’s Signature)

Full Name : DR. NOR AIDA ZURAIMI MD NOAR

Position : SENIOR LECTURER

Date :

____

(Co-supervisor’s Signature)

Full Name : DR. MOHD ZUKI SALLEH

Position : PROFESSOR

Date :

STUDENT'S DECLARATION

I hereby declare that the work in this thesis is based on my original work except for quotations and citations which have been duly acknowledged. I also declare that it has not been previously or concurrently submitted for any other degree at Universiti Malaysia Pahang or any other institutions.

____

(Student's Signature)

Full Name : MOHD SHAHRIDWAN BIN RAMLI

ID Number : MSE15001

Date :

MATHEMATICAL MODELLING OF WAVE IMPACT ON LANDWARD-INCLINED AND SEAWARD-INCLINED SEAWALLS

MOHD SHAHRIDWAN BIN RAMLI

Thesis submitted in fulfillment of the requirements
for the award of the degree of
Master of Science

Centre for Mathematical Sciences

UNIVERSITI MALAYSIA PAHANG

NOVEMBER 2019

ACKNOWLEDGEMENTS

Alhamdulillah, praise be to Allah for His blessings. I am grateful and would like to convey my thanks to my supervisor, Dr. Nor Aida Zuraimi Md Noar for her invaluable guidance and limitless support during my study. The constant encouragement and continuous assistance helped me immensely in making this research possible. Thank you for everything. I am honoured to be her student.

My sincere thanks also goes to my co-supervisor, Prof Madya Dr. Mohd Zuki Salleh, who has always supported and spared his time for me.

My special thanks also to Miss Fadhlyya Arawaney for being the best research partner I could have. She helped me a lot during my study. I also learnt a lot from her. I wish her all the best in her research project.

My deepest appreciation goes to father and my late mother for their prayers and true love. Also to my brothers and sisters for their continuous support.

Finally, I acknowledge my sincere indebtedness and gratitude to my family especially my beloved wife, Siti Wan Aminah Wan Norudin for always giving her full support and encouragement. She has always been there in all my ups and downs throughout this research journey and is the top motivation for me to complete my study

ABSTRAK

Struktur pantai dan lautan tertakluk kepada beban gelombang terpisah yang mungkin mencapai $690kNm^{-2}$. Untuk mengurangkan beban ini, kita mungkin mencondongkan permukaan benteng ke arah lautan ataupun ke arah daratan. Walau bagaimanapun, tidak dijelaskan bahawa kecerunan banteng boleh mengurangkan kesan gelombang dan eksperimen menggunakan model baru-baru ini menunjukkan bahawa benteng yang condong mungkin terdedah kepada beban lebih tinggi daripada benteng yang menegak. Dipengaruhi oleh penemuan ini, kami melakukan kajian secara teori mengenai pengaruh kecerunan benteng terhadap kesan gelombang. Model-model kesan gelombang matematik terhadap benteng yang condong ke arah lautan dan daratan dipertimbangkan dengan menggunakan lanjutan model Cooker iaitu benteng laut yang menegak. Teori impuls tekanan yang dicadangkan oleh Cooker diterapkan ke dalam dua masalah ini yang akan memudahkan masalah yang bergantung pada masa dan sangat tidak linear dengan mempertimbangkan masa integrasi tekanan selama jangka waktu utuk impak tekanan impuls. Penyelesaian masalah ini ditemui dengan menyelesaikan Persamaan Laplace untuk sempadan tertentu. Teori perturbasi diterapkan ke dalam model-model ini dan masalahnya diselesaikan dengan menggunakan MATLAB. Hubungan antara tekanan impuls dan sudut kecenderungan dinding disiasat. Keputusan menunjukkan terdapat persamaan dengan kajian eksperimen. Telah didapati bahawa tekanan impuls paling rendah berlaku apabila kecenderungan kecil berlaku menghampiri tembok yang menegak. Kajian juga menunjukkan bahawa tekanan impuls meningkat apabila impak permukaan meningkat. Tekanan gelombang meningkat kepada 17% untuk tembok yang condong ke arah daratan dan 20% untuk tembok yang condong ke arah lautan jika dibandingkan dengan tembok yang menegak pada kecenderungan sudut 10° dengan impak permukaan 0.5. Cadangan reka bentuk untuk tembok didapati konservatif.

ABSTRACT

Shoreline and ocean structures are subjected to breaking wave loads which may reach $690kNm^{-2}$. To reduce these loading, we might slope the exposed surface seaward or landward. However, it is unclear that sloped walls can reduce the wave impact and recent models tests indicated that sloped walls might be exposed to higher loads than vertical walls. Motivated by these findings, we perform a theoretical study of wave impacts on sloped seawalls. The mathematical models of wave impacts on landward-inclined and seaward-inclined seawalls are considered by using an extension of Cooker's model for vertical seawalls. The pressure impulse theory proposed by Cooker is applied into these two problems which simplify the highly time-dependent and very nonlinear problem by considering the time integral of the pressure over the duration of the impact pressure-impulse. The solution to this problem is found by solving Laplace's Equation for specific boundary condition. The perturbation theory is applied into these models and the problems are solved by using MATLAB. The correlation between the pressure impulse and the inclination angle of the wall is investigated. The results are found to be in good agreement with the experimental study. It was found that the lowest pressure impulse occurs when the small inclination happens near to the vertical wall. Study also shows that pressure impulse increases as impact region increases. Breaking wave pressures increase to 17% for landward inclined wall and to 20% for seaward inclined wall compared to vertical wall at 10° incline with impact region of 0.5. Design recommendations were found to be conservative.

TABLE OF CONTENT

LIST OF TABLES

LIST OF FIGURES

LIST OF SYMBOLS

ε	Angle of Seawall
B	Boundary
ρ	Density of Water
μ	Dimensionless Constant of Impact Region
F	Force
g	Gravity Acceleration
H	Height/ Depth of the Wall
u	Velocity
x	Horizontal Direction
t	Impact Time
$L_{\circ}$	Length
u_{nb}	Normal Component of the Approach Velocity
n	Normal Direction
p_{pk}	Peak Pressure
β	Porosity
P	Pressure Impulse
p_s	Pressure of Incident Wave
$U_{\circ}$	Typical Impact Velocity
t_a	Time After the Impact
t_b	Time Before the Impact
Δt	Time Taken During the Impact
u_a	Velocity After the Impact
u_b	Velocity Before the Impact
y	Vertical Direction

LIST OF ABBREVIATIONS

BEM	Boundary Element Method
CFD	Computational Fluid Dynamics
DID	Department of Irrigation and Drainage
FSI	Fluid-Structure Interaction
GIS	Geographic Information System
MNRE	Ministry of Natural Resource & Environment
MOA	Ministry of Agriculture & Agro-based Industry
NAHRIM	National Hydraulic Research Institute of Malaysia
SPH	Smoothed Particle Hydrodynamics
SPM	Shore Protection Manual
TCEC	Technical Coastal Engineering Centre
VOF	Volume of Fluids
VOWS	Violent Overtopping by Waves at Seawalls

CHAPTER 1

INTRODUCTION

1.1 Research Background

Wind blowing over the surface area of an ocean causes the formation of waves. As a carrier of energy, when a wave strikes the surface of any structure, it can cause a huge spray of water rising up into the air.

There are forces or pressures that are acting on these structures. These forces or pressures are divided into two categories. They are pulsating pressure, also known as quad static, and impulse pressure or known as impact (Allsop, Vicinanza & McKenna, 1996). These pressures striking the structures often cause damage.

Seawalls are built by the authorities to protect beaches and coastlines from being damaged by erosion. Seawalls are also a type of seaside safeguard developed where the ocean, and related waterfront forms, affect specifically upon the landforms of the drift. The inspiration behind a seawall is to secure zones of human residence, preservation and recreation from the activity of tides, waves, or torrents. There are a few types of seawall designs as shown in Figure 1.1.

A breakwater is constructed and used to provide a calm lagoon for ships and protect harbour facilities. As ports open to rough seas, breakwaters play an important function in their operations. The purpose of a breakwater is to diminish the power of wave activity in inshore waters and consequently lessen seaside disintegration or provide safe harbourage. Therefore, the history of a breakwater has been one of much damage and failures (Takahashi, 1996). Figure 1.2 shows a simple structure of breakwater.

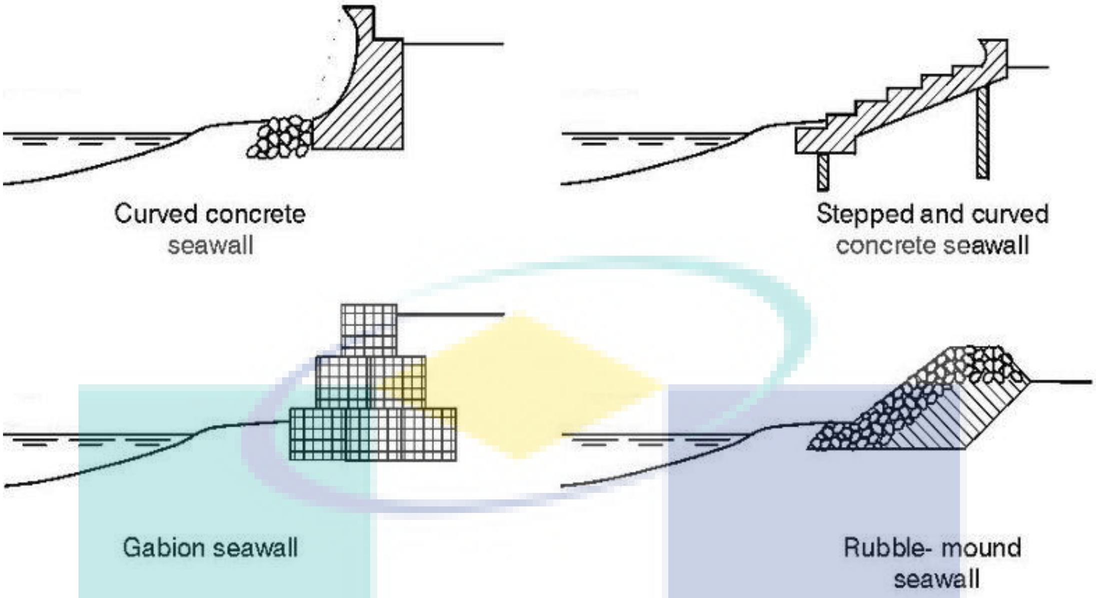

Figure 1.1 Examples of seawalls, image taken from Coastalwiki

Source: Mangor (2019)

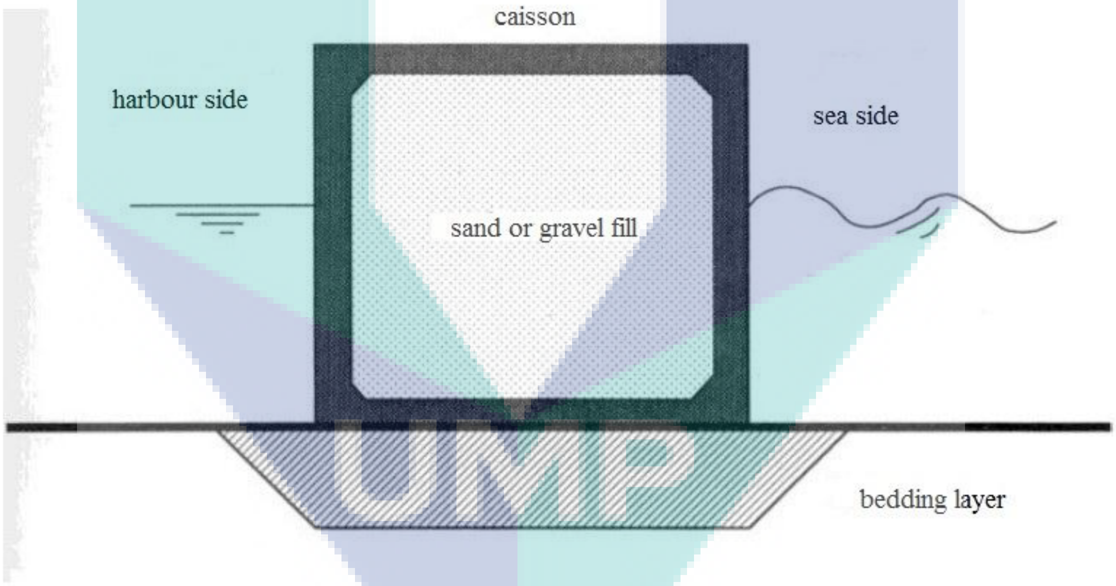

Figure 1.2 A simple structure of breakwater, image taken from European Coast

Source: Md Noar (2012)

Hence, it is really important to study the significance of wave impact on a wall. The design of the seawall or breakwater should be considered. The engineers and designers should design a proper seawall or breakwater that can reduce this impact. The cost to design this seawall or breakwater also should be considered. A poorly designed seawall or breakwater may lead to structural failure as waves erode the base of the seawall. This also requires constant maintenance that is time consuming and costly. Among the initial significant cases of damage was in a series of failures of a large rubble mound breakwater recorded in 1930 (Oumeraci, 1994). Since then, many studies have been conducted in order to develop and enhance the stability of seawalls or breakwaters. Waves breaking on and impacting structures has been studied theoretically and experimentally in the coastal engineering field.

Coastal engineering has attracted a lot of researchers interested in investigating and carrying out experiments to determine wave impact on coastal structures. These experiments used either scaled down models or were conducted in full scale. Some researchers investigated this topic using theoretical studies. The results were compared and a good agreement was found. Their results have contributed a lot to the coastal engineering field and have improved the development of seawalls and breakwaters. A few researchers investigated landward-inclined and seaward-inclined seawalls. Most of the research on landward-inclined and seaward-inclined seawalls were conducted empirically.

One of the earliest research work in coastal engineering was carried out by Bagnold (1939). He contributed to this field by investigating the high peak value of pressure using a wave tank model. Cooker and Peregrine (1991) proposed a mathematical model for the pressure impulse theory. Cooker and Peregrine (1995) then modified Cooker's previous model from using exponential terms into hyperbolic terms in Fourier series. They also stated the pressure impulse is equal to the integral of the pressure within the duration of the impact. This resulted in a simplified, but much more stable, model of wave impact on the coast.

Mitsuyasu, Hase, and Sibayama (1958) carried out an experiment and stated the correlation between impact pressure and inclination of the wall. Okamura (1993) compared his result by using a theoretical study and a good agreement of pressure impulse was found from altering the inclination of the wall. Kirkgöz (1991) studied the impact pressure of breaking waves on a sloping seawall and did an experiment on a backward sloping wall. Neelamani and Sandhya (2005) conducted an experiment on the surface roughness effect of a landward-inclined seawall in incident random wave fields.

This research is a continuity of the work of Md Noar (2012) involving wave impact on the rectangular model. Md Noar and Greenhow (2015b) had extended Cooker's model to breakwaters with a ditch or berm by using a basis function method and a hybrid collocation method of the pressure impulse. In this research two more models will be considered; a landward-inclined seawall and a seaward-inclined seawall.

The perturbation theory will be applied into these two cases to validate the results of this study. Then, the same theory as proposed by Cooker will be extended and compared with previous research. The pressure impulse will be found by varying the angle of the seawall. These quantities will be very helpful from a practical point of view for engineers or designers to build a seawall.

In this case, a mathematical formulation will be studied theoretically to investigate the pressure impulse on landward-inclined and seaward-inclined seawalls. A mathematical theory will then be applied to these two problems; a landward-inclined and seaward-inclined seawall. Finally, the results of the two cases will be displayed graphically.

1.2 Problem Statement

Malaysia has 4800 km of coastline. Recent coastal erosion has resulted in damage to mangrove forests, agricultural lands, road communication links and recreational beaches. Midun (1988) states that coastal erosion is a natural phenomenon resulting from the interactions between natural processes and the system. The natural process for coastal erosion is caused by waves. Out of the 4800 km of coastline, about 1300 km (27%) are at present subject to erosion. Coastal erosion has an adverse effect economically and socially. Many socio-economic activities such as agriculture, housing and urbanisation, transportation and recreation are affected and most of the agricultural land is seriously threatened in the west coast of Peninsular Malaysia. In order to prevent the erosion, there are long term and short term plans. The short term plan involves building structural solutions like the construction of revetments and seawalls. Meanwhile the long term plan, in order to minimise the high cost of protective works in the future, will involve taking into account erosion for every development, planning and construction of facilities at affected areas.

As an example, in the case of Tanjung Piai in Johor, the occurrence of erosion has been reported since the 1930s. Critical erosion has been estimated to happen at a rate of 2-4 m/year at the western coast of Tanjung Piai (Abdullah, 1992). Awang, Jusoh, and Hamid (2014) through the Department of Irrigation and Drainage (DID) reported that erosion rapidly increased after the dredging of a navigation channel in 2002. Since Tanjung Piai has a high socio-economic value for fisheries and eco-tourism, the erosion affects the socio-economic situation of the local residents. Awang, Jusoh, and Hamid (2014) also stated that heavy shipping activities around Tanjung Piai generated waves and disturbed the growth of mangrove trees.

As a result, a few methods were proposed to mitigate the erosion in Tanjung Piai. While erosion still occurred along the east coast of Tanjung Piai, a 707m seawall was built in 2006 to protect the coastal area from further erosion. In 2003 and 2006, geotextile tubes filled with sand and laid parallel to the shoreline were installed to reduce the wave heights. Between 2007 and 2009, a 270m long rock revetment was constructed to protect the west of Tanjung Piai. Lastly, in 2010, since erosion was still occurring, a 1700 m long soft rock combined with 220m of revetment were built along the west and east coasts in order to protect Tanjung Piai from further erosion.

Figure 1.3 shows the destruction caused by coastal erosion at Tanjung Piai. Many trees and plants were destroyed due to the coastal erosion.

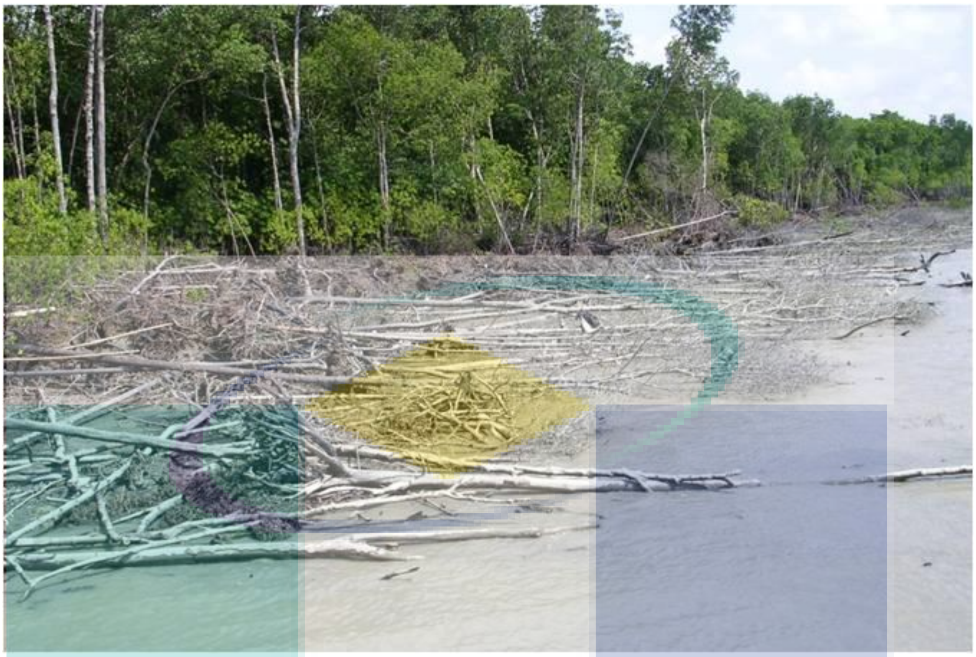

Figure 1.3 Erosion in Tanjung Piai, Johor, image taken from DID
Source: Reka (2017)

Meanwhile, Toriman (2006) stated that at Kuala Kemaman in Terengganu, the erosion happened in a coastal area and caused a high impact to the community in Kuala Kemaman. The first effect is a physical dimension which involved the coastal monitoring due to severe erosion and the second effect is the human dimension which affected on human activities and economy. It caused problem among the coastal community especially in terms of their security. They were losing their homes and their cemetery was also affected. The erosion was also affecting the fishing community of Kuala Kemaman. Figure 1.4 shows the destruction caused by coastal erosion that occurred in Kuala Kemaman. The seawall was built to minimise or prevent the erosion of the shore.

Figure 1.4 Erosion in Terengganu, image taken from New Strait Times
Source: David (2016)

The increase in coastal erosion has affected about 1,282 ha or about 1% a year since 1990 in annual mangrove area losses in some major states in Peninsular Malaysia (Sahriman, Samad, Zainal, Ghazali & Abbas, 2017). The Setiu estuary and Chendering in Terengganu are among the areas experiencing serious erosion (McAlister & Nathan, 1987). The huge waves that strike the coastline during the northeast monsoon were accepted as a hypothetical cause among researchers. This season, which occurs annually from November to February, has waves that are larger than normal due to the strong onshore winds and thus can cause comparatively more damage (Husain & Yaakob, 1988; Mastura, 1987). Husain, Yaakob, and Saad (1995) investigated the variability of beach erosion during the northeast monsoon between Penarek and Setiu Lama. This investigation demonstrates that in spite of the fact that the larger waves of the northeast monsoons may, all in all, be erosional in nature, their net impact on particular stretches of coastlines might be reliant upon site-particular elements including the bathymetry of the landward-inclined territories fronting the coastline and the impact of island covers.

Jaafar, Yusoff, and Ghaffar (2017) reported that coast erosion occurs almost every year in the east coast of Peninsular Malaysia, especially in Kampung Kemeruk in Kota Bharu, Kelantan. Coastal areas are sensitive areas and tend to be vulnerable to various threats such as erosion. If this situation is left unattended without appropriate action to curb aggravated erosion problems, it indirectly affects the quality of life of local communities. The negative impact of this disaster on humans is not only the destruction of property and residential areas, but also threatens the lives of the population inhabiting the coastal area. Therefore, studies on beach erosion are important because our country has a very long coastal area of 4,800 km. In addressing this problem, the steps taken by the authorities such as building seawalls, renovation steps, river estuary repairs and displacement development has been implemented in order to reduce coastal erosion.

Larger waves represent a notable risk to individuals and resources near the coastline, generally due to their size during storms (Wdowinski, Bray, Kirtman & Wu, 2016; Whittaker, Raby, Fitzgerald & Taylor, 2016). Mohd, Maulud, Begum, Selamat, and Karim (2018) in their study titled "The Impact of Shoreline Changes to Pahang Coastal Areas" covered Cherating to Pekan along the shore of the state of Pahang. These areas are on the east coast of Peninsular Malaysia fronting the South China Sea. Along the 10 areas of the Pahang coast, the aggregate length of shoreline changes was observed to be around 14 km (14035.10 m), Pantai Balok and Tanjung Agas were exceptionally affected with a land loss of 26.8 ha and 94.7 ha, respectively. The seaside territories from Cherating to Pekan experienced a high defencelessness with a disintegration rate of 1.8 to 20.9 meter (m) every year (yr). The worst degree of disintegration was found on the seaside territories of Pantai Balok, Kelab Golf Pahang, Taman Gelora, Kampung Cherok Paloh and Tanjung Agas with rates of 13.5 to 20.9 m/yr. For the most part, the beach front zones of Pahang are subjected to a higher disintegration process than growth (Mohd, Maulud, Begum, Selamat & Karim, 2018). Coastal erosion estimation amid the upper east rainstorm also provides data about the progression of shorelines along Tanjung Lumpur to Cherok Paloh, Pahang and a huge portion of the stations have experienced erosion during the time of the study (Azid et al., 2015).

Rameli and Jaafar (2015) assessed coastline changes utilising GIS geospatial procedures on Carey Island which is located off the Morib coast, Selangor, Malaysia. He reported on the suspicion that both deposition and erosion affect the changes in shoreline position. An investigation of available topographical maps showed that the process of deposition and erosion occurred at the same time. Be that as it may, coastal erosion occurred frequently in Carey Island while the deposition process occurred frequently in Morib.

There are a few more examples of seawall construction in Malaysia. Figure 1.5 shows the seawall constructed in Tanjung Piai, Johor. Lastly, Figure 1.6 displays a seawall built in Georgetown, Pulau Pinang. All these seawalls were built by the government to prevent or reduce coastal erosion which has resulted in the destruction of the environment.

Figure 1.5 Seawall in Tanjung Piai, Johor, image taken from Berita Harian
Source: Ibrahim (2019)

Figure 1.6	Seawall in Georgetown, Pulau Pinang, image taken from the Star
Source: Ali (2018)

Since 1970, the only organisation involved in coastal management is the Department of Irrigation and Drainage (DID). Today, among the duties of the DID is to monitor and implement projects to control coastal erosion. DID also carries out some research in coastal management and provides data or information to others to control coastal erosion. The DID also manages the mitigation of floods in Malaysia. Figure 1.7 shows DID satellite office in Sarawak.

Figure 1.7	DID satellite office in Sarawak, image taken from DID Sarawak
Source: Aman (1970)

In the quest to improve coastal management and making it more efficient, the Technical Coastal Engineering Centre (TCEC) was established in 1987 to control critical coastal erosion and provide technical advice on construction projects.

Similarly, the National Hydraulic Research Institute of Malaysia (NAHRIM) is a government institute under the Malaysian Ministry of Natural Resources and Environment which leads the research and provides consultancy in matters of hydraulic and water environment. NAHRIM offers expert consulting services in all areas of hydrothermal engineering including river engineering, coastal engineering, water resources development, and water and environmental quality. NAHRIM was established in September 1993 under the Ministry of Agriculture Malaysia before transferred to Ministry of Natural Resources and Environment in 2004. Figure 1.8 shows hydraulic lab at NAHRIM Seri Kembangan, Selangor.

Figure 1.8 Hydraulic lab at NAHRIM Seri Kembangan, Selangor
Source: Arkib (2014)

Based on the facts presented, the erosion occurring in Malaysia will become more serious without preventive measures. Tanjung Piai is one of the examples related to this problem. In the physical dimension, it causes damage to mangrove forests, agricultural lands, road communication links and recreational beaches. Meanwhile in the human dimension, it affects the socio-economic value of fisheries and eco-tourism and also affects human security in terms of losing their homes. Overcoming these problems costs a lot of money and is time consuming. The government is forced to spend a lot of money building seawalls or breakwaters to overcome this problem. A lot of money is also spent to allocate funding to NAHRIM, TCEC and DID to carry out research in this field to overcome the erosion problem.

In the course of this research, a mathematical modelling and mathematical formulation will be studied to help engineers and designers build a proper and effective seawall. The results will be compared to previous studies to find a good agreement and for analysis. The results might be helpful in cutting the cost of designing a seawall and reducing pressure impulse on a seawall. They also might help engineers and designers to build an effective seawall to overcome erosion effectively.

1.3 Research Questions

a) How to formulate mathematical models of the pressure impulse-theory for landward-inclined and seaward-inclined seawals?

b) How does the small angle of inclination from the vertical structures affect the pressure impulses on the wall?

c) Do the seaward-inclined and landward-inclined seawalls produce minimum pressure impulse?

1.4 Research Objectives

This study has the following objectives:

a) To extend the mathematical model and equations in the fluid motion of the landward-inclined and seaward-inclined seawalls.

b) To apply the perturbation method for solving the mathematical formulations of landward-inclined and seaward-inclined seawalls.

c) To develop MATLAB algorithms for solving the mathematical formulations of the wave impact for the landward-inclined and seaward-inclined seawalls.

d) To provide simplified and much more stable results in models of wave impact on coastal structures.

1.5 Scope and Limitation of the Study

This research aims to extend the pressure impulse theory on the landward-inclined and seaward-inclined seawalls. We will study the effect of a small angle of inclination and also declination in vertical structures. This research is divided into two phases; the first phase is to modify the mathematical modelling of a landward-inclined and seaward-inclined seawall. This will be achieved through extending the pressure impulse theory used by Cooker and Peregrine (1991). Next, Cooker's model is altered based on these two problems i.e. a landward-inclined and seaward-inclined seawalls.

In terms of the limitation of the study, research involving theoretical methods is quite rare in Malaysia. Hence, it is harder to find sources of theoretical methods in Malaysia for comparison. There are only a few organisations involved in this field and they are not very interested in pressure impulse towards seawalls. Furthermore, most of the resources concerning inclined seawalls are found in studies from 1980 to 2000. However, most researchers tend to study this field by conducting experiments either using a model or using a full scale measurement. Hence, it is quite difficult to find a latest resource that used a theoretical approach for this research.

In addition, only Cooker's model from 1991 is applicable and works for our method. In other words, the verification of this model and method has been done successfully.

Finally, the perturbation method only works on a seaward-inclined or landward-inclined seawalls of angle less than 15°. Angles larger than 15° will give error results. The assumption in every one of the issues in this postulation is the liquid is inviscid and incompressible.

1.6 Significance of the Study

This research able to contribute to the understanding of the landward-inclined and seaward-inclined seawall by theoretical studies. It is better if any researcher studies this problem using a model or full scale measurement so we can compare the results of the study. This study might then help engineers to estimate the pressure impulse on the wall for certain geometries.

This study is expected to be considered by engineers and designers to predict the design of wave load conditions in order to help ensure the stability of the structures. Referring to this study might help a designer or engineer to estimate and minimise the cost to build a proper seawall.

1.7 Research Methodology

The first phase is preliminaries studies. During the literature study phase, the preliminary background of wave impact on the seawall was reviewed and the method used by previous authors was studied. The scope of the research was identified.

The next second phase is derivation of mathematical model. During this phase, the pressure impulse theory which proposed by Cooker and Peregrine (1991) was imposed, and two-dimensional model for water wave impact on vertical wall which modelled by Cooker and Peregrine (1991) was applied.

The third phase is to develop a mathematical formulation of each problem. From the mathematical model, the fluid is assumed to be compressible and inviscid. The governing equations and boundary conditions was applied to Laplace's equations.

The next phase is to solve the mathematical formulation. During this phase, the formulation was solved by using perturbation method. Then the results were shown using MATLAB.

The last phase is result analysis and discussion. At this final phase, the results were analysed. For the validation of the results, the later studies or experiments work by previous research was compared.

1.8 Outline of the Thesis

The thesis has been divided into six chapters, and each chapter will be elaborated significantly including the explanation and discussion of the pressure impulse theory. In these two problems, we assume the fluid is incompressible and inviscid.

Chapter 2 provides a comprehensive review of previous studies by researchers in this field. It provides a review of pressure impulse on seawalls, breakwaters and overtopping. The review of these studies will be explained experimentally and theoretically. It also discusses a literature review of the perturbation method since this method is applied in this model.

Chapter 3 will cover the explanation of the pressure impulse theory. It will include Cooker's theory. It will also explain the governing equation in this chapter. Furthermore, the method to be applied will be introduced in this chapter.

The mathematical modelling of a landward-inclined seawall is introduced in Chapter 4. It is then followed by the mathematical formulation of a landward-inclined seawall. The methodology of the research is discussed briefly in this chapter. The methods should be followed to achieve the objectives of the research and to obtain accurate results. We will discuss the result of pressure impulse on a landward-inclined seawall. The results will be analysed and presented in tables and graphs. The results of previous studies will also be discussed and compared to the current results.

Chapter 5 briefly discusses the mathematical modelling of a seaward-inclined seawall. The mathematical formulation of this problem will be discussed. The methodology of the research is also discussed briefly in this chapter. The methods should be followed to achieve the objectives of the research and to obtain accurate results. We will then examine the aftereffect of pressure impulse on a seaward-inclined seawall. The outcomes will be examined and introduced in tables and charts. In addition, the correlation of past investigations will be examined and contrasted with current outcomes.

Finally, Chapter 6 will conclude all the results and objectives of the research. It will also cover the recommendations for further work in order to improve the current mathematical model or to test a new mathematical model in other structural designs.

CHAPTER 2

LITERATURE REVIEW

2.1 Introduction

The coastal engineering field has attracted researchers who wish to investigate the wave impact on the seawall. There have been several research works in this field, both experimentally and theoretically. Bagnold (1939) was among the earliest person researching wave impact and focused on the nature of the shock pressure of wave striking on the vertical seawall. The research in this field has been developed theoretically and experimentally whether in full scale measurement or using a model and they mostly agreed with Bagnold's observations.

The results of laboratory experiments (Bagnold, 1939; Chan & Melville, 1988; Hattori, Arami & Yui, 1994; Ingram, Gao, Causon, Mingham & Troch, 2009; Kirkgöz, 1991; Pullen, Allsop, Bruce & Pearson, 2009) and full-scale measurements (Bullock, Crawford, Hewson, Walkden & Bird, 2001; Bullock, Obhrai, Peregrine & Bredmose, 2007; Cuomo, Allsop, Bruce & Pearson, 2010; Hofland, Kaminski & Wolters, 2011) have contributed to the knowledge of wave impact pressures and its effects on coastal structures. The theoretical approach has also contributed a lot to this field, (Cooker & Peregrine, 1992; Md Noar & Greenhow, 2015a, 2015b; Okamura, 1993). This is vital knowledge in improving the design of coastal structures such as breakwaters and seawalls.

2.1.1 Model Scale

A model scale is most generally a physical representation of an object which maintains accurate relationships between all important aspects of the model, although absolute values of the original properties need not be preserved. This enables the demonstration of some properties of the original object without examining the original object itself. As a result, the researchers have given us new results or detail and also some improvements for us to study the characteristics of wave impact pressure.

An experiment was conducted to study the problem of wave pressure on vertical walls by using a wave tank model (Bagnold, 1939). The study clearly stated that when waves strike a wall, they are likely to yield high shock pressure in a very short time. Bagnold (1939) also stated that in a very short time, Δt, the pressure goes up to its high peak value, p_{pk} and normally the time taken is from 1 to 10 ms. He also proposed the pressure impulse, P as the integral of pressure over the period of impact.

Kirkgoz (1982) conducted an experiment to study the breaking wave impact on vertical walls. He claimed that the breaking wave with its front face parallel to the wall produces the greatest shock pressures. He then continued his study by conducting a new experiment, and found that the backward landward-inclined and forward landward-inclined wall may experience higher impact pressure than a vertical wall (Kirkgöz, 1991).

Chan and Melville (1988) conducted an experiment on the impact pressure due to deep-water breaking on surface piercing flat plate. They stated that the dynamics of trapped air during impact may cause a higher pressure and pressure oscillations. Chan (1994) also had the same result in an experiment on deep water plunging-wave impact on a vertical wall. The result was compared theoretically by Cooker and Peregrine (1991) and a good agreement was found.

Hattori, Arami, and Yui (1994) found that the highest impact pressures of very short duration happened when small air bubbles were trapped between the wall and the vertical wave during the impact. Ingram, Gao, Causon, Mingham, and Troch (2009) conducted a numerical modelling work package to study impulsive wave overtopping at coastal structures. The simulation shows impulsive, aerated, near overtopping jets dominated the overtopping process on a vertical seawall. Pullen, Allsop, Bruce, and Pearson (2009) did a comparison between field and laboratory measurements of mean overtopping and spatial distribution on a vertical seawall. The study shows there are no scale effects that need to be considered when comparing between field and laboratory tests but the wind effect needed to be accounted and corrected for accordingly.

Kisacik, Troch, Van Bogaert, and Caspeele (2014) investigated uplift impact forces on a vertical wall with an overhanging horizontal cantilever slab. In a little scale test set-up under wave impact (imprudent) loads, a vertical wall with an overhanging flat cantilever piece is tested. An arrangement of parameters overseeing the expectation of wave stacking on the structure is examined. From the breaking wave kinematics and impact loads experiment, the result of a prediction model of uplift impact force is introduced.

Using a model test, a numerical simulation of wave impact on a rigid wall using a two–phase compressible Smoothed Particle Hydrodynamics (SPH) method was studied by Rafiee, Dutykh, and Dias (2015). A SPH strategy in light of the SPH–ALE plan was utilised for demonstrating two-stage streams with extensive thickness proportions and sensible sound velocities. The SPH plot was additionally enhanced to go around the elastic flimsiness that may happen in the SPH recreations. The distinction in the area of the effect weight was related to the interface thickness in the level set reproductions though the proposed SPH conspire was equipped for displaying sharp interfaces between the stages.

Kocaman and Ozmen-Cagatay (2015) explored dam-break induced shock waves impact on a vertical wall by doing trial tests and Volume of Fluids, VOF-based on Computational Fluid Dynamics, CFD simulations. New research facility tests were done in a rectangular flume with a smooth even wet bed for two distinctive tailwater levels. The discoveries demonstrate that the effect of dam-break surge wave on a downstream end divider causes wave reflection against the divider and a negative wave event moving upstream with undulations on a free surface. Holloman, Deshpande, and Wadley (2015) investigated an impulse transfer during sand impact with a solid block. During this experiment, a vertical pendulum device was utilised to tentatively explore the impulse and pressure connected by the effect of wet engineered sand upon the level surface of a back upheld strong aluminium test square. The experimental study shows that the momentum transferred to the test structure and is assumed to be equivalent to the incoming sand's free field momentum, with the possibility that the sand stagnates against a planar surface upon impact.

Shih (2016) studied random wave impact on highly pervious pipe breakwaters through a physical experiment. This examination explored the execution of a pervious pipe screen breakwater introduced before a seawall to reduce the wave impact force and wave pressure. The outcomes demonstrated that pervious pipe snags set vertically before a dike can viably moderate and decrease the wave impact by more than 70%.

An investigation of offshore breaking wave impacts on a large offshore structure was carried out by Hu, Mai, Greaves, and Raby (2017). The discoveries are significant to offshore and beach front structures in distinguishing the outrageous loads, maximum pressure and most extreme run-up required for their design. There are four types of wave impact recognized in the tests. They are slightly breaking, flip-through, large air pocket and broken wave impacts. The outcome demonstrates a good agreement was found in the four wave impact types between numerical expectations and experimental measurements of surface height, run up and impact zone. This study has demonstrated various types of wave impact will affect the highest wave run-up and maximum load. Hence, this study is required to be considered separately for design purposes.

Van Doorslaer, Romano, De Rouck, and Kortenhaus (2017) investigated the impact on a storm wall caused by non-breaking waves overtopping a smooth inclining embankment. An experimental modelling was conducted at three unique scales which are small, middle and large scale in order to quantify such effects. The tested geometry was a smooth inclining embankment. The forces from the waves overtopping the dams in the range of 20 to 40 kN/m model scale in the dimensionless freeboard (Rc/Hm0) scope of 1 to 2 was demonstrated as a result. Compared to impact forces on vertical walls as computed by the Shore Protection Manual (SPM), it is much lower. The diminishment of wave overtopping should be possible by introducing a versatile or changeless storm wall.

A nonlinear wave interaction with curved front seawalls was investigated by De Chowdhury, Anand, Sannasiraj, and Sundar (2017) in the Ursell number ranging from 8 to 16. Analyses have been conducted to gauge the dynamic weight on these seawalls under the activity of customary monochromatic waves. Two diverse numerical models have been utilised to break down the deliberate information: An in-house SPH molecule based model and the business CFD bundle ANSYS-FLUENT. The SPH arrangement contains a few imperative nonlinear viewpoints likewise uncovered in the investigations. The correlation of estimated and reenacted weights along the bended front demonstrates the ability of the SPH models in anticipating the idea of run-up and overtopping, if it happens.

Extreme wave run-ups and pressures on a vertical seawall were studied by Ning et al. (2017). Correlations with exploratory information demonstrate that the stretched out numerical model can precisely foresee extraordinary wave run-ups and pressures on a vertical seawall. The impacts of the wave spectrum bandwidth, the position of the wall and the wave nonlinearity on the wave run-up and the greatest wave load on the vertical seawall are explored by doing parametric research.

Qin, Tang, Xue, Hu, and Guo (2017) conducted a numerical study of wave impact on the deck-house caused by freak waves by using a model test. An improved strategy is proposed to surmise the deck-house wall as an Euler beam with a middle of an intermediate elastic bearings. By applying an understood iterative calculation, the Fluid-Structure Interaction (FSI) is applied. Three re-creations are worked up, including a customary wave impact against a rigid wall, a laboratory scale freak wave impact against a flexible wall, and the deck-house impact caused by a full-scale freak wave. By contrasting the neighbourhood pressure between the elastic deck and the elastic deck close to the vertical wall, it was discovered that the hydro elasticity altogether impacts the liquid area close to the elastic body.

Song and Zhang (2018) studied the boundary element study of wave impact on a vertical wall with air entrapment. This research intends to accomplish the total procedure of simulation for wave impact with air entanglement utilising Boundary Element Method, BEM. A multi scale calculation with the assistance of an extended organised framework is presented for the nearby impact zone. Impacts of the pneumatic force on the effect procedure with air entanglement are likewise examined, where a logical conclusion due to the law of conservation is applied to clarify the discoveries. The impact of the air ensnared between a vertical wall and an overturning wave also assumes a fundamental part in the physical procedure of wave impact. Jensen (2018) investigated a solitary wave impact on a vertical wall. Wave impact on a vertical wall is explored in a physical and numerical wave tank. In a wave tank, a flip-through was moving quickly vertical because of a stream and a case with an extremely soaked wave was produced. Next, the front was relatively vertical and the measurement of impact pressure was 60% higher than the flip-through case where the greatest pressure is discovered. Due to the impact and once-over process, an articulated double pressure peak is recorded for measurement of pressure.

In the latest research, Marzeddu, Stagonas, Gironella, and Sánchez-Arcilla (2018) investigated an experimental set-up and calibration errors for mapping wave-breaking. In concurrence with existing literature, researchers characterised adjustment capacities are accounted for to decrease the error in many estimations. However, in logical inconsistency to past work, straight and nonlinear fit capacities are stated to yield measurably indistinct outcomes. This study investigates the primary parameters influencing the precision and error of pressure result prompted by laboratory set-up and calibration system.

2.1.2 Full-Scale Measurement

Full-scale measurement is the experimentation of real-life situation in real location that will give an overview of the problem being measured and using large scale measurement. Bullock, Crawford, Hewson, Walkden, and Bird (2001) studied the influence of air and scale wave impact pressures at Admiralty Breakwater, Alderney. They found that the aeration level of seawater is higher than freshwater. They also noticed the peak pressure of freshwater waves is larger than the peak pressure of seawater waves. Subsequently, they concluded that the entrained air caused the maximum impact pressure to be lower. Bullock, Obhrai, Peregrine, and Bredmose (2007) investigated again the characteristics of the impact waves and used large-scale regular wave tests on sloping and vertical walls. They proposed that in some cases, the high level of aeration can increase the force and impulse on the wall. They noticed that at a sloping wall, the pressures, force, and impulse will be lower compared to a vertical wall.

Cuomo, Allsop, Bruce, and Pearson (2010) conducted a full measurement experiment in Barcelona within the framework of the Violent Overtopping by Waves at Seawalls (VOWS) on breaking wave loads at vertical seawalls and breakwaters. A simple and intuitive set of prediction formula was introduced for quasi-static, impact forces and overturning moments and it produced a good agreement with the new measurement. They compared the previous measurements from physical model tests at small and large scale with this new prediction formula and found encouraging results.

Hofland, Kaminski, and Wolters (2011) carried out a full scale measurement of pressure fields on a vertical seawall. They collaborated with the Joint Industry Project Sloshel in LNG tanks using high spatial and temporal resolution. The flip-through impact was found to have caused the highest peak pressure and force but it was also found to happen very rarely in a random wave field. Peregrine (2003) stated that violent pressure caused the flip-through to occur; it occurs without impact of liquid on the wall, independent of the global dynamics and is a local phenomenon.

Stagonas, Marzeddu, Cobos, Conejo, and Muller (2016) studied the use of a pressure mapping system for measuring wave impact induced pressures. A set-up and an adjustment strategy were proposed and utilised for this work. The framework was approved against a pressure transducer and load cell measurement and for a scope of waves breaking on a vertical seawall. Using an extensive number (120 estimations for each case considered) of breaking and broken waves communicating with the wall, the peak pressure profiles and the pressure distribution maps detailed by the framework concur well with results obtained by utilising pressure transducers. It was found that through cautious alignment and set-up the pressure mapping framework has the ability to furnish pressure distribution maps with a decent precision.

2.1.3 Theoretical Work

Weggel and Maxwell (1970) modelled the wave impact on vertical walls and solved the wave equation in a compressible fluid. A similar work was done by Partenscky and Tounsi (1989).

Cooker and Peregrine (1991) had modelled the wave as a rectangular region filled by fluid. They compared their theory (1991) with experimental works by Weggel and Maxwell (1970) and also by Partenscky and Tounsi (1989). They compared the shape of distribution of peak pressure using the chosen impact region, μ by the previous experimenters using their own mathematical model and found a good agreement. Presently, Cooker's model (1991) is extended in this study. Subsequently, Cooker and Peregrine (1995) applied the theory to study the impact of deep water waves, the impact in a container, the impact of a water sheet on still water and a triangular wave. They found that the pressure impulse field is insensitive to variations of the wave shape where the distance is greater than half of the water depth from the impact region.

Okamura (1993) investigated the impulsive pressure due to wave impact on a sloping wall. He studied the relation between the maximum pressure impulse and the inclination angle of a wall. The results showed that the pressure impulse has a maximum value in the case of a near vertical wall.

Two methods had been applied in order to find wave impacts on rectangular structures i.e. hybrid collocation method and a basis function method (Md Noar, 2012). The hybrid collocation method was applied into the berm and ditch problem and a wall with a deck. Meanwhile, the basis function method was applied into a missing block problem and structures with baffles. The difference between the hybrid collocation method and the basis function method is at the matching interface. For the hybrid collocation method, the equation and derivatives will be matched by collocation points distributed over the depth. In contrast, for the basis function method, both equations and their derivatives will be multiplied by basis function and then integrated over the depth.

Cooker (2013) created a model of water impact onto a porous breakwater. He found that there are two types of flow, depending on the porosity, β of the barrier. He considered the small value of β giving an insight into the sudden changes in flow and the high pressures that occur when a wave impacts a nearly impermeable seawall. Mamak and Guzel (2013) studied the wave impact pressures on curved seawalls. The results showed that the pressure impulse model can be used to model the wave impact pressures and their distribution on curved seawall models with good accuracy. A slight decrease has been observed in pressures for increasing radii of curvatures, especially in the case where the water depth at the wall was 14 cm. The location of the maximum impact pressure was found to occur above the still water level for all cases tested in this study.

Md Noar and Greenhow (2015b) developed a simple analytical model for the pressure impulse and then applied it to a vertical seawall with berm and ditch and a vertical seawall with a missing block. They found that the berm has only a small effect on the pressure impulse on the seawall while within the ditch, repeated pressure impulses may liquefy the seabed there and may destabilize the wall. For the missing block case, they found that the pressure impulse decreases when the width of the missing block increases. Md Noar and Greenhow (2015a) modelled a vertical baffle at a free surface, a vertical baffle in front of a wall, a vertical baffle at a deck in front of a seawall and a vertical baffle on the seabed in front of a wall.

Akbari (2017) conducted a theoretical study of the simulation of wave overtopping using an enhanced SPH method for different coastal structures. Based on the idea of surface viscosity initially presented by Xu (2010), this issue was illuminated by altering the consistency of surface particles. This change can be utilised for both Incompressible and Weakly Compressible SPH strategies and its usage is simple and computationally productive as well. By this research, free surface boundary was simulated more precisely by methods for the presented alteration. As a result, the approximated values especially the wave-overtopping rate turn out to be more accurate.

Paprota, Staroszczyk, and Sulisz (2018) investigated the Eulerian and Lagrangian modelling of a solitary wave attack on a seawall. The two approaches i.e. the semi-analytical method and the SPH method were applied to investigate the problem of a solitary wave attack. The expectations of the two approaches were contrasted by differing wave regimes for which the two strategies produced satisfactory outcomes. The after-effects of numerical re-creations have demonstrated that both proposed techniques foresee basically a similar free-surface profiles for rushes of little and direct amplitudes. For maximum waves, a few errors between the after-effects of the two methods happen. By comparing these two models results with empirical data, a good agreement was found with experimental data of wave crest and maximum wave run-up at a wall.

Based on this research, theoretical work is chosen. A rectangular region filled by fluid from Cooker and Peregrine (1991) has been extended into two models of wave impact on seaward-inclined seawall and landward-inclined seawall. Pressure impulse theory is discussed in chapter three.

2.1.4 Perturbation Method

The perturbation theory method will be applied in this research for these two problems in Chapter 3 and Chapter 4 i.e. the mathematical modelling of a landward-inclined and a seaward-inclined seawall respectively. After the results have been obtained, we will run the coding in MATLAB to illustrate them in tables and figures.

Perturbation theory leads to an expression for the desired solution in terms of a formal power series in a small parameter, ε, known as the perturbation series that quantifies the deviation from the exactly solvable problem. The leading term in this power series is the solution of the exactly solvable problem while further terms describe the deviation in the solution. Perturbation theory comprises mathematical methods for finding an approximate solution to a problem by starting from the exact solution of a related, simpler problem. A critical feature of the technique is a middle step that breaks the problem into solvable and perturbation parts. Perturbation theory is applicable if the problem at hand cannot be solved exactly, but can be formulated by adding a small term to the mathematical description of the exactly solvable problem. Consider

$$x = x_0 + \varepsilon x_1 + \varepsilon^2 x_2 + \cdots \tag{2.1}$$

Here, x_0 is the known solution to the exactly solvable initial problem and $x_1, x_2, \dots$ are the higher order terms. For small ε these higher order terms are successively smaller. An approximate "perturbation solution" is obtained by truncating the series, usually by keeping only the first two terms.

A few researchers have recently applied the perturbation method in their studies. Mirzazadeh and Ayati (2016) applied the perturbation method for a system of Burger equation. They noticed the method is very simple and effective. The computational difficulties of other methods are reduced in this model. All calculations with simple manipulations can also be made.

Claude, Duigou, Girault, and Cadou (2017) investigated an eigensolution to a vibroacoustic interior coupled problem with the perturbation method. As a result, they proposed to apply a perturbation method to compute the eigenvalues of a vibroacoustic interior coupled problem. Because it only requires a linear solver and a subroutine to realize matrix-vector product, this proposed method is much easier to implement in computational software

Moutsinga, Pindza, and Mare (2018) studied the perturbation and transform methods for pricing under pure diffusion models with affine coefficients. They introduced an efficient method in order to solve the system of Riccati differential equation. The Laplace and perturbation methods are combined in this technique as a part of an algorithm to the exact solution of the nonlinear Riccati equation. As a conclusion, they proposed to solve nonlinear systems of stiff Riccati differential equations arising in finance by combining the Laplace and perturbation methods.

CHAPTER 3

PRESSURE IMPULSE THEORY

3.1 Introduction

During the impact of waves on a seawall, the horizontal of the waves is immediately brought to rest. This sudden and unexpected change of the wave's motion is accompanied by a large pressure, p over a short time acting on the wall and also through the fluid. Since wave impacts occur for a very short time, typically $10^{-2}s$ or may be less, it is appropriate to define the pressure impulse.

The first definition of pressure impulse P had been proposed by Cooker and Peregrine (1991) as the integral of pressure with respect to time:

$$P(x,y) = \int_{t_b}^{t_a} p(x,y,t)\,dt \tag{3.1}$$

The notation t_b is the time before the impact while t_a is the time after the impact. Next, x and y are the Cartesian coordinates of position and p is pressure.

The peak pressure, p_{pk} (typically $4 \times 10^5 Nm^{-2}$) can also be estimated from a calculation of the value of P, by assuming that during the impact the pressure is approximately triangular, and $\Delta t = t_a - t_b$ are known. It can be referred in Figure 3.1.

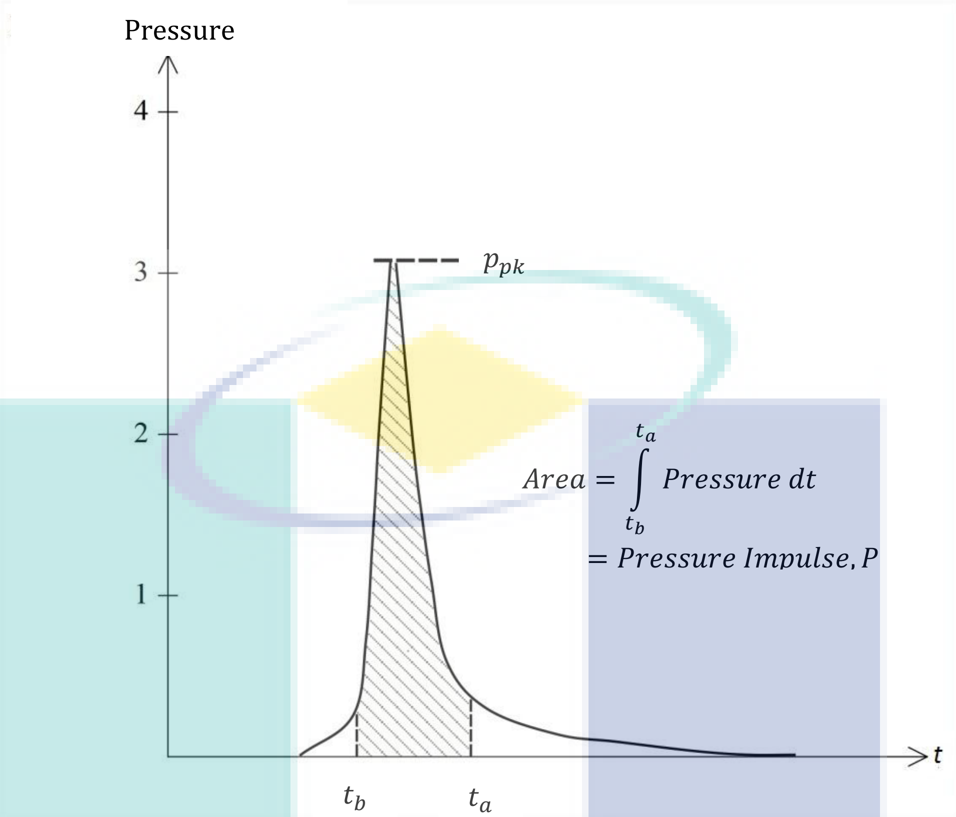

Figure 3.1 The sketch of pressure as a function of time

Under the fixed wave condition (at a point on the wall) the pressure impulse is approximately constant although the peak pressure will vary unpredictably (Bagnold, 1939). Therefore,

$$P = p_{pk}\frac{\Delta t}{2} \qquad 3.2$$

It can be expressed as:

$$p_{pk} = \frac{2P}{\Delta t} \qquad 3.3$$

But since Δt is uncertain, the peak pressure p_{pk} is also an uncertain estimation. This is the reason the pressure impulse, P, is chosen to study the wave impact on a rigid structure and to get the peak pressure. For a high impact p_{pk} can be very high and Δt very small, but the product of Equation 3.2 will stay finite and approximately constant for wave impact from similar waves. In a comparison of their result with an experimental measurement, they stated that this theory uses simple boundary conditions and produces an approximate solution for other wave shapes in more complex geometries. Therefore, we refer to the model of Cooker and Peregrine (1991) which is a two-dimensional model for water wave impact on a vertical wall.

3.2 Cooker's Model

Cooker and Peregrine (1991, 1995) created a mathematical model for the pressure impulse theory for impact between a region of incompressible and inviscid. Cooker's model from 1991 was designed for the pressure impulse theory of an impact region. Figure 3.2 represents a model of a two-dimensional vertical seawall. The full line is the wave after the impact while the dotted line is the incoming waves. The area between dotted line and full line is the impact zone.

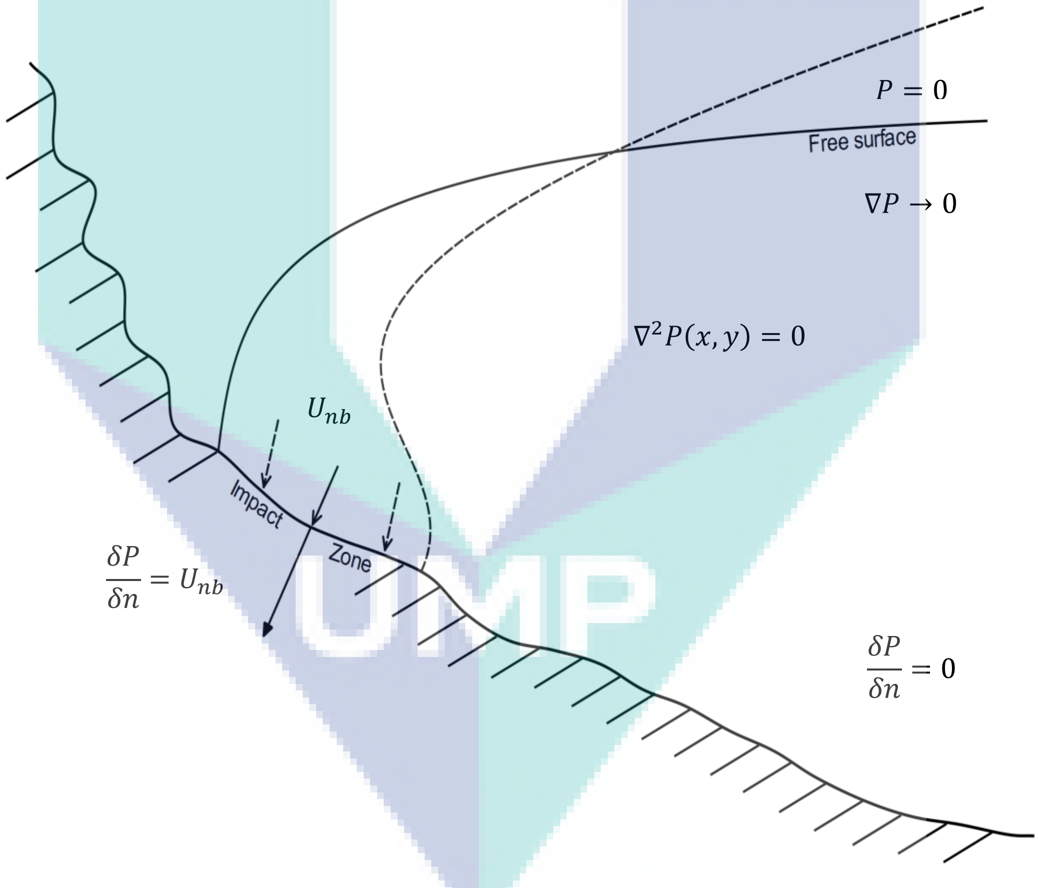

Figure 3.2 The sketch of a realistic wave impact

Cooker and Peregrine (1991) modelled the real situation as a rectangular shaped region filled by fluid where the seabed is at $y = -H$ while the seawall is at $x = 0$, and the free surface is at $y = 0$. The fluid domain is defined by $x \geq 0, -H \leq y < 0$ and μ

is a parameter that describes the impact region, $-\mu H \leq y < 0$. This can be shown in Figure 3.3.

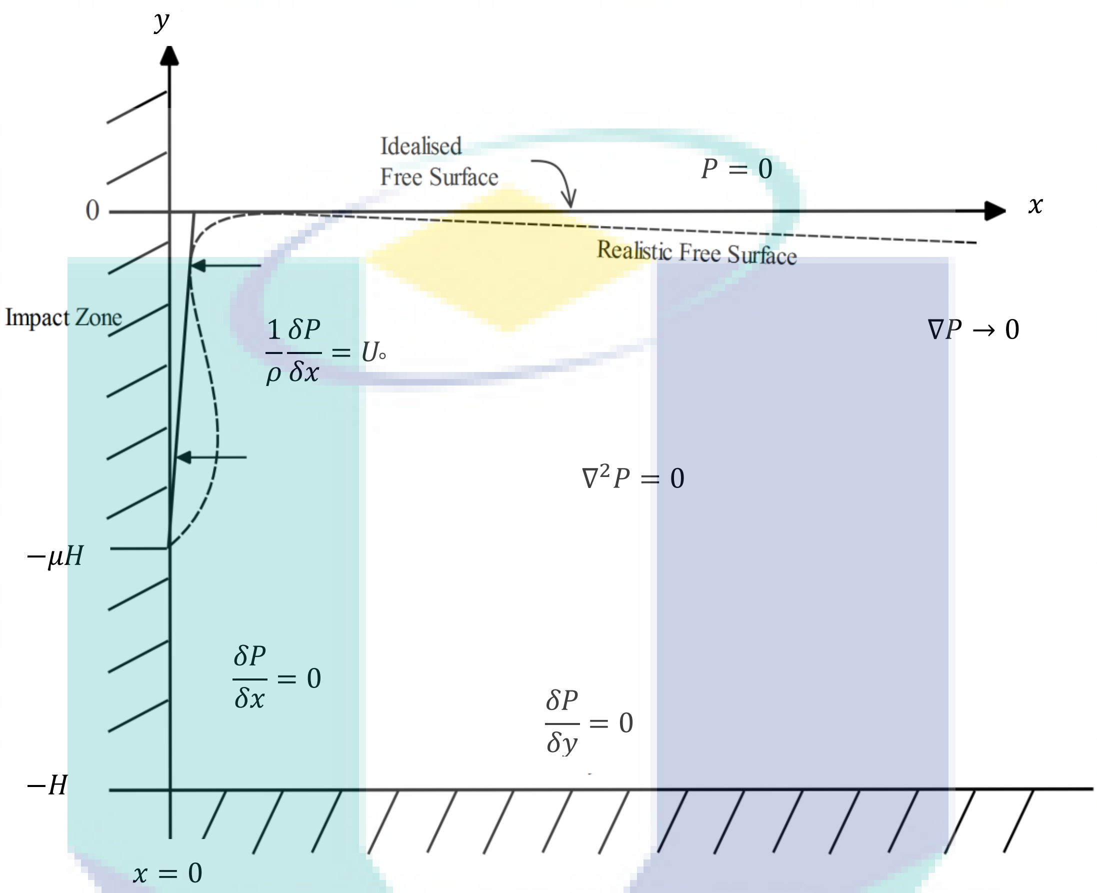

Figure 3.3 Cooker's model in 1991

The notations used in Figure 3.3 are defined as:

$0 \leq \mu \leq 1$: a dimensionless constant indicating how much of the wall is hit

$H > 0$: total water depth at time impact, from seabed to the top of the wave

$U_{\circ}$: a typical impact velocity

Cooker and Peregrine (1995) then improved their mathematical model from 1991, changing from using exponential terms to hyperbolic terms. They stated that the exponential will decay when $x \to \infty$ (Cooker & Peregrine, 1991) and transformed the previous model into a specific boundary, $x = B$ instead of $x \to \infty$. The new model is illustrated in Figure 3.4.

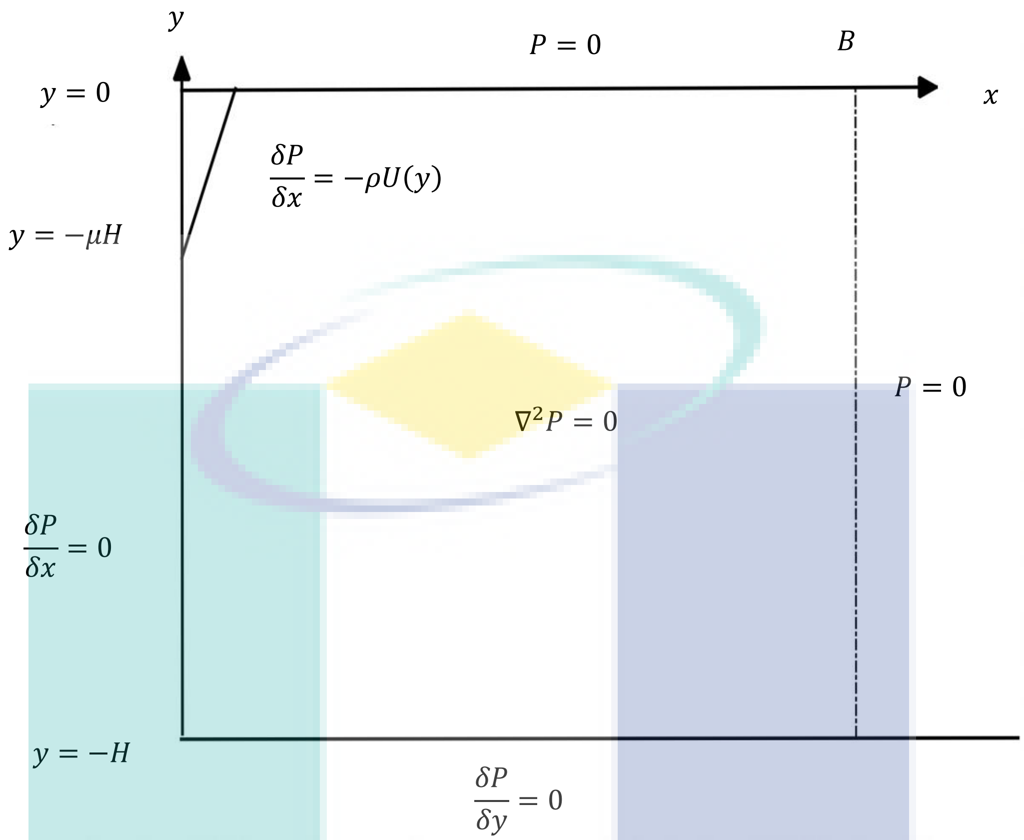

Figure 3.4 Cooker's model in 1995

Cooker and Peregrine (1995) stated that the rectangular region is full with an ideal fluid domain by neglecting any cushion of air. Bagnold (1939) suggested the greatest pressure impulse happens due to an adiabatic compression over a large area of thin air cushion and the wave front must be almost plane and parallel to the wall at the moment of impact. This model was developed by Faltinsen and Timokha (2011) theoretically. However, we will not consider it here.

3.3 Governing Equation

The governing equations for this problem are based on the mathematical model suggested by Cooker and Peregrine (1991, 1995). The fluid is said to be incompressible and inviscid. The boundary conditions are displayed in Figure 3.4. Let's say $U_\circ$, $L_\circ$, Δt, ρ, g, u and p_s are typical impact velocity, length, time, water density, gravitational acceleration, velocity and pressure, respectively, for the incident wave. Euler's equations made dimensionless with respect to these scaling are:

$$\frac{\delta \underline{u}}{\delta t}+\left(\frac{U_\circ \Delta t}{L_\circ}\right)(u.\nabla)\underline{u}=-\left(\frac{\Delta t p_s}{\rho U_\circ L_\circ}\right)\nabla p-\left(\frac{g\Delta t}{U_\circ}\right)\underline{j} \qquad 3.4$$

$$G_1 \qquad\qquad G_2 \qquad\qquad G_3$$

The notation $\underline{j}$ in Equation 3.4 is a unit vector directing upwards. Cooker and Peregrine (1991) had labelled G_1, G_2 and G_3 as dimensionless groupings and they are discussed as follows.

For a sudden impact, the impact time is much less than the time scale of the evolution of the wave as a whole, i.e $\Delta t \ll L_\circ/U_\circ$. Then, based on Equation 3.4, $G_1 = U_\circ \Delta t/L_\circ \ll 1$, and the nonlinear term can be neglected. Next, $G_3 = g\Delta t/U_\circ \ll 1$, then the last term in Equation 3.4 is so small and can be neglected. Besides that, as for $G_2 = \Delta t p_s/\rho U_\circ L_\circ$, we can have a balance between the first and third term in Equation 3.4. Cooker and Peregrine (1991) proves this is consistent with the statement:

"Impulse exerted on the wall~Incident wave momentum"

Neglecting the small terms in Equation 3.4 yields:

$$\frac{\delta \underline{u}}{\delta t}=-\left(\frac{\Delta t p_s}{\rho U_\circ L_\circ}\right)\nabla p \qquad 3.5$$

By choosing $\Delta t p_s = |U_\circ| = L_\circ = 1$, i.e. $p_s = (\rho U_\circ L_\circ/\Delta t)$. From this case, considered here we can choose to non-dimensionalise problem by the characteristic length, time and velocity become the water depth, duration of impact and velocity of impact directly. Then Equation 3.5 indicated that pressure impulse is scaled by $\rho U_\circ L_\circ$. Equation 3.5 becomes:

$$\frac{\delta \underline{u}}{\delta t}=-\frac{1}{\rho}\nabla p \qquad 3.6$$

over a short interval, ∇t.

Now, the integration of Equation 3.6 with respect to time through the impact interval, $[t_b, t_a]$ gives

$$u_a - u_b = -\frac{1}{\rho}\nabla p \tag{3.7}$$

The notation of u_a is velocity after impact and u_b is velocity before impact, $\nabla . u_b$ and $\nabla . u_a$ will vanish ($\nabla . u_b = 0,\ \nabla . u_a = 0$) by taking the divergence of Equation 3.7. Therefore, it shows that the pressure impulse satisfies Laplace's equation:

$$\nabla^2 P = 0 \tag{3.8}$$

Equation 3.8 does not contain time, hence we can solve the boundary-value problem in a fixed domain which is a mean position for the fluid during the impact. In the fluid domain, the boundary conditions are applied to Laplace's equation as follows:

a) At the free surface, where pressure is constant and taken to be zero reference pressure.

$$P = 0 \tag{3.9}$$

b) At points on a fixed rigid boundary, in contact with the liquid before and after the impulse, the normal velocity is zero and it gives

$$\frac{\delta P}{\delta n} = 0 \tag{3.10}$$

c) When the liquid meets a solid boundary during impact, the change in normal velocity gives the normal derivative of pressure impulse. For the simplest case of a stationary or moving rigid boundary,

$$u_{nb} = \frac{1}{\rho}\frac{\delta P}{\delta n} \tag{3.11}$$

The notation u_{nb} is the normal component of the approach velocity of the liquid. The subscript n_b denotes the components normal to the boundary. Conditions b) and c) are easily altered to account for moving rigid boundaries including the case where the impact causes a rigid body to move.

d) When liquid meets liquid two boundary conditions are needed on the common interface. One is that the pressure impulse is continuous:

$$P_1 = P_2 \tag{3.12}$$

Considering the change in velocity on each side of the interface gives

$$u_{1nb} - u_{2nb} = \frac{1}{\rho_1}\frac{\delta P_1}{\delta n} - \frac{1}{\rho_2}\frac{\delta P_2}{\delta n} \tag{3.13}$$

The subscript n_b denotes the components normal to the boundary and subscript b denotes the liquid velocities immediately before the impact. In all the above cases, an inelastic impact is assumed.

The solution of the boundary value problem for the first model by Cooker and Peregrine (1991) in Figure 3.3 is solved using the separation of variables in Laplace's equation and Fourier analysis giving

$$P(x, y) = \sum_{n=0}^{\infty} a_n \sin\left(\frac{\lambda_n y}{H}\right) exp\left(-\frac{\lambda_n x}{H}\right) \tag{3.14}$$

with $a_n = 2\rho U_\circ H(\cos(\mu\lambda_n) - 1)/\lambda_n^2$ where $\lambda_n = (n + 1/2)\pi$ and the constant a_n is determined by solving boundary conditions with given $\delta P/\delta x$ at $x = 0$, the wall

$$\left.\frac{\delta P}{\delta x}\right|_{x=0} = \sum_{n=1}^{\infty} -a_n\lambda_n \sin(\lambda_n y) = f(x) = \begin{cases} -\rho U_\circ, & -\mu H \le y \le 0 \\ 0, & -H \le y < 0 \end{cases} \tag{3.15}$$

Cooker and Peregrine (1995) had modified the previous model (Cooker & Peregrine, 1991) from using exponential terms to using hyperbolic terms in Fourier series and a new solution was found, as shown in Figure 3.4. But, this change still satisfies Laplace's equation. Thus, the new model solution in Figure 3.4 in the Fourier series can be stated as:

$$P(x,y) = \sum_{n=0}^{\infty} a_n \sin\left(\frac{\lambda_n y}{H}\right) \frac{\sinh\left(\frac{\lambda_n (x-B)}{H}\right)}{\cosh\left(\frac{\lambda_n B}{H}\right)} \qquad 3.16$$

with $a_n = \int_{-\mu H}^{0} (2\rho U_{\circ}/\lambda_n^2)\, sin(\lambda_n y/H) dy$, where $\lambda_n = (n + 1/2)\pi$

The results of pressure impulse on the wall of Cooker's model (1991) are shown in Figure 3.5, Figure 3.6, Figure 3.7 and Figure 3.8. From these results, it can be stated as impact region, μ increases, pressure impulse, P are increasing. It can be seen from peak pressure, p_{pk} from these figures. As we can see, when value of impact region, μ has been increased from 0.1 to 0.5, peak pressure is increasing from 0.057 to 0.290. It can be seen from Figure 3.5 and Figure 3.6. Next, impact region, μ is increase from 0.8 until 1.0. The results from Figure 3.7 and Figure 3.6 show the peak pressure, p_{pk} increase from 0.510 to 0.730. From these figures, Cooker's result shows as, μ increases, pressure impulse, P are increasing.

Cooker's result (1991) can be shown in Table 3.1. The impact region, μ can be related with pressure impulse, P.

Table 3.1 The result of Cooker's model (1991)

Impact Region, μ	**5°**
0.1	0.058
0.5	0.290
0.8	0.510
1.0	0.720

Source: Cooker (1991)

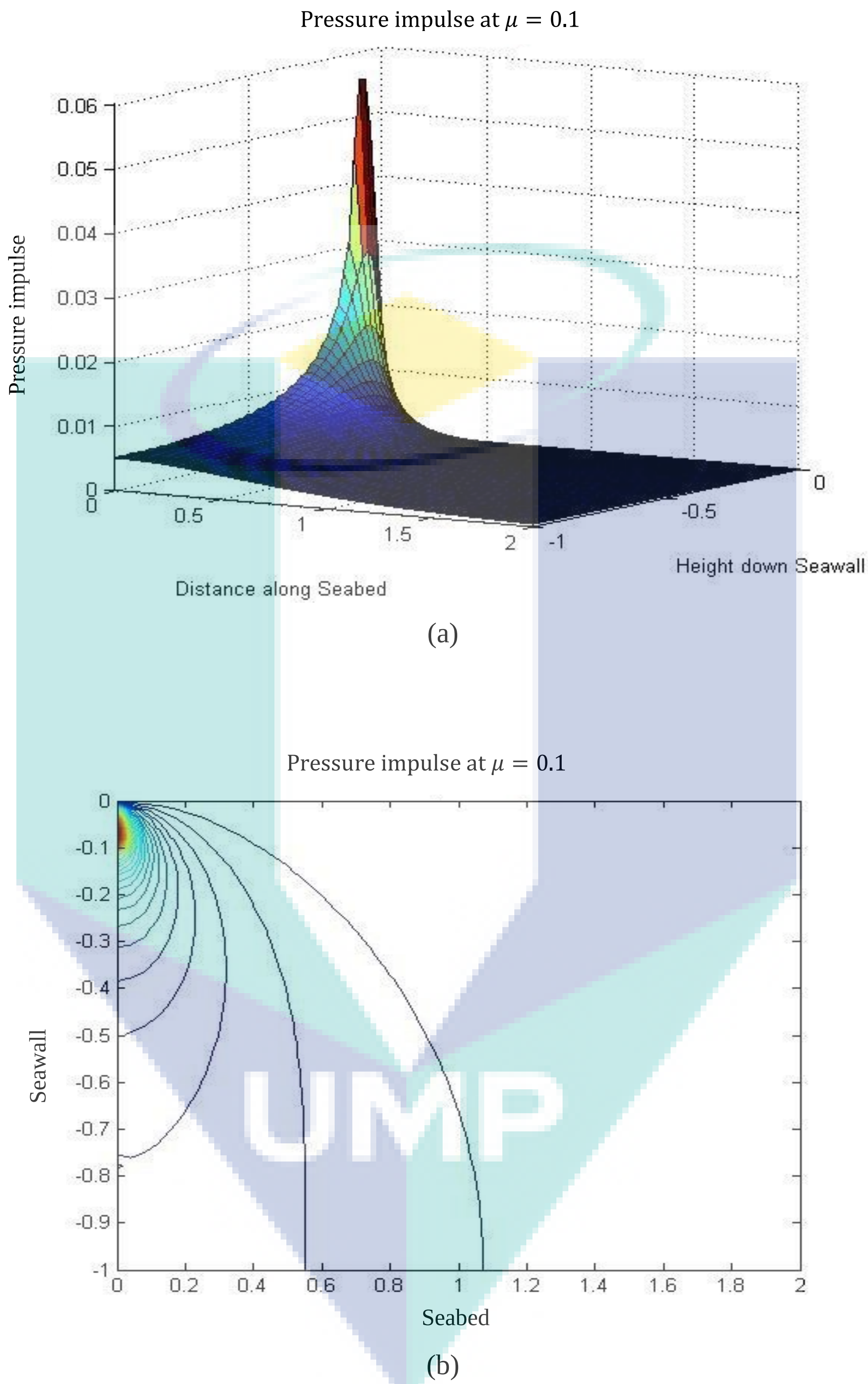

Figure 3.5 3D plot, (a) and contour plot, (b) with $\mu = 0.1$

Pressure impulse at $\mu = 0.5$

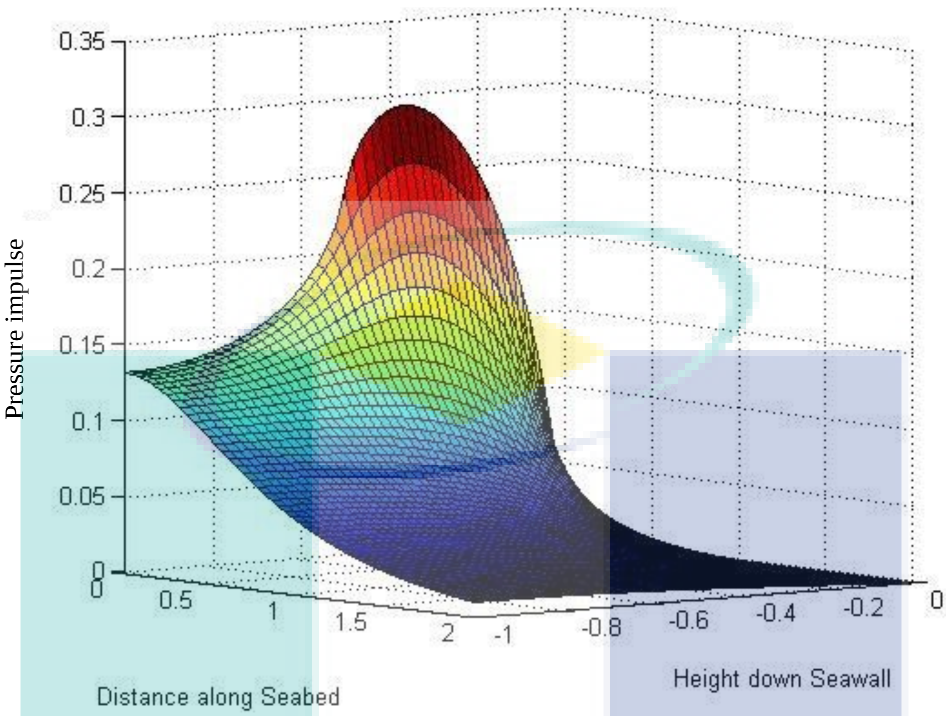

(a)

Pressure impulse at $\mu = 0.5$

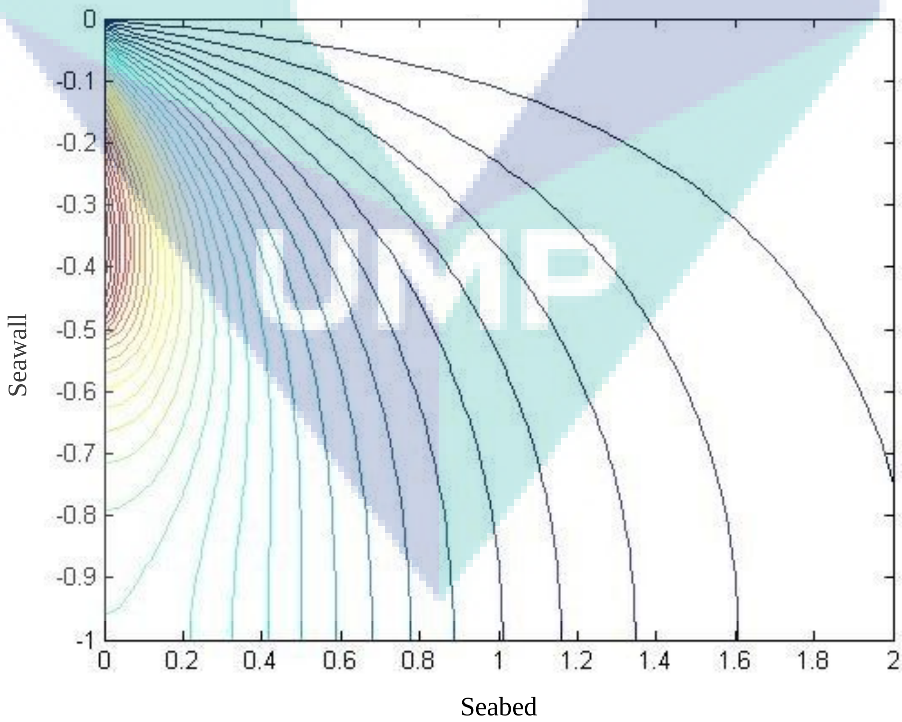

(b)

Figure 3.6 3D plot, (a) and contour plot, (b) with $\mu = 0.5$

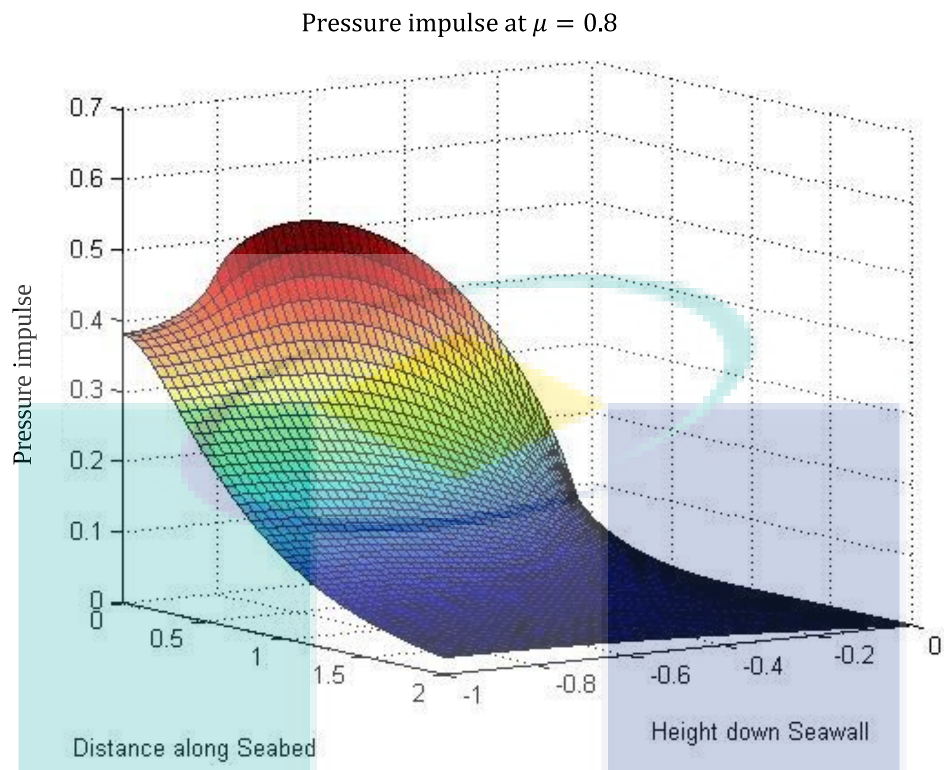

(a)

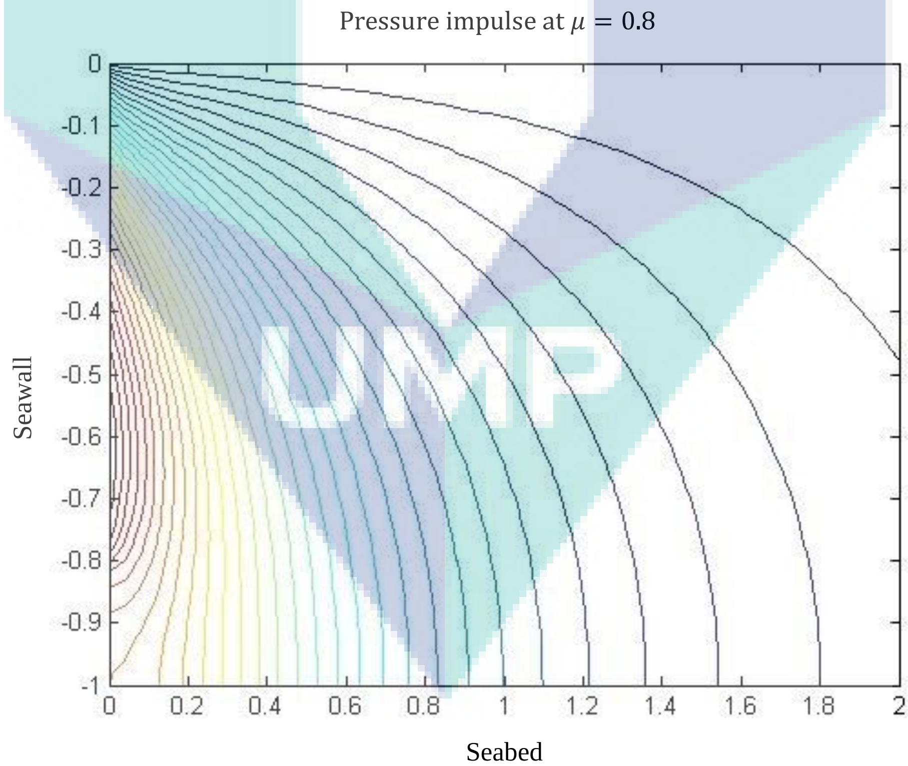

(b)

Figure 3.7 3D plot, (a) and contour plot, (b) with $\mu = 0.8$

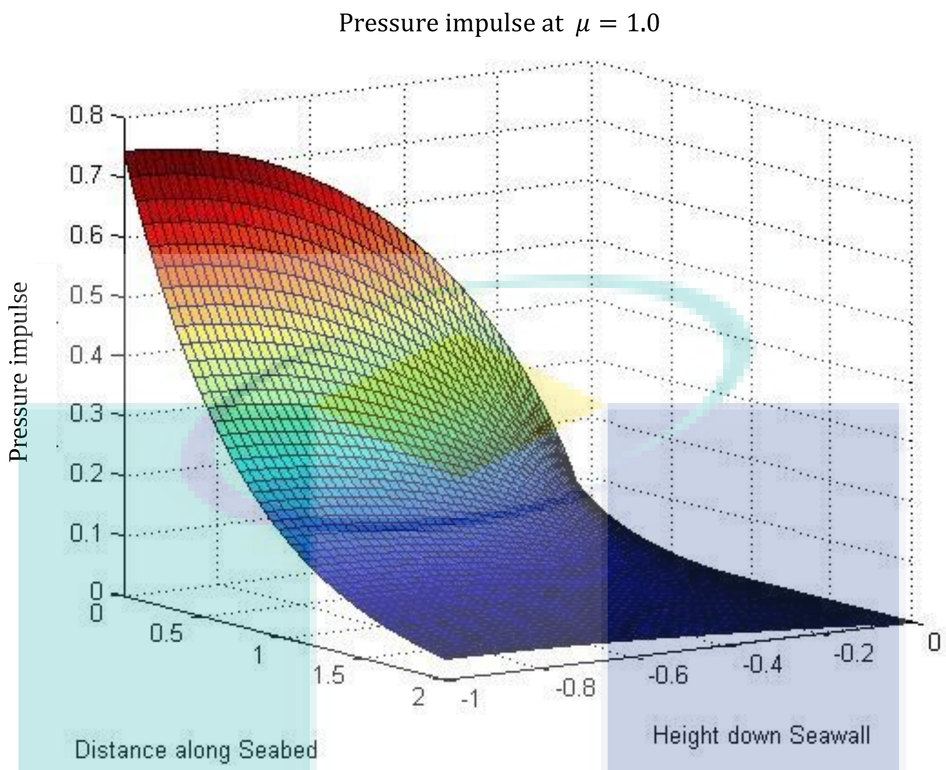

(a)

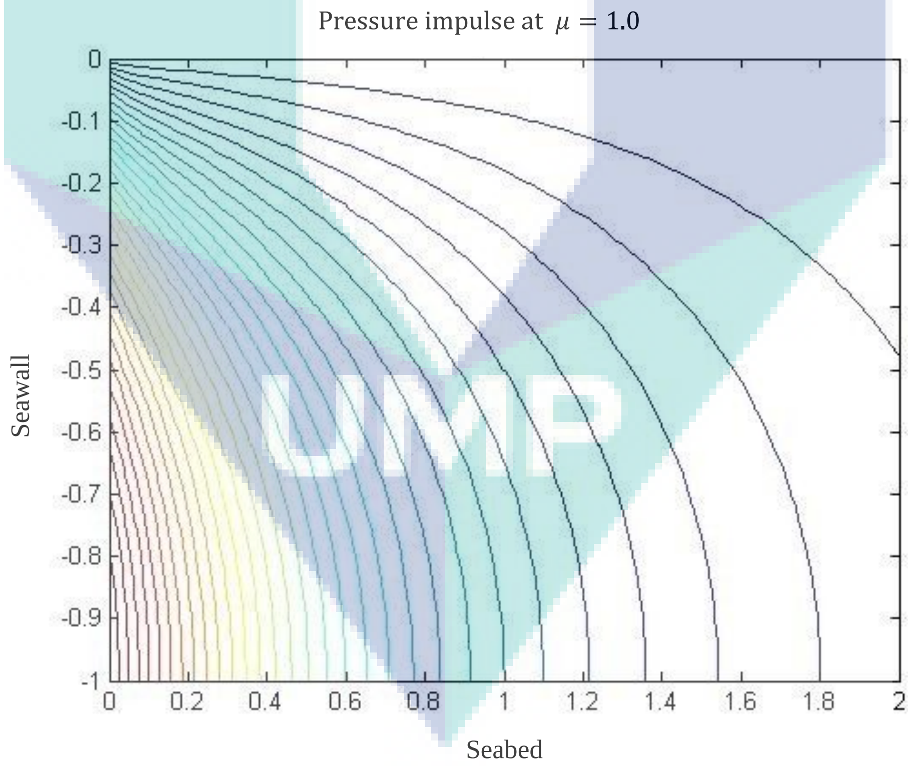

(b)

Figure 3.8 3D plot, (a) and contour plot, (b) with $\mu = 1.0$

3.4 Non-Dimensionalisation

We have non-dimensionalised our calculation for most of the problems in this thesis. By taking Cooker's Model from Figure 3.4 as a concrete illustration, the required boundary conditions in this current problem may be described as a non-dimensionalised by culling incipient non-dimensional factors in view of variables that normally show up in the problem. Prime (') variables indicate non-dimensionalised quantities.

$$x = x'H, \qquad y = y'H, \qquad B = B'H, \qquad P = P'\rho U_{\circ}H \tag{3.17}$$

The corresponding derivatives are variable

$$\delta x = \delta x'H, \qquad \delta y = \delta y'H, \quad \delta P = \delta P'\rho U_{\circ}H \tag{3.18}$$

On the wall, substituting the non-dimensional variable quantity into Equation 3.11 gives

$$\frac{\delta P}{\delta x'H} = -\rho U(y) = -\rho U_{\circ} \tag{3.19}$$

to become

$$\frac{\delta P}{\delta x'} = -\rho U_{\circ}H \tag{3.20}$$

and

$$\frac{\delta P}{\delta x'} = -1 \tag{3.21}$$

The comparative advances are rehashed to other boundary conditions and the solution, as opposed to presenting another notation for all variables. The prime notation is dropped and gives us the dimensionless boundary value problem for pressure impulse. It is illustrated in Figure 3.9.

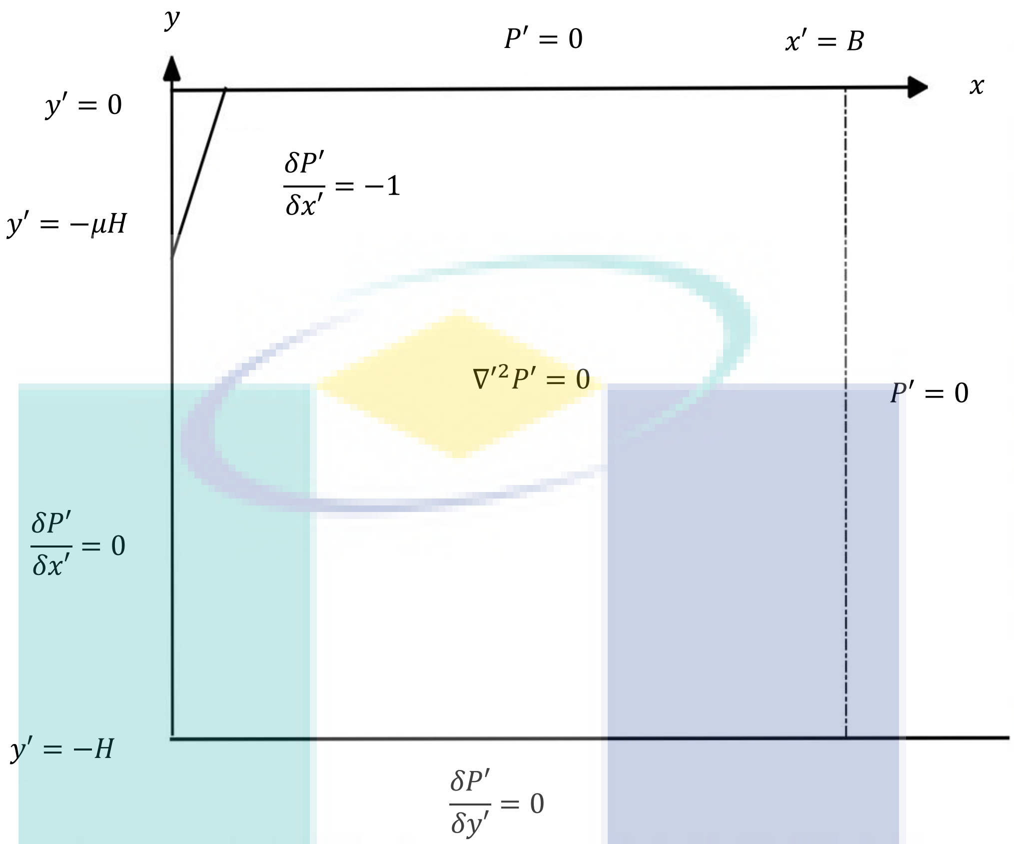

Figure 3.9 The dimensionless boundary value problem for pressure impulse

Subsequently, the Fourier series of dimensionless solution moves toward becoming

$$P(x, y) = \sum_{n=0}^{\infty} a_n \sin(\lambda_n y) \frac{\sinh\big(\lambda_n (x - B)\big)}{\cosh(\lambda_n B)} \qquad 3.22$$

With $a^n = \int (-2/\lambda_n) \sin(\lambda_n y) dy$ where $\lambda_n = (n + 1/2)\pi$

Equation 3.21 then becomes

$$P(x, y{:}\, \mu) = \sum_{n=0}^{\infty} \int \frac{-2}{\lambda_n^2} (1 - \cos(-\mu\lambda_n)) \sin(\lambda_n y) \frac{\sinh(\lambda_n (x - B))}{\cosh(\lambda_n B)} \qquad 3.23$$

The physical parameter can be found in this problem. The quantity unit and dimensions are mentioned in Table 3.1. P can be shown as a dimensionless quantity by

$$P = \int_{t_b}^{t_a} p\,dt = \frac{[T][M][L][T^{-2}]}{L^2} = [M][T^{-1}][L^{-1}] \quad 3.24$$

Furthermore, it has a similar dimension to

$$\rho U_\circ H = [M][L^{-3}][L][T^{-1}][L] = [M][T^{-1}][L^{-1}] \quad 3.25$$

Finally, the scaling pressure for pressure impulse, P is given by

$$P = \frac{P'}{\rho U_\circ H} \quad 3.26$$

Table 3.2 Physical quantities

Physical Quantity	Symbol	SI Unit	Dimensions
Velocity	$U_\circ$	ms^{-1}	$[L][T^{-1}]$
Depth	H	m	$[L]$
Density	ρ	kgm^{-3}	$[M][L^{-3}]$
Area	A	m^2	$[L^2]$
Impact Time	t	s	$[T]$
Force	F	$kgms^{-2}$	$[M][L][T^{-2}]$
Pressure Impulse	P	$kgm^{-1}s^{-1}$	$[M][L^{-1}][T^{-1}]$

3.5 Convergence Test

In order to verify and validate the numerical convergence of the summation in Equation 3.8, we truncate the sums at $n = N$, then examine the effect of varying the value of N on the results. The convergence can be tested numerically or analytically.

To look at the infinite analytically, we will apply the Integral Test to show the series is convergent (Stewart & Bair, 2009). By taking the infinite total of Equation 3.14, the equation will be

$$P(x, y: \mu) = \sum_{n=0}^{\infty} \frac{\cos(\mu\lambda_n) - 1}{\lambda_n^2} \sin\left(\frac{\lambda_n y}{H}\right) exp\left(\frac{-\lambda_n x}{H}\right) \quad 3.27$$

Where $\lambda_n = (n + 1/2)\pi$.

Next, $a^n = \sum_{n=0}^{\infty} (\cos(\mu\lambda_n) - 1/\lambda_n^2) \sin\left(\frac{\lambda_n y}{H}\right) exp\left(\frac{-\lambda_n x}{H}\right)$.

The slowest convergence case happens when $x = 0$, $y = H$ and $\mu = 1.0$. As we can see, the value of N can be set at 100 as there is not much of a difference in the pressure output and position of maximum pressure on the wall for N in a range of values.

From the result illustrated by Table 3.3, an acceptable accuracy can be obtained through the truncation of Fourier series at $N = 10$ until $N = 100$. The percentage of difference for each result is calculated which truncates at $N = 100$ where it is assumed to be convergent. Table 3.2 shows that the Fourier series can be truncated at $N = 50$ because there is only a 0.061% difference compared to $N = 100$. The results indicate an acceptable accuracy at $N = 50$ to $N = 100$.

Table 3.3 Pressure changes for values of N at $y = -0.125$ and $\mu = 1.0$

N	Pressure	% Difference from $N = 100$
10	0.26772	1.520
20	0.26332	0.110
30	0.26327	0.125
40	0.26392	0.120
50	0.26344	0.061
60	03.6361	0.038
70	0.26367	0.030
80	0.26352	0.003
90	0.26365	0.020
100	0.26360	0.000

The convergence of peak pressure is presented numerically at $x = 0$ and $y = -0.125$ by the next graph in Figure 3.10 for different values of N and by using $\mu = 0.1$. It clearly shows the pressure impulse of Cooker's model converging when the value of N is increasing.

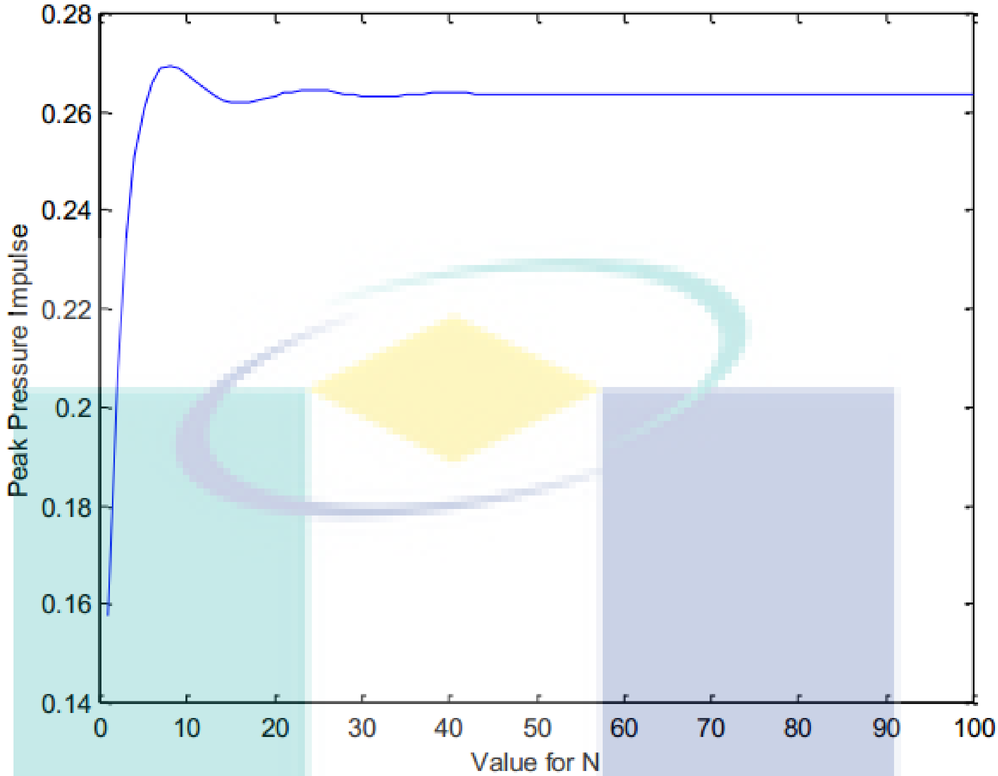

Figure 3.10 Convergence of Cooker's model

CHAPTER 4

MATHEMATICAL MODELLING OF A LANDWARD-INCLINED SEAWALL

4.1 Introduction

A literature study shows that Kirkgöz (1978) set up an experiment of a model of seawall at angles of 0° and 30°. He noticed that the average impact pressure was greater at 30° compared to 0°.

Kirkgöz (1991) investigated the impact pressure of breaking waves on vertical and backward sloping walls by conducting laboratory experiments. He found that the impact pressure on backward and forward sloping walls was higher compared to those on vertical walls. Neelamani and Sandhya (2005) studied the surface roughness effect of vertical and landward-inclined seawalls in incident random wave fields. They found that seawalls at 50° and 60° inclinations received more wave pressure due to the plunging effects compared to vertical walls. Therefore, the purpose of the present chapter is to investigate how a small angle of inclination on vertical structures affect the pressure impulses on the wall by using the pressure-impulse theory. Pressure impulse might increase or decrease when the angle of inclination is increased.

4.2 Mathematical Modelling of a Landward-Inclined Seawall

The model of a landward-inclined seawall is illustrated in Table 4.1. The bottom of the wall is represented by x_w, but the domain is still similar to Cooker's theory. We need to apply the perturbation theory in order to solve this problem. The notation ε represents the angle of the wall from a vertical line in a positive clockwise direction. In this case, it is less than zero making it a negative value.

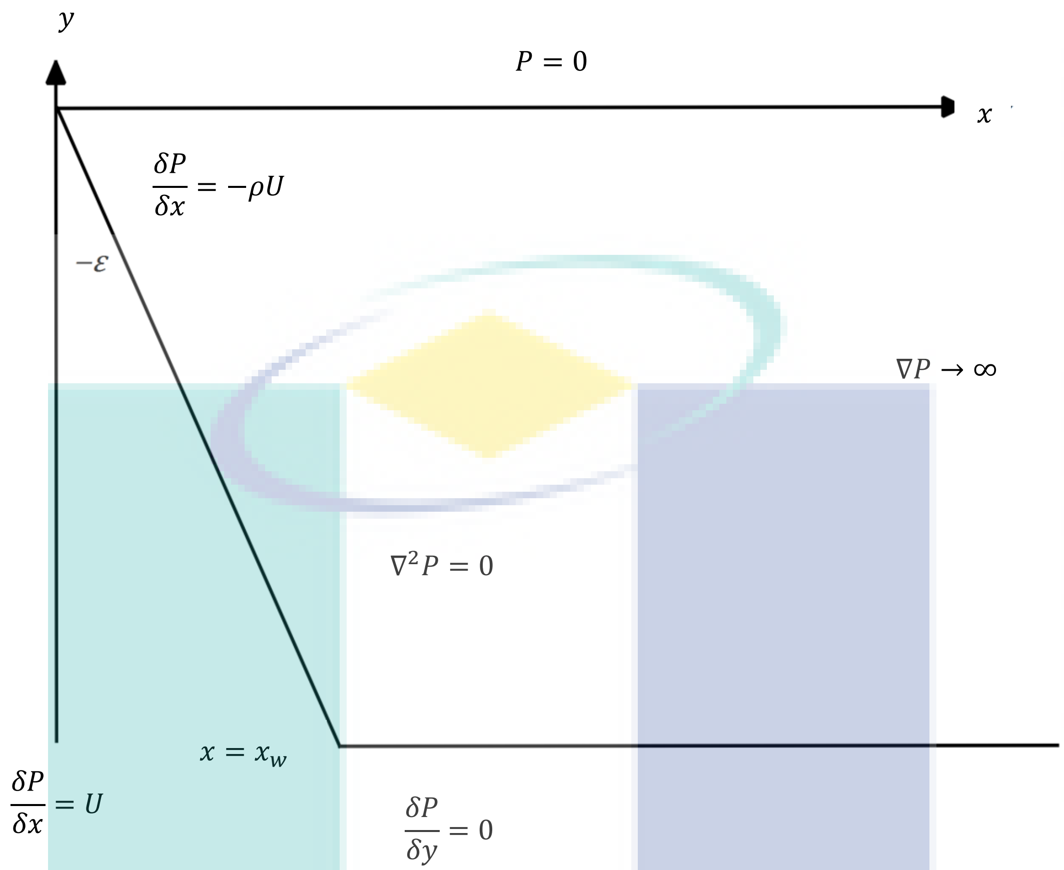

Figure 4.1 Model of a landward-inclined seawall

4.3 Mathematical Formulation of a Landward-Inclined Seawall

Cooker's model in Figure 3.4 is modified. Therefore, we consider a new altered equation from Equation 3.1 as follows

$$P(x, y; \varepsilon) = \sum_{k=0}^{\infty} P^k(x, y)\varepsilon^k \qquad 4.1$$

This problem becomes a series of problems for various types of order of ε, with each new order depending on the previous one. P, ε and k are pressure impulse, angle of a landward-inclined wall and number of terms, respectively.

Each of P^k term is given by:

$$P^k(x, y) = P^k e^{-\lambda_n x} \sin \lambda_n y \qquad 4.2$$

The wall is assumed to be flat. The model can be explained by this triangle where H is the depth and x_w is the bottom of the wall,

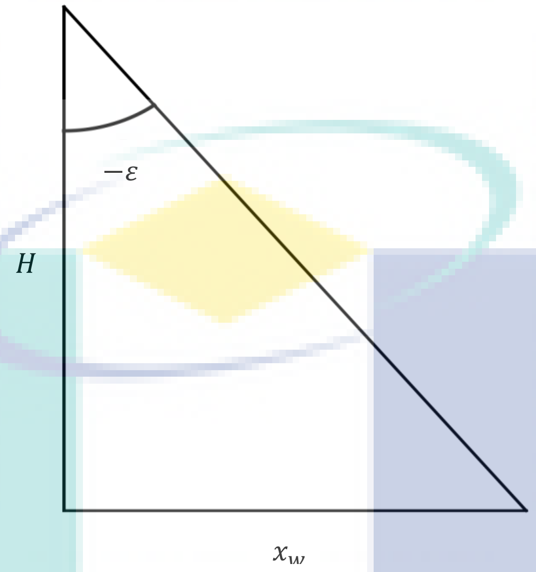

Figure 4.2 Triangle of a model of a landward-inclined seawall

From Table 4.2, the equation of $\tan\varepsilon$ can be described as

$$\tan\varepsilon = \frac{x_w}{H} \qquad 4.3$$

Now, the value of x will be defined as

$$x = \frac{x_w}{H}y = y\tan\varepsilon, \quad -H < y < 0 \qquad 4.4$$

Since the wall is flat, it can be described as in Figure 4.3.

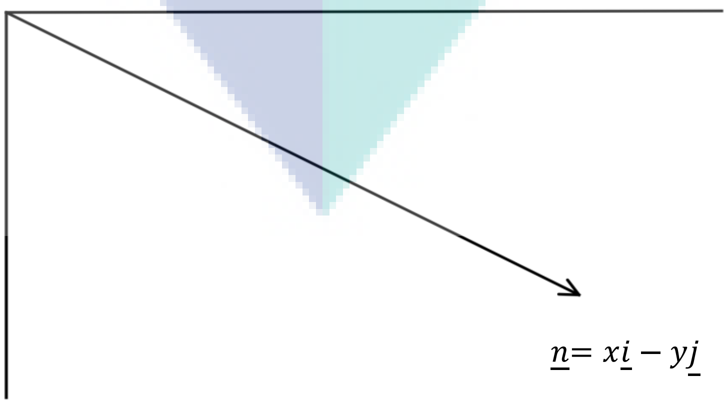

Figure 4.3 Direction of a flat wall

From Figure 4.3, the value of $\underline{n}$ can be defined by

$$\underline{n} = \cos\varepsilon \underline{i} - \sin\varepsilon \underline{j} \tag{4.5}$$

Now, the boundary condition of the wall impacted by the water waves become

$$\frac{\delta P}{\delta n} = \nabla P.n = \cos\varepsilon \frac{\delta P}{\delta x} - \sin\varepsilon \frac{\delta P}{\delta y} = -\rho U_{\circ} \cos\varepsilon \tag{4.6}$$

Therefore, Equation 4.6 will give

$$\frac{\delta P}{\delta n} = -\rho U_{\circ} \cos\varepsilon \tag{4.7}$$

For the region of the seawall in constant contact, the boundary condition is

$$\frac{\delta P}{\delta x} = \tan\varepsilon \frac{\delta P}{\delta y} \tag{4.8}$$

Since $= y \tan\varepsilon$, therefore from Equation 4.4 and $\delta P/\delta n = -\rho U_{\circ} \cos\varepsilon = 0$. The following approximations are given for small ε by using Taylor Series,

$$\tan\varepsilon \approx \varepsilon + \frac{\varepsilon^3}{3} + \cdots \tag{4.9}$$

The perturbation theory applied to this model gives the solution

$$P = \sum_{k=0}^{\infty} P^k \varepsilon^k = P^0 + \varepsilon P^1 + \varepsilon^2 P^2 + \varepsilon^3 P^3 + \cdots \tag{4.10}$$

Equation 4.10 will then be approximated for small ε , and the perturbation solution to the boundary conditions gives

$$P_x^0 + \varepsilon\left(P_x^1 - P_y^0\right) + \varepsilon^2\left(P_x^2 - P_y^1 - \frac{P_x^0}{2}\right) + \varepsilon^3\left(P_x^3 - P_y^2 - \frac{P_x^1}{2} - \frac{P_y^0}{6}\right) + \cdots$$
$$= -\rho U_\circ \cos\varepsilon = -\rho U_\circ \left(1 - \frac{\varepsilon^2}{2}\right) + 0(\varepsilon^4) \qquad 4.11$$

Since $\cos\varepsilon = \left(1 - \frac{1}{2}\varepsilon^2\right)$.

Then, each of the P_x^k and P_y^k terms is expanded by using Taylor Series at $x = 0$, giving

$$P_x^k = P_x^k(0,y) + xP_{xx}^k(0,y) + \frac{x^2}{2}P_{xxx}^k(0,y) + \frac{x^3}{6}P_{xxxx}^k(0,y) + \cdots \qquad 4.12$$

$$P_y^k = P_y^k(0,y) + xP_{yx}^k(0,y) + \frac{x^2}{2}P_{yxx}^k(0,y) + \frac{x^3}{6}P_{xxx}^k(0,y) + \cdots \qquad 4.13$$

Note that, from Equation 4.9, value of $x = y\tan\varepsilon \approx \left(\varepsilon + \frac{1}{3}\varepsilon^3\right)y$

Then, the Taylor Series of Equation 4.12 becomes:

$$P_x^k = P_x^k(0,y) + \varepsilon y P_{xx}^k(0,y) + \frac{\varepsilon^2 y^2}{2}P_{xxx}^k(0,y)$$
$$+\frac{\varepsilon^3}{3}\left(yP_{xx}^k(0,y) + \frac{y^3}{2}P_{xxxx}^k(0,y)\right) + \cdots \qquad 4.14$$

Next, the Taylor Series of Equation 4.13 becomes:

$$P_y^k = P_y^k(0,y) + \varepsilon y P_{yx}^k(0,y) + \frac{\varepsilon^2 y^2}{2}P_{yxx}^k(0,y)$$
$$+\frac{\varepsilon^3}{3}\left(yP_{yx}^k(0,y) + \frac{y^3}{2}P_{yxxx}^k(0,y)\right) + \cdots \qquad 4.15$$

The boundary condition takes the following form, as we neglect $0(\varepsilon^4)$ and greater terms. By substituting Equation 4.14 and Equation 4.15 into Equation 4.11:

$$P_x^0+\varepsilon yP_{xx}^0+\frac{\varepsilon^2y^2}{2}P_{xxx}^0+\frac{\varepsilon^3}{3}\left(yP_{xx}^0+\frac{y^3}{2}P_{xxxx}^k(0,y)\right)+\cdots$$
$$+\varepsilon\left(P_x^1+\varepsilon yP_{xx}^1+\frac{\varepsilon^2y^2}{2}P_{xxx}^1-P_y^0-\varepsilon yP_{yx}^0-\frac{\varepsilon^2y^2}{2}P_{yxx}^0\right)+\cdots$$
$$+\varepsilon^2\left(P_x^2+\varepsilon yP_{xx}^2-P_y^1-\varepsilon yP_{yx}^1-\frac{1}{2}P_x^0-\frac{1}{2}\varepsilon yP_{xx}^0\right)+\cdots$$
$$+\varepsilon^3\left(P_x^3-P_y^2-\frac{1}{2}P_x^1-\frac{1}{6}P_y^0\right)=-\rho U_\circ\left(1-\frac{\varepsilon^2}{2}\right) \quad 4.16$$

The conditions for the boundary condition of the above equation to remain true. It can be found by equating the coefficients of the powers of ε for both sides of Equation 4.16.

Now, we are going to compare each coefficient of ε^0, ε^1, ε^2 and ε^3.

For the solution of ε^0,

$$P_x^0=\begin{cases}0, & -H<y<-\mu H\\ -\rho U_\circ, & -\mu H<y<0\end{cases} \quad 4.17$$

This is similar to Cooker's solution in Equation 3.15.

For the solution of ε^1,

$$P_x^1=P_y^0-yP_{xx}^0 \qquad -H<y<0 \quad 4.18$$

For the solution of ε^2 ,

$$P_x^2=\begin{cases}P_y^1+\dfrac{P_x^0}{2}-y\left(P_{xx}^1-yP_{yx}^0\right)-\dfrac{y^2P_{xxx}^0}{2}, & -H<y<-\mu H\\ P_y^1+\dfrac{P_x^0}{2}-y\left(P_{xx}^1-yP_{yx}^0\right)-\dfrac{y^2P_{xxx}^0}{2}+\rho U_\circ, & -\mu H<y<0\end{cases} \quad 4.19$$

For the solution of ε^3,

$$P_x^3-\frac{P_x^1}{2}-\frac{P_y^0}{6}-y\left(P_{xx}^2-P_{yx}^1-\frac{P_{xx}^0}{6}\right)$$
$$-\frac{y^2}{2}\left(P_{xxx}^1-P_{yxx}^0\right)-\frac{y^3P_{xxxx}^0}{6}, \qquad -H<y<0 \quad 4.20$$

Next, the first order solution, $O(\varepsilon^1)$ is going to be solved. The nth term of P_n^k can be separated on the left hand side by multiplying each condition by $\sin\left(\frac{\lambda_n y}{H}\right)$ and then it is integrated over$(-H, 0)$. This can be solved by applying the orthogonality of $\left(\sin\left(\frac{\lambda_n y}{H}\right), n \in N\right)$. But, since the orthogonality does not always apply to the right hand side, it will be left with an infinite sum. Hence, each P_n^{k-1} and P_n^{k-2} are defined. Then, these coefficients are determined by integral of products from the set $\left(\sin\left(\frac{\lambda_n y}{H}\right), \cos\left(\frac{\lambda_n y}{H}\right), y^n, n \in N\right)$. In order to find the first order solutions of ε^1, Equation 4.18 is multiplied by $\sin(\lambda_n y)$ and then it is integrated over $(-H, 0)$. It gives:

$$\int_{-H}^{0} P_x^1 \sin\left(\frac{\lambda_n y}{H}\right) dy = \int_{-H}^{0} \left(P_y^0 - yP_{xx}^0\right) \sin\left(\frac{\lambda_n y}{H}\right) dy \qquad 4.21$$

Then, the derivatives in Equation 4.21 can be calculated,

$$P_x^1(0, y) = -\sum_{n=0}^{\infty} \lambda_n P_n^1 \sin\left(\frac{\lambda_n y}{H}\right) \qquad 4.22$$

$$P_y^0(0, y) = \sum_{n=0}^{\infty} \lambda_n P_n^1 \cos\left(\frac{\lambda_n y}{H}\right) \qquad 4.23$$

$$P_{xx}^0(0, y) = -\sum_{n=0}^{\infty} \lambda_n^2 P_n^0 \sin\left(\frac{\lambda_n y}{H}\right) \qquad 4.24$$

Next, we substitute Equation 4.22, Equation 4.23 and Equation 4.24 into Equation 4.21 which leads to the following approximation for the first order solution:

$$P(x, y) = P^0(x, y) + \varepsilon P^1(x, y) \qquad 4.25$$

By substituting the Equation 4.25,

$$P(x, y) = \sum_{n=0}^{\infty} P_n^0 e^{-\lambda_n x} \sin\left(\frac{\lambda_n y}{H}\right) + \varepsilon \sum_{n=0}^{\infty} P_n^1 e^{-\lambda_n x} \sin\left(\frac{\lambda_n y}{H}\right) P^1(x, y) \qquad 4.26$$

$$P(x,y) = \sum_{n=0}^{\infty} (P_n^0 + P_n^1) e^{-\lambda_n x} \sin\left(\frac{\lambda_n y}{H}\right) \qquad 4.27$$

$$P(x,y) \approx \sum_{n=0}^{N} (P_n^0 + P_n^1) e^{-\lambda_n x} \, sin\left(\frac{\lambda_n y}{H}\right) \qquad 4.28$$

The second order solution, $O(\varepsilon^2)$ is going to be solved. A solution of $P^2(x,y)$ will be found by using a similar method to $P^1(x,y)$. Equation 4.19 will be multiplied by $\sin(\lambda_n y)$ and integrated over $(-H, 0)$. Hence, it will give:

$$\int_{-H}^{0} P_x^2 \sin\left(\frac{\lambda_n y}{H}\right) dy = \int_{-H}^{0} \left(P_y^1 - y\left(P_{xx}^1 - P_{yx}^0\right) - \frac{y^2}{2} P_{xxx}^0\right) \sin\left(\frac{\lambda_n y}{H}\right) dy \qquad 4.29$$

Calculating the relevant derivatives and substituting them into Equation 4.19 leads to the following approximation for the second term, $P^2(x,y)$ and therefore the second order solution is

$$P(x,y) = P^0(x,y) + \varepsilon P^1(x,y) + \varepsilon^2 P^1(x,y) \qquad 4.30$$

Finally it can be approximated as,

$$P(x,y) = \sum_{n=0}^{\infty} (P_n^0 + \varepsilon P_n^1 + \varepsilon^2 P_n^2) \, e^{-\lambda_n x} \, sin\left(\frac{\lambda_n y}{H}\right) \qquad 4.31$$

$$P(x,y) \approx \sum_{n=0}^{N} (P_n^0 + \varepsilon P_n^1 + \varepsilon^2 P_n^2) \, e^{-\lambda_n x} \, sin\left(\frac{\lambda_n y}{H}\right) \qquad 4.32$$

4.4 Result and Discussion of Landward-Inclined Seawall

The results of our mathematical model will be discussed in this section. The results of our study will also be confirmed and verified to ensure our study, method and calculation are accurate and correct. This is done by comparing our results with Cooker's results from 1991 and 1995. In addition, some previous studies related to our research will be included in this chapter. We will then discuss the relevance and compare the results. The results will be represented by diagrams, figures or tables and will be analysed.

4.5 Validation of Result for Landward-Inclined Seawall

Table 4.1 shows the comparison of pressure impulse from Cooker's model (1991) and a landward-inclined wall's model. It can be seen from the results that the values of the pressure impulse from Cooker's model (1991) and landward-inclined wall's model are exactly equivalent. Although the value of impact region, μ is varied, we still get the same result. We can therefore validate that our method is correct since we found a good agreement with Cooker's results.

Table 4.1 Comparison of Cooker's model and a landward-inclined wall model

Impact Region, μ	Cooker's Model	Landward-inclined Model
0.1	0.058	0.058
0.5	0.290	0.290
0.8	0.510	0.510
1.0	0.720	0.720

Source: Cooker (1991)

Figure 4.4, Figure 4.5, Figure 4.6 and Figure 4.7 show that the values of peak pressure from Cooker's model and landward-inclined wall's model are equivalent. When comparing a landward-inclined wall's model at angle $\varepsilon = 0°$ with Cooker's model at the value of impact region, μ when $\mu = 0.1$, $\mu = 0.5$, $\mu = 0.8$ and $\mu = 1.0$, we can see that although we increased the value of μ, a landward-inclined wall's model still gives consistent results which are equivalent to Cooker's results.

When we tested at $\mu = 0.1$ until $\mu = 1.0$, the pressure impulse keeps increasing similar to Cooker's model (1991). Therefore, the results obtained from a landward-inclined wall's model are still similar to Cooker's results (1991).

Hence, we can conclude that even though the value of μ always varies, the results obtained are consistent following Cooker's model (1991). Therefore, a landward-inclined wall's model is said to be correctly verified by this comparison. Our method previously can also be verified.

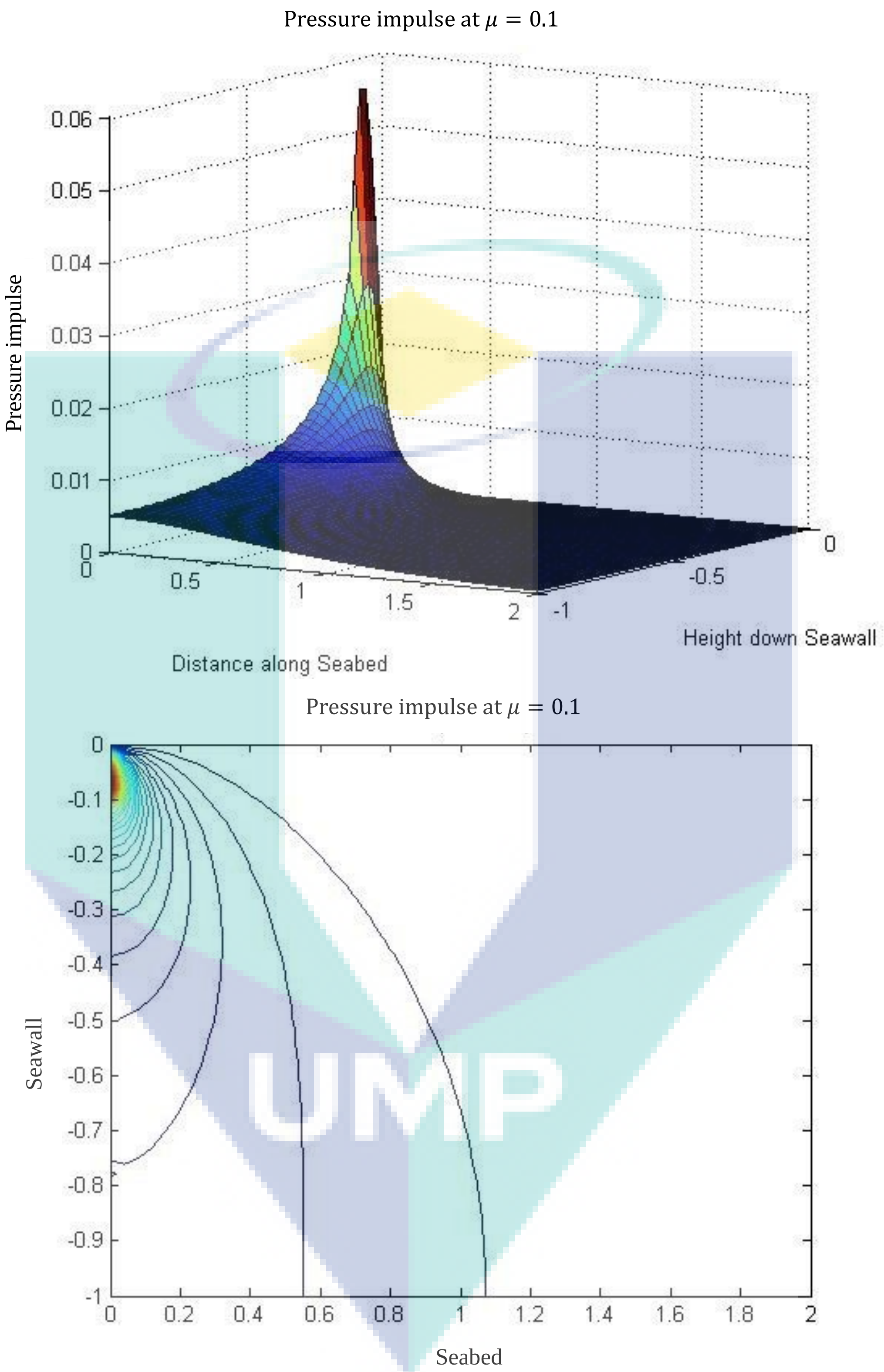

(a)

Figure 4.4 Comparison between Cooker's model, (a) and landward-inclined model at 0°, (b) when $\mu = 0.1$

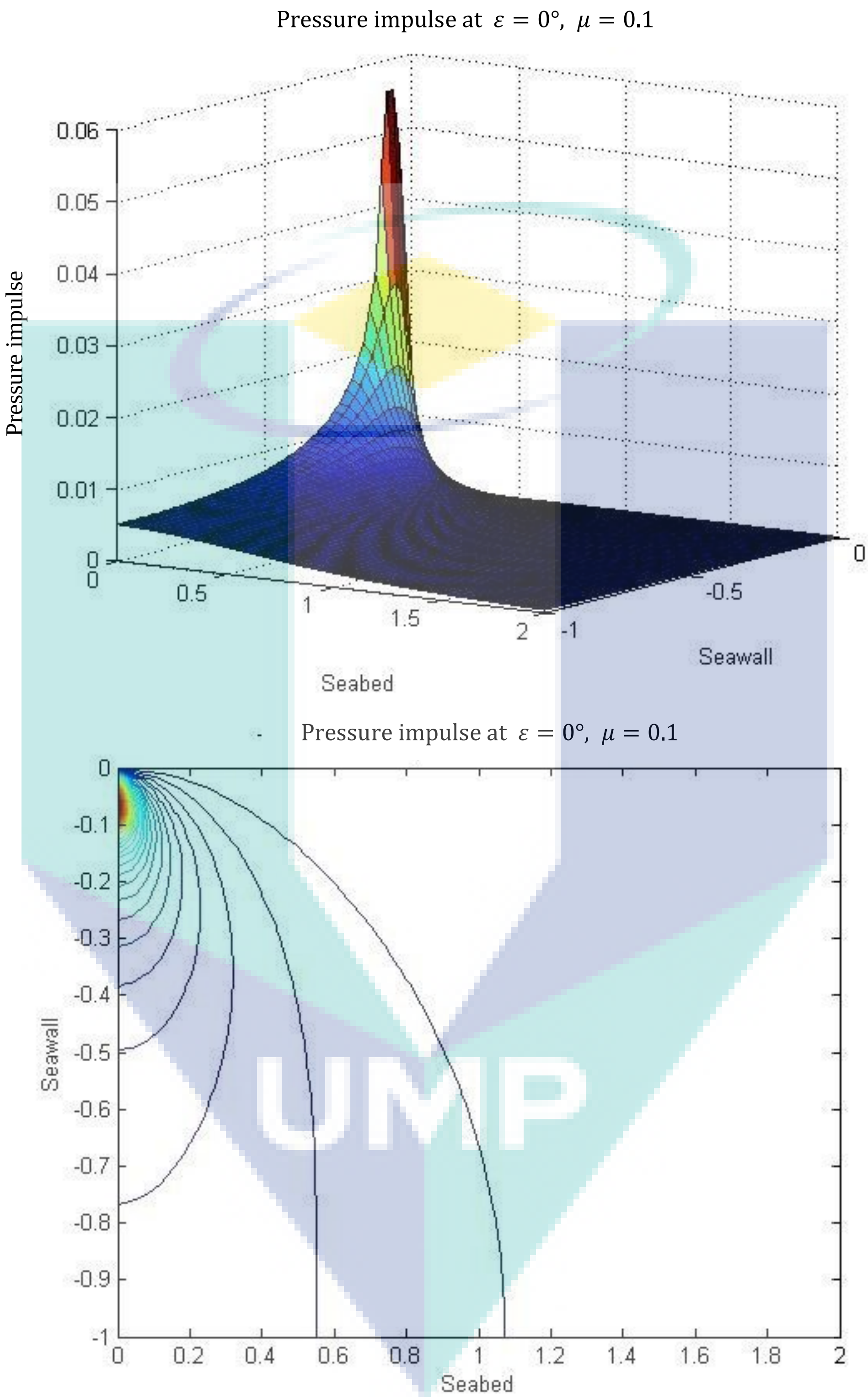

(b)

Figure 4.4 Continued

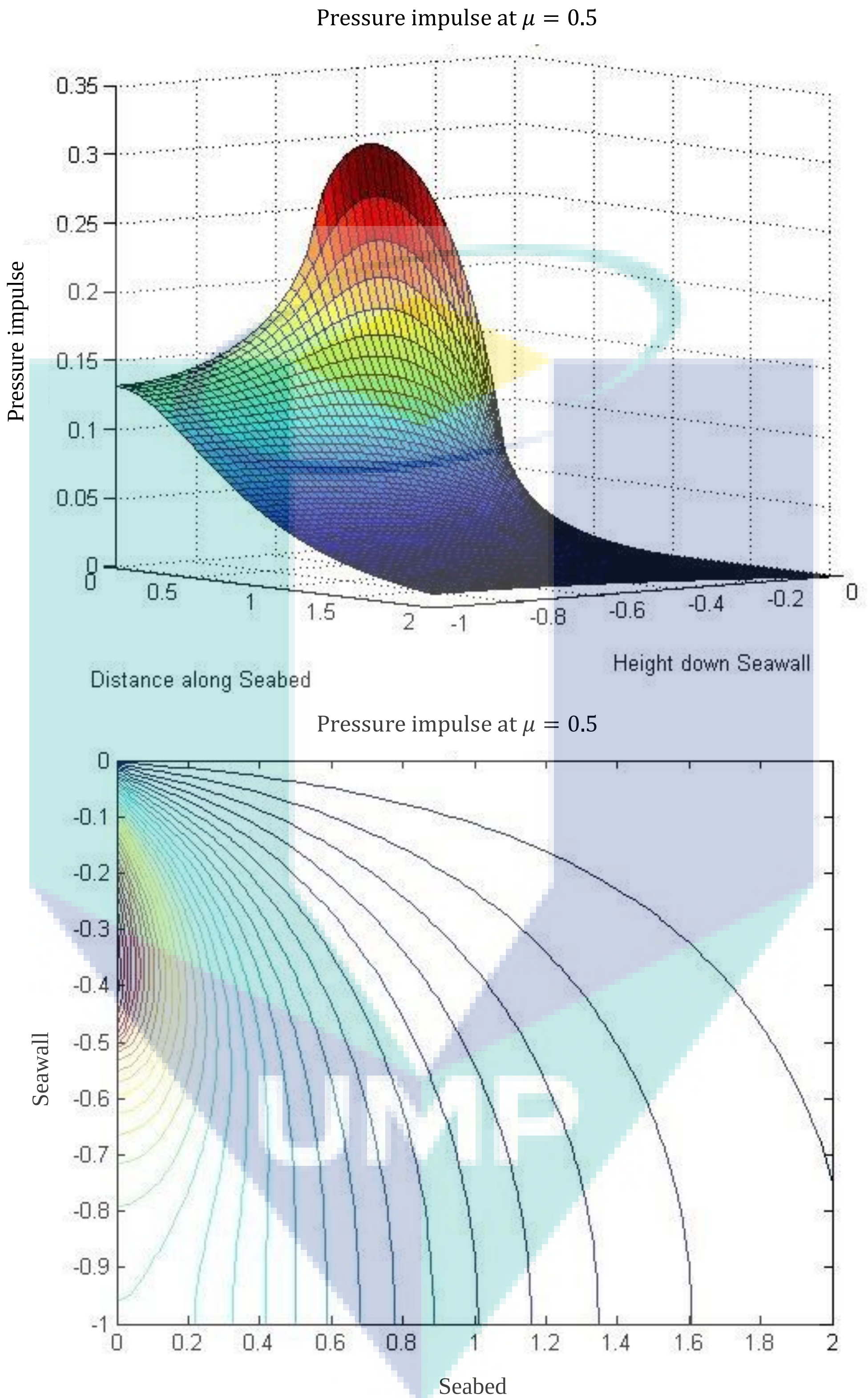

(a)

Figure 4.5 Comparison between Cooker's model, (a) and landward-inclined model at 0°, (b) when $\mu = 0.5$

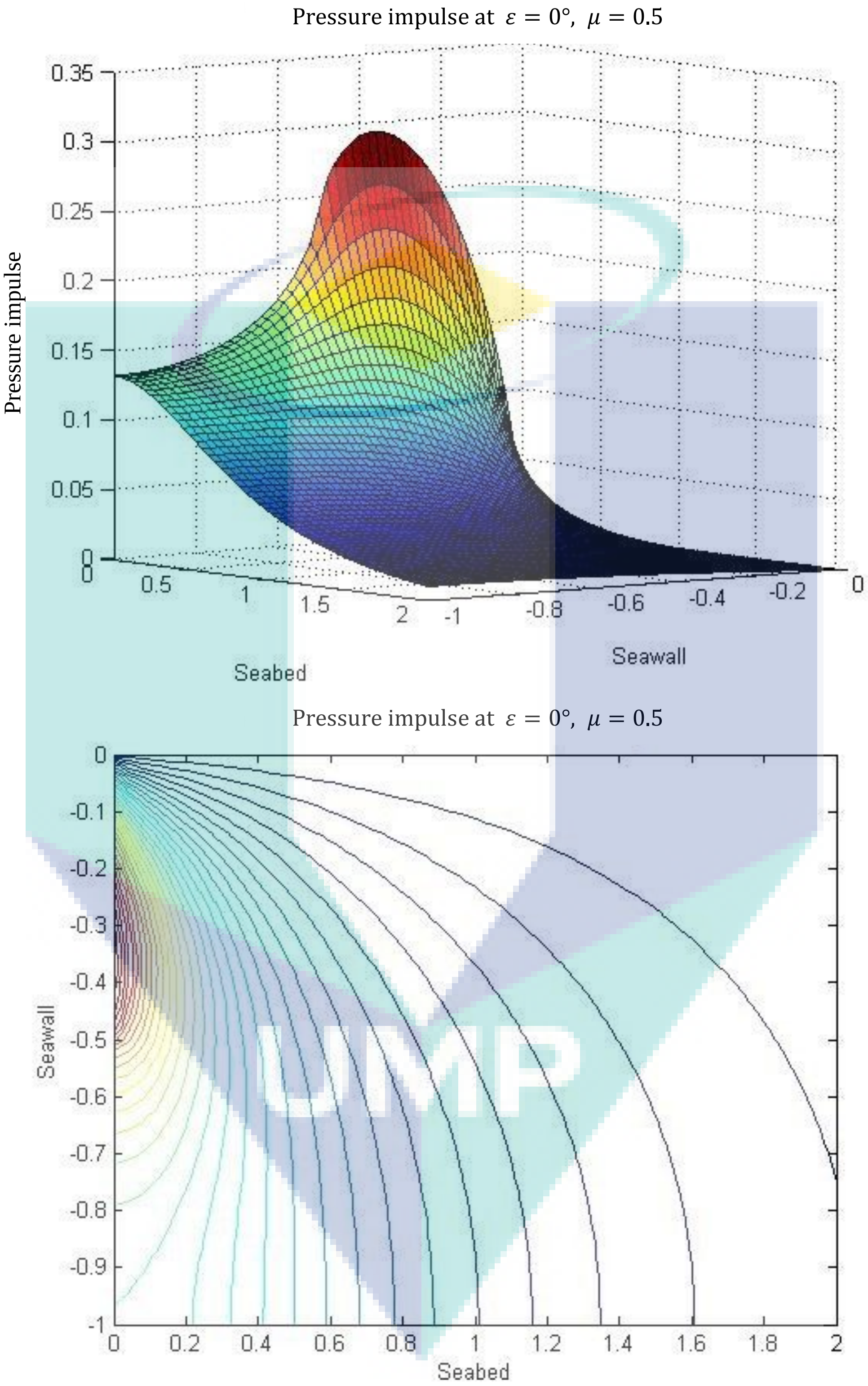

(b)

Figure 4.5 Continued

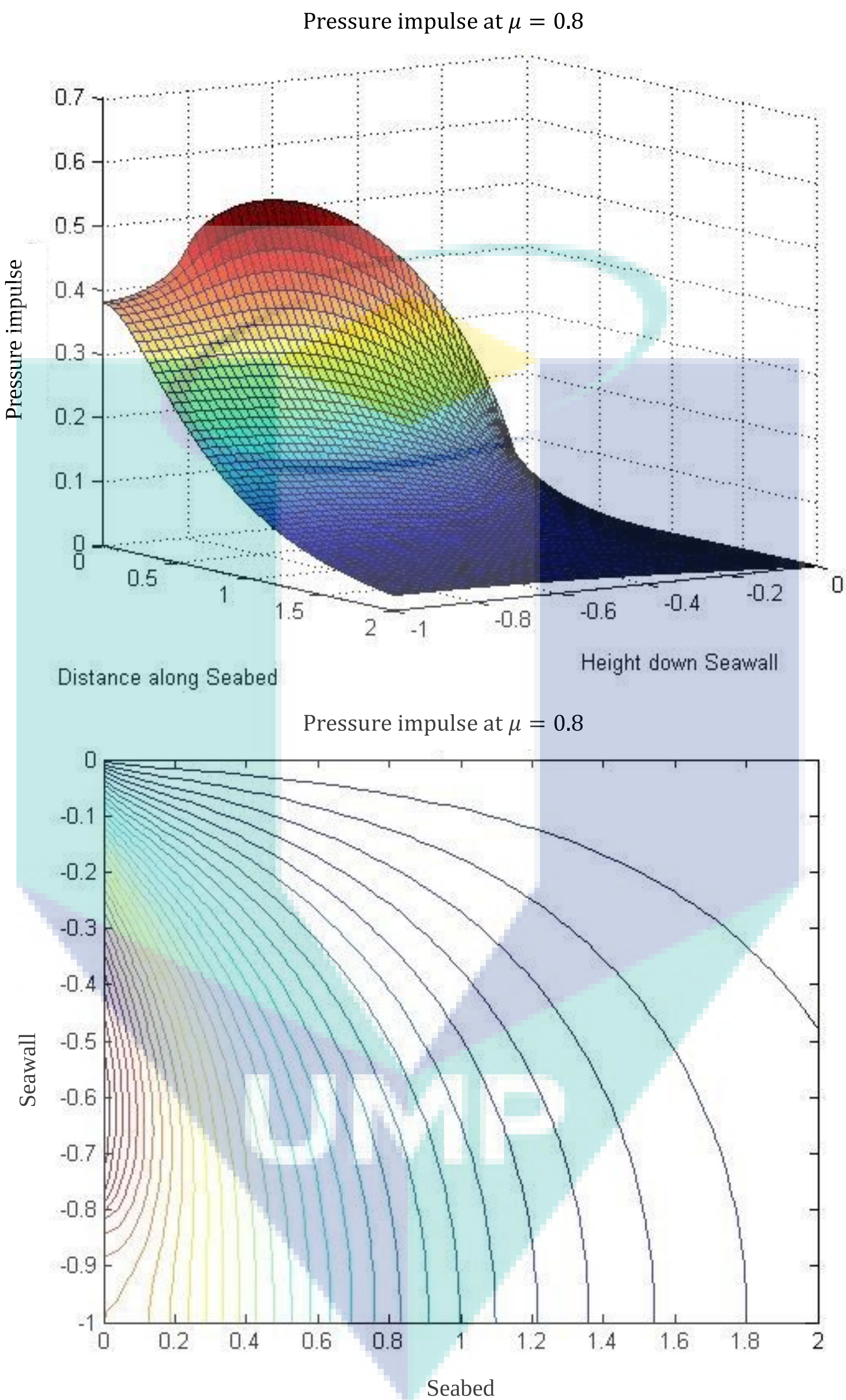

(a)

Figure 4.6 Comparison between Cooker's model, (a) and landward-inclined model at 0°, (b) when $\mu = 0.8$

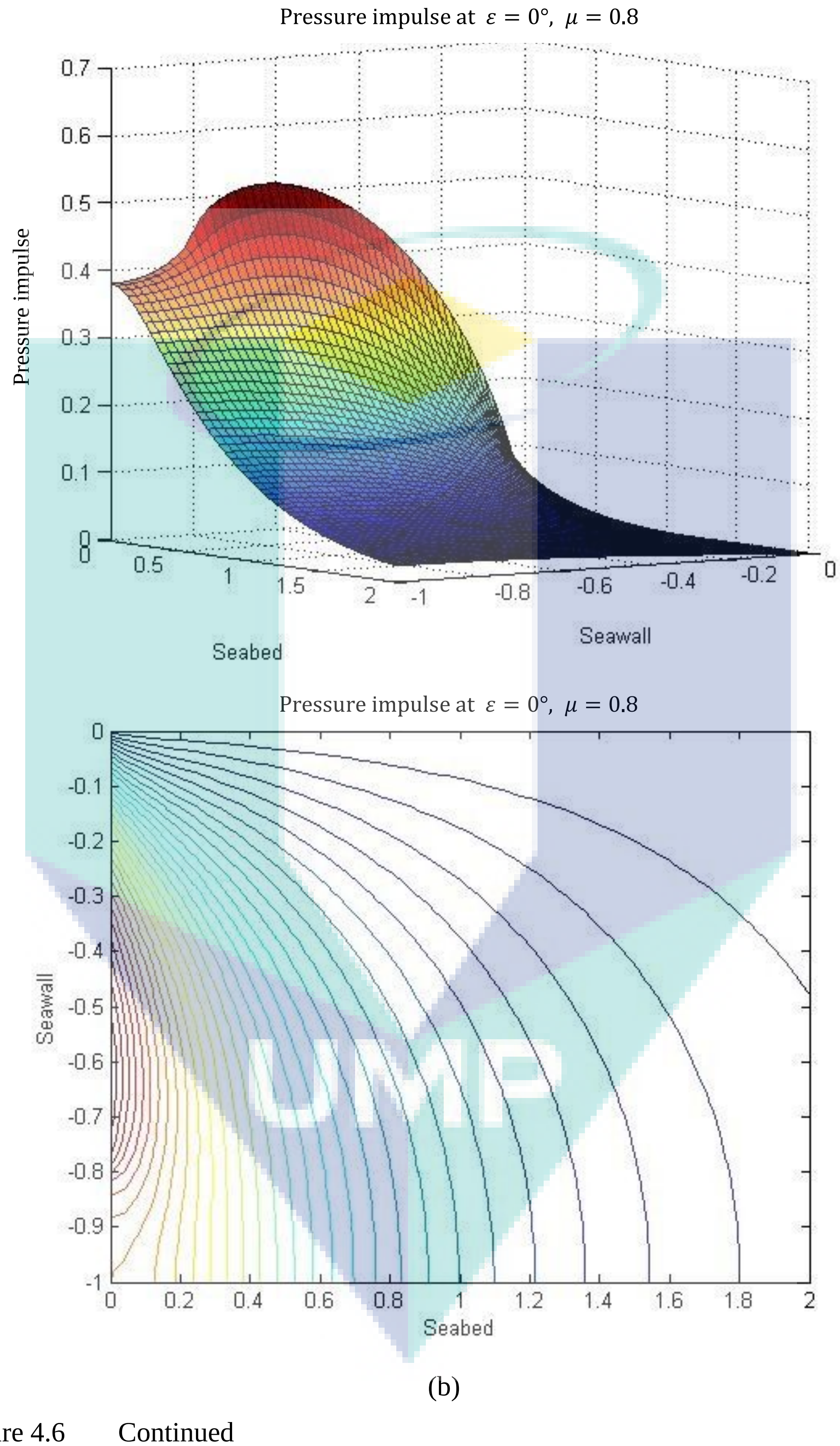

(b)

Figure 4.6 Continued

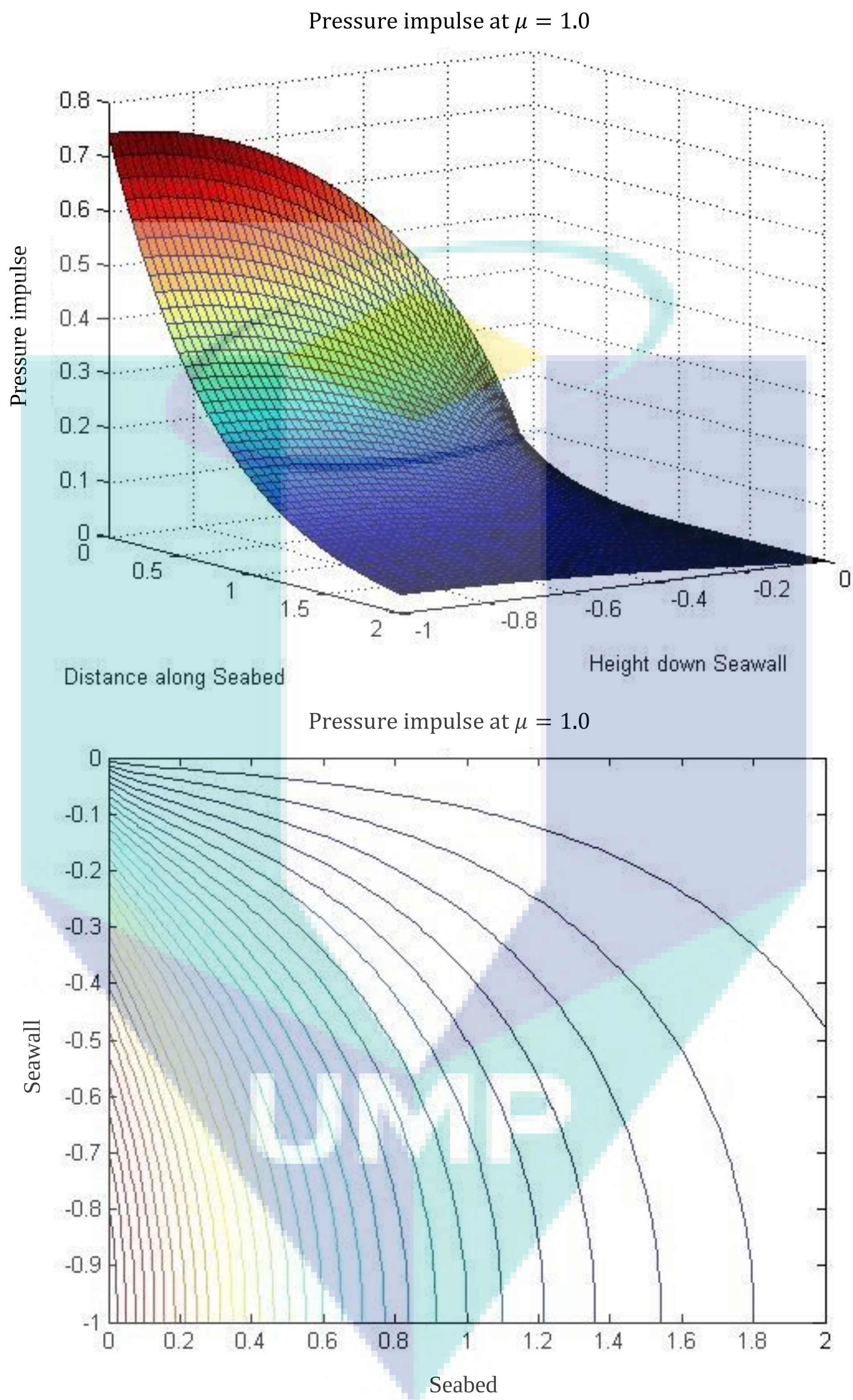

(a)

Figure 4.7 Comparison between Cooker's model, (a) and landward-inclined model at 0°, (b) when $\mu = 1.0$

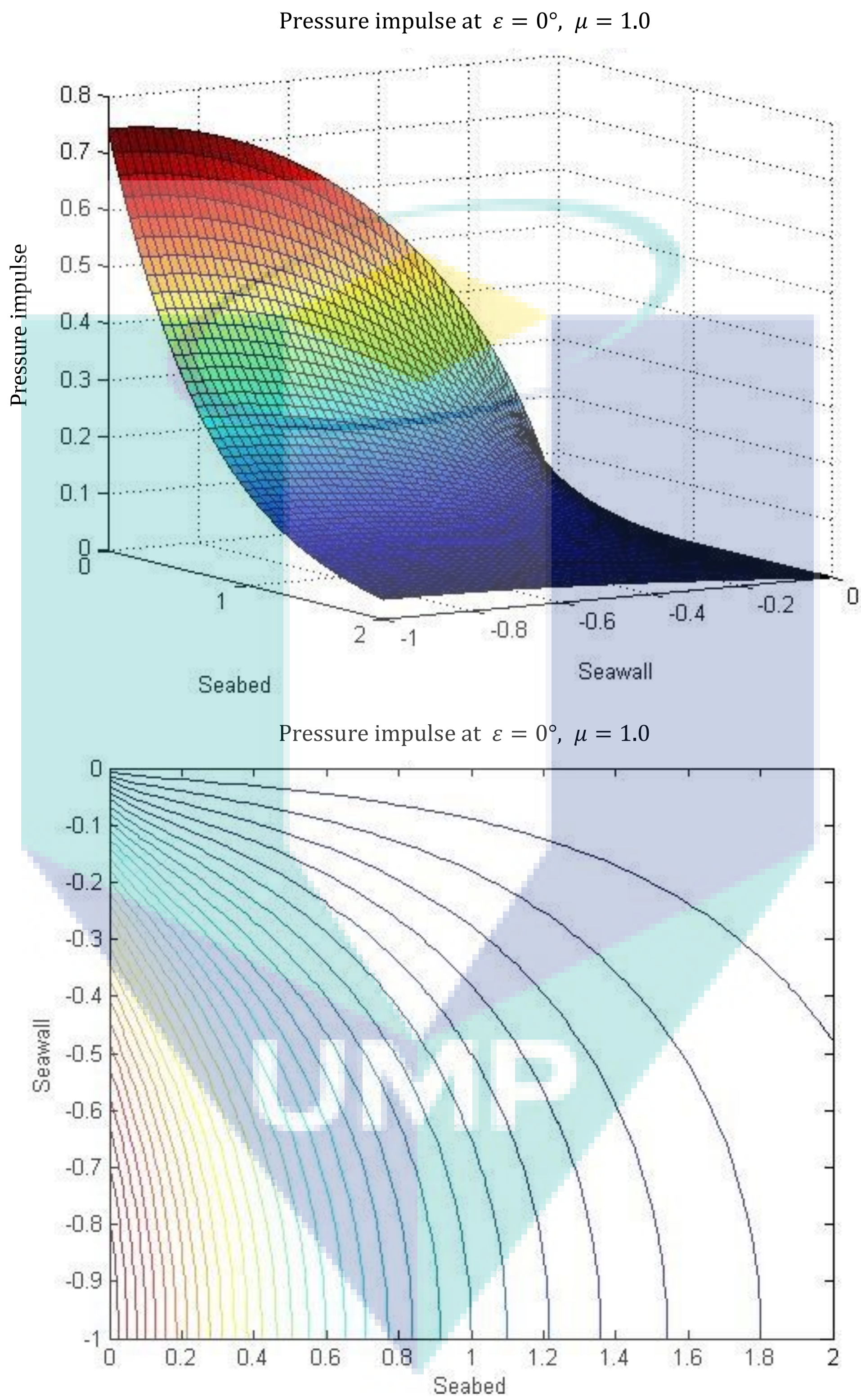

(b)

Figure 4.7 Continued

4.6 The Effect of Varying Impact Zone towards Pressure Impulse

We will discuss how varying the impact zone, μ will affect the pressure impulse. We only tested at an angle of inclination for the seawall, $\varepsilon = 5°$ at different values of μ. Table 4.2 shows the effect of varying the impact region, μ at the angle of 5°.

Table 4.2 The effect of varying impact region at angle of 5°

Impact Region, μ	**5°**
0.1	0.068
0.5	0.310
0.8	0.530
1.0	0.790

From Figure 4.8, Figure 4.9, Figure 4.10 and Figure 4.11 below, we can see that the value of peak pressure will vary as we vary the value of μ. We are testing the value of impact region, μ when $= 0.1$, $\mu = 0.5$, $\mu = 0.8$ and $\mu = 1.0$ for the angle of $\varepsilon = 5°$.

As we can see, pressure impulse increased by 0.242 when we increased the value of impact region, μ from 0.1 to 0.5. After we increased the value of impact region, μ from 0.5 to 0.8, pressure impulse increased by 0.220. When the value of impact region, μ was increased again from 0.8 to 1.0, pressure impulse also increased by 0.260.

We can therefore conclude that if the value of impact region, μ increases, the value of pressure impulse also increases.

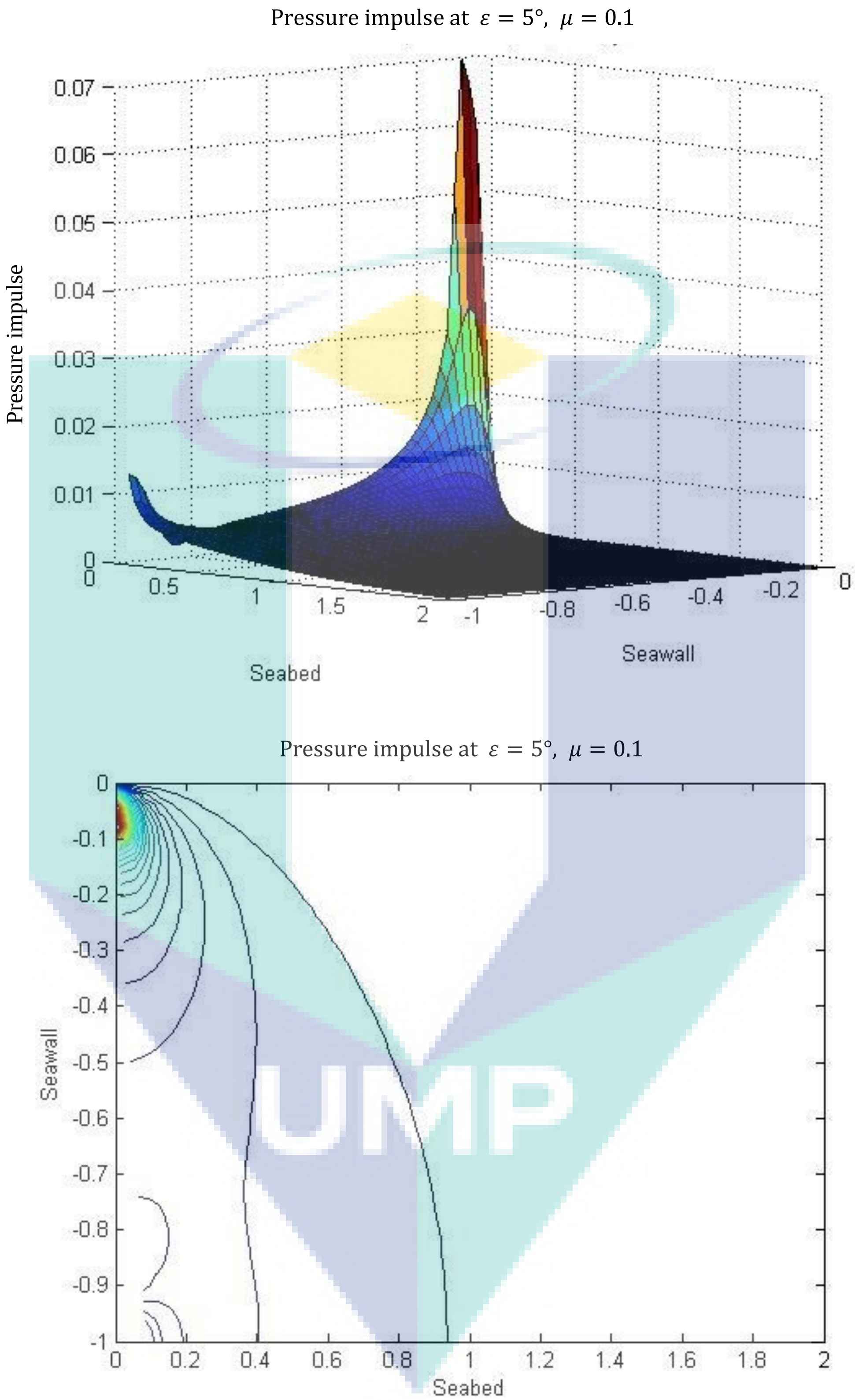

Figure 4.8 The effect of varying impact region, $\mu = 0.1$ at angle of $5°$

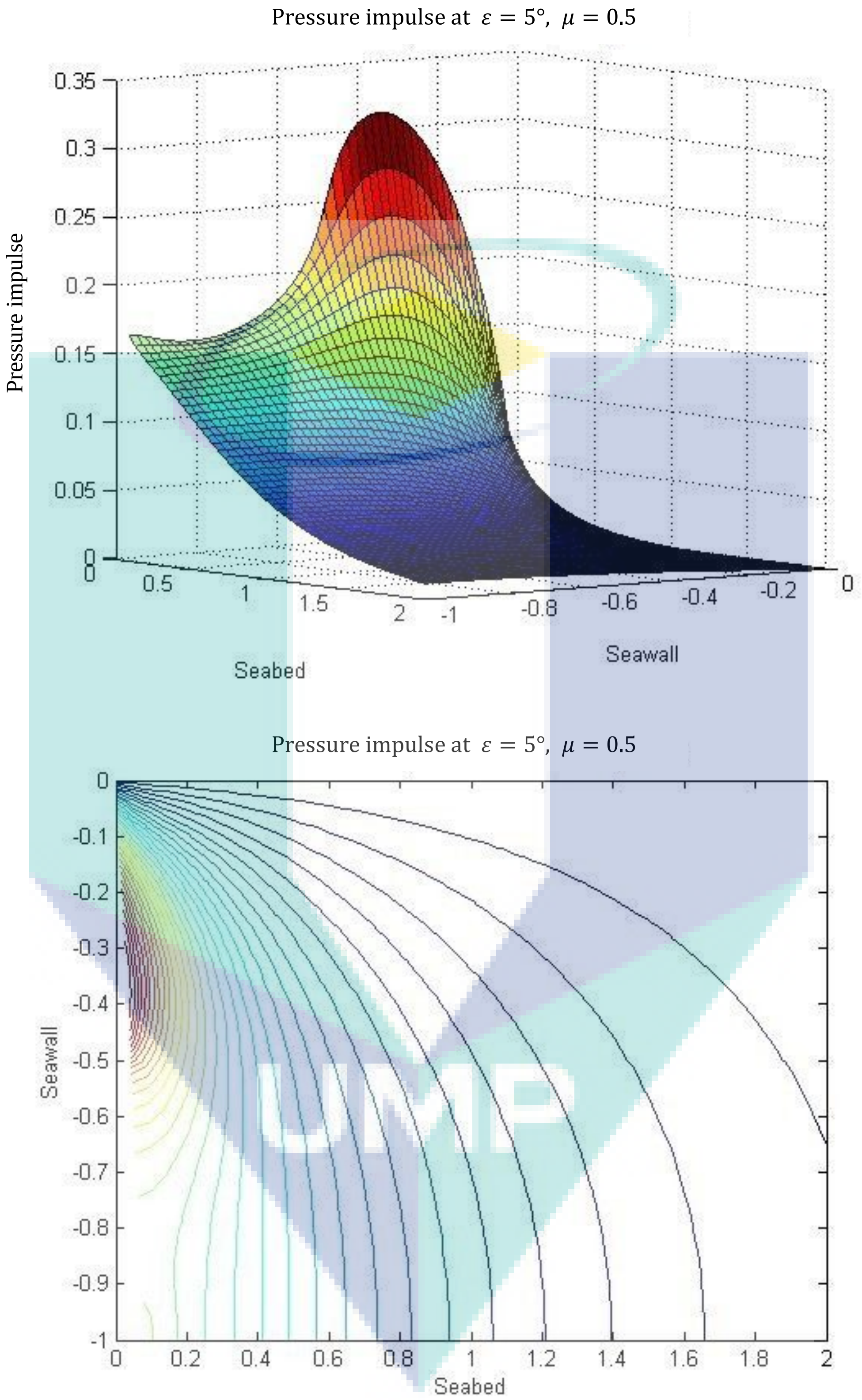

Figure 4.9 The effect of varying impact region, $\mu = 0.5$ at angle of 5°

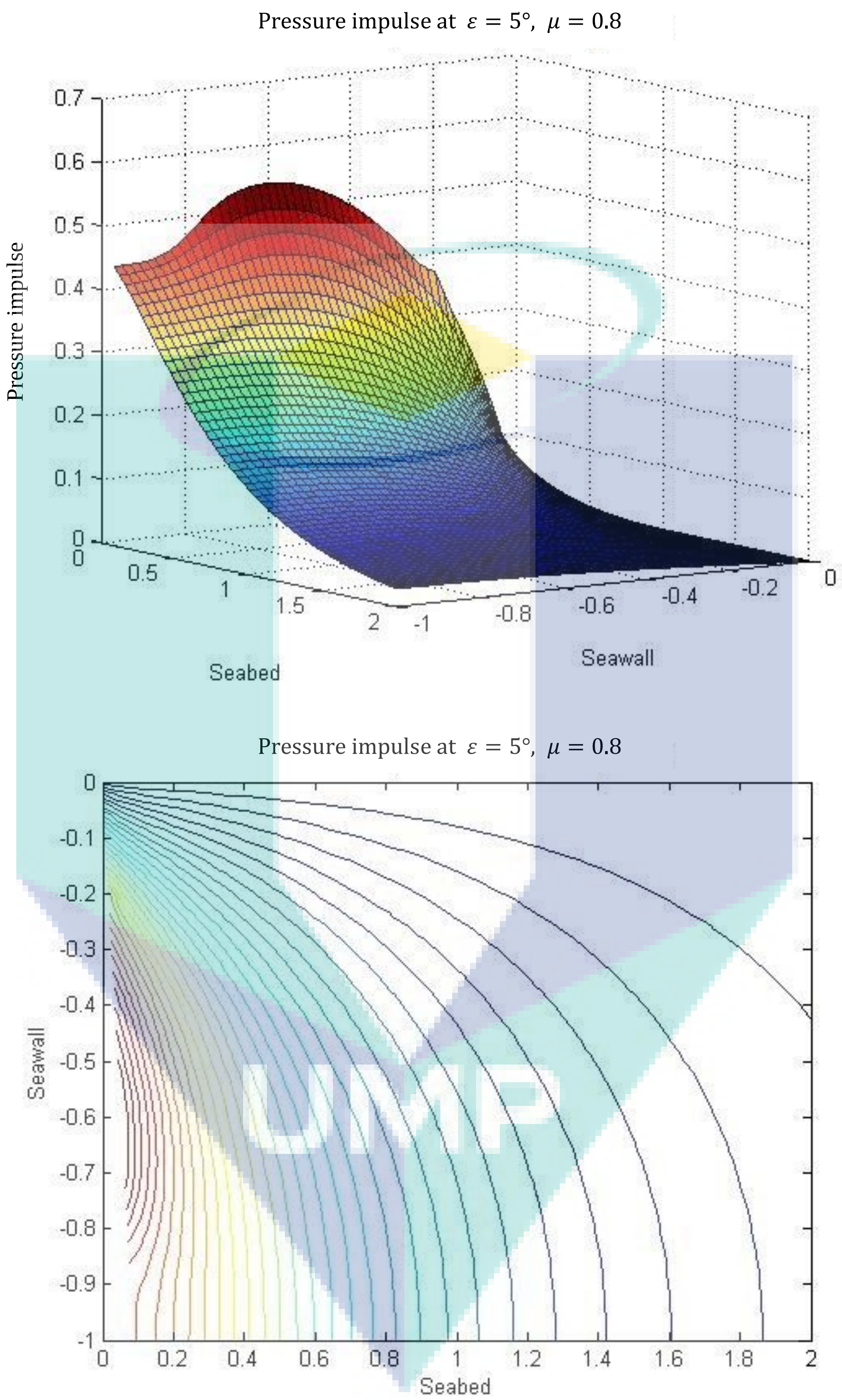

Figure 4.10 The effect of varying impact region, $\mu = 0.8$ at angle of 5°

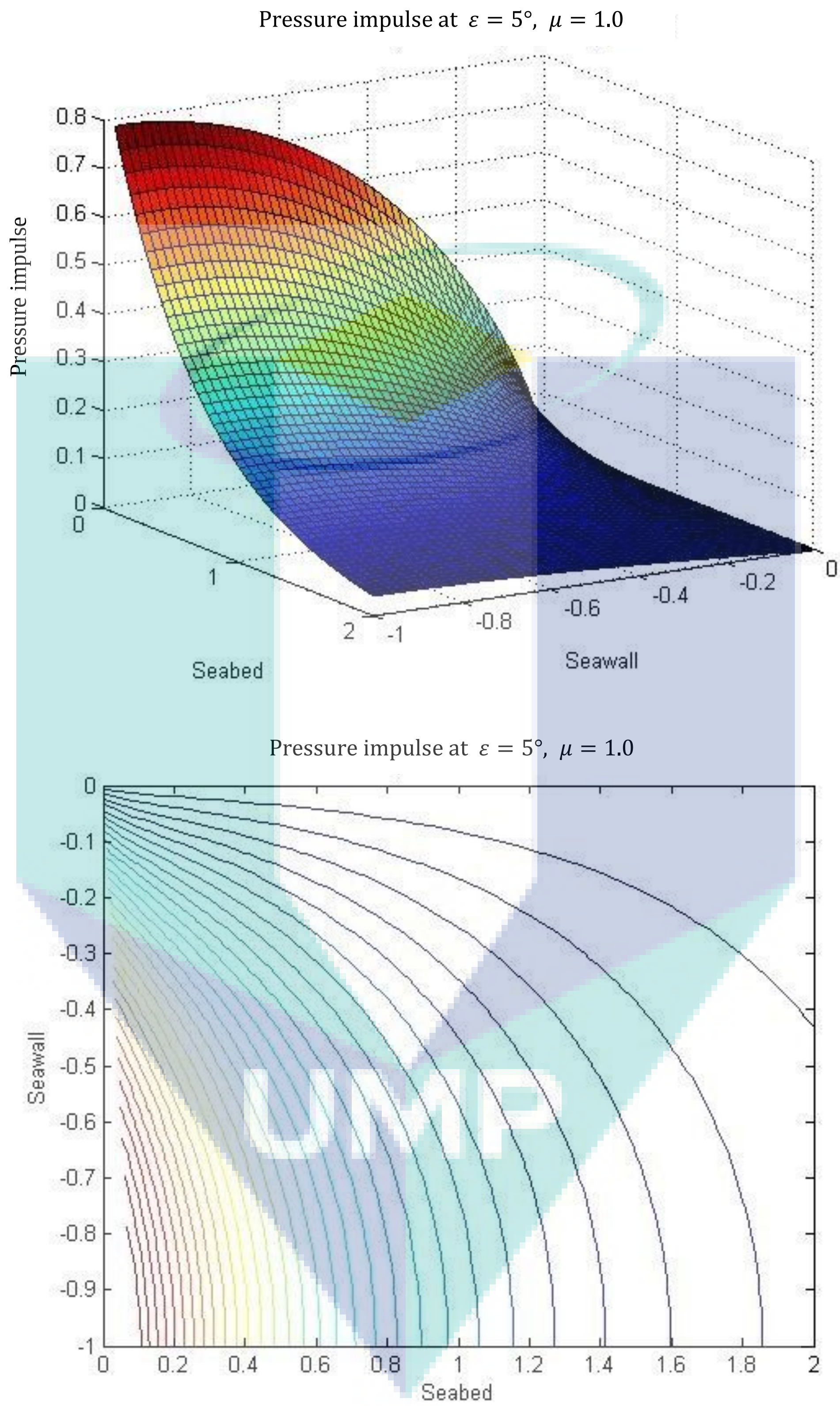

Figure 4.11 The effect of varying impact region, $\mu = 1.0$ at angle of 5°

4.7 The Effect of Varying Angle of Inclination towards Pressure Impulse

The values of pressure impulse as the angle of a landward-inclined seawall increases are shown below in Table 4.3. A landward-inclined wall's model was tested at different angles of $\varepsilon = 5°$ and $\varepsilon = 10°$. The values of impact region, μ are varied to get a better result and to be compared to each value of angle, ε. The results were recorded and compared in Table 4.3.

Table 4.3 Comparison a landward-inclined seawall model at $\varepsilon = 5°$ and $\varepsilon = 10°$

Impact Region, μ	**5°**	**10°**
0.1	0.068	0.078
0.5	0.310	0.340
0.8	0.530	0.570
1.0	0.790	0.820

From the above table, at impact region of $\mu = 0.1$, the pressure impulse on a landward-inclined seawall at an angle of $\varepsilon = 10°$ is slightly higher than the pressure impulse on a landward-inclined-inclined seawall at angle of $\varepsilon = 5°$ by 0.010.

At impact region of $\mu = 0.5$, the pressure impulse at angle of 10° is greater than at angle of 5° by 0.030. The trend of increasing impact pressure continues when μ is increased to 0.8 and 1.0 while the angle is increased from 5° to 10°.

Therefore, we can conclude that peak pressure impulse on a landward-inclined seawall increases as the angle of inclination of the seawall is increased.

Figure 4.12 and Figure 4.13 indicate the peak pressure impulse at $\mu = 0.1$ for angle of inclination, ε values of 5° and 10. The difference between these two figures is observed.

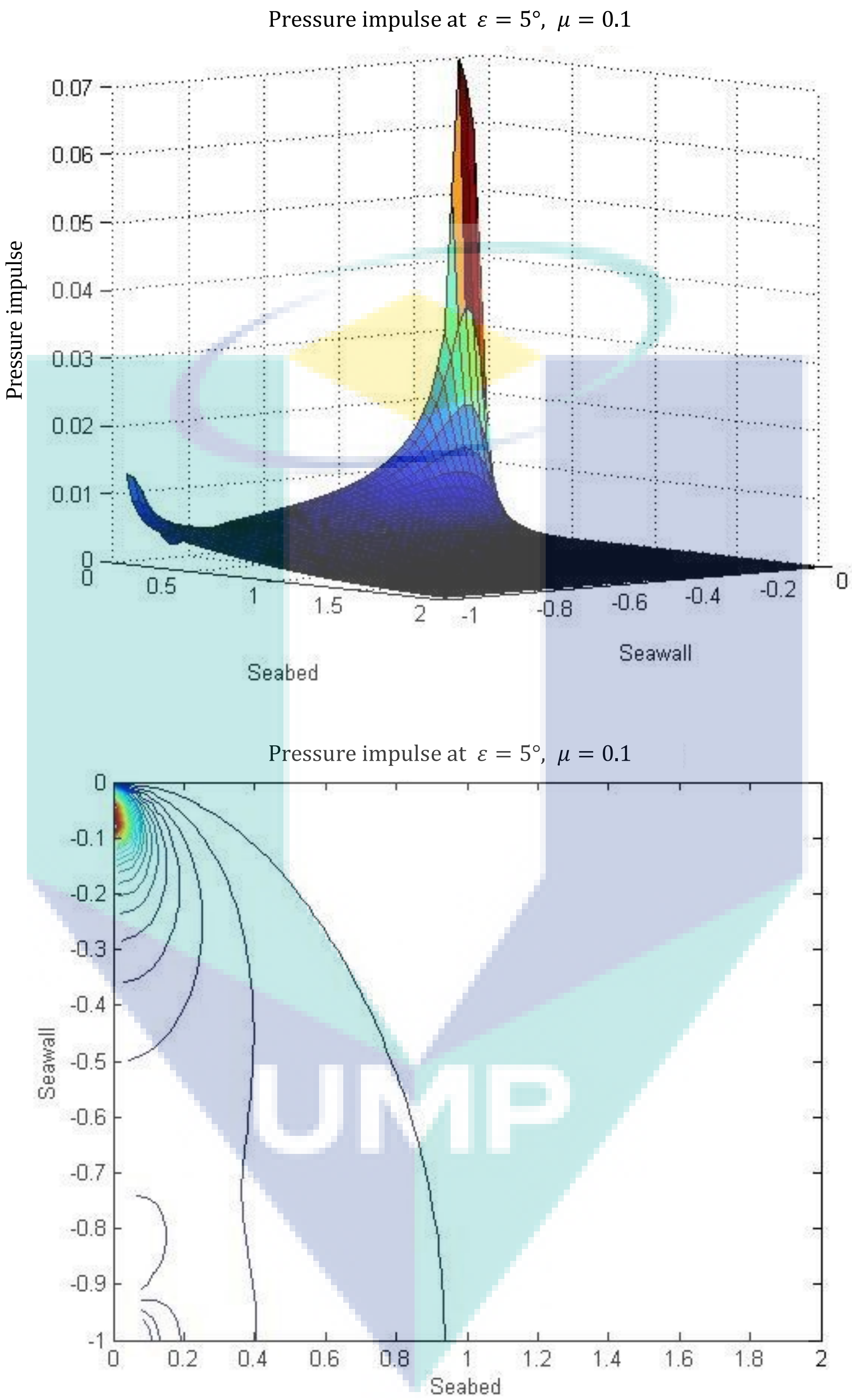

Figure 4.12 The pressure impulse on landward-inclined model at 5° as $\mu = 0.1$

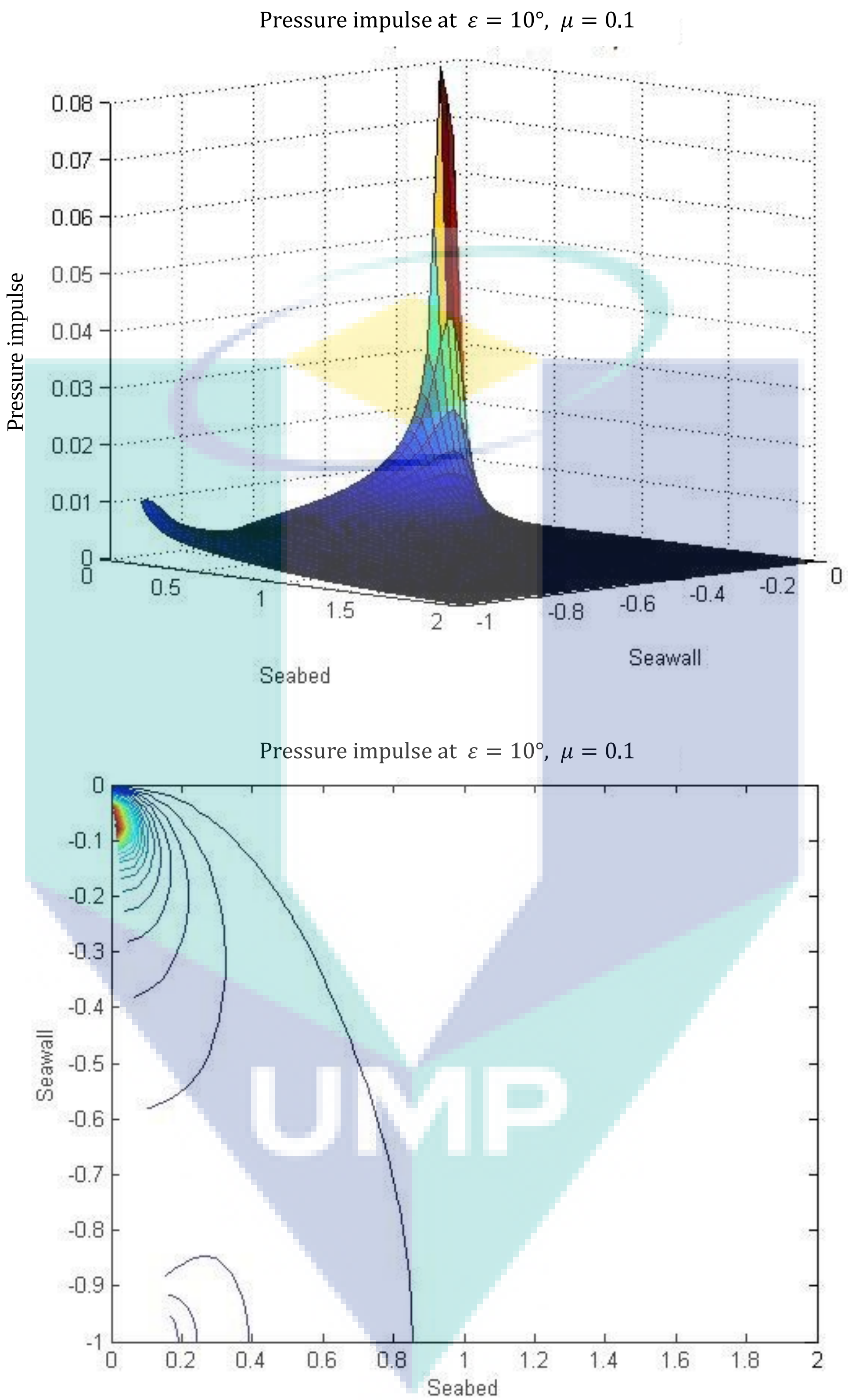

Figure 4.13 The pressure impulse on landward-inclined model at $10°$ as $\mu = 0.1$

We are now going to compare the pressure impulse at $\mu = 0.5$ as ε increases from $5°$ to $10°$. Figure 4.14 and Figure 4.15 show the difference between these two figures.

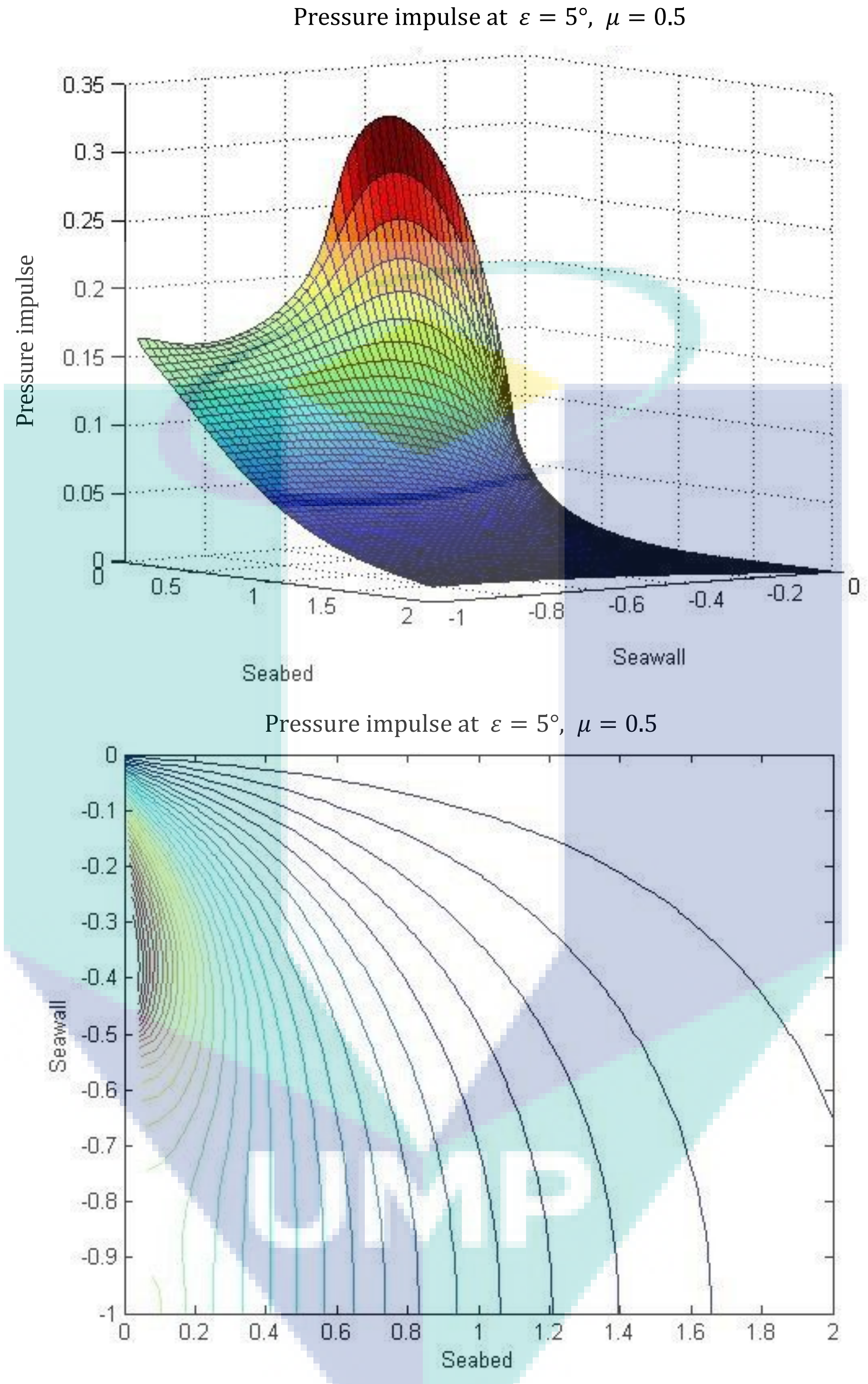

Figure 4.14 The pressure impulse on landward-inclined model at at 5° as $\mu = 0.5$

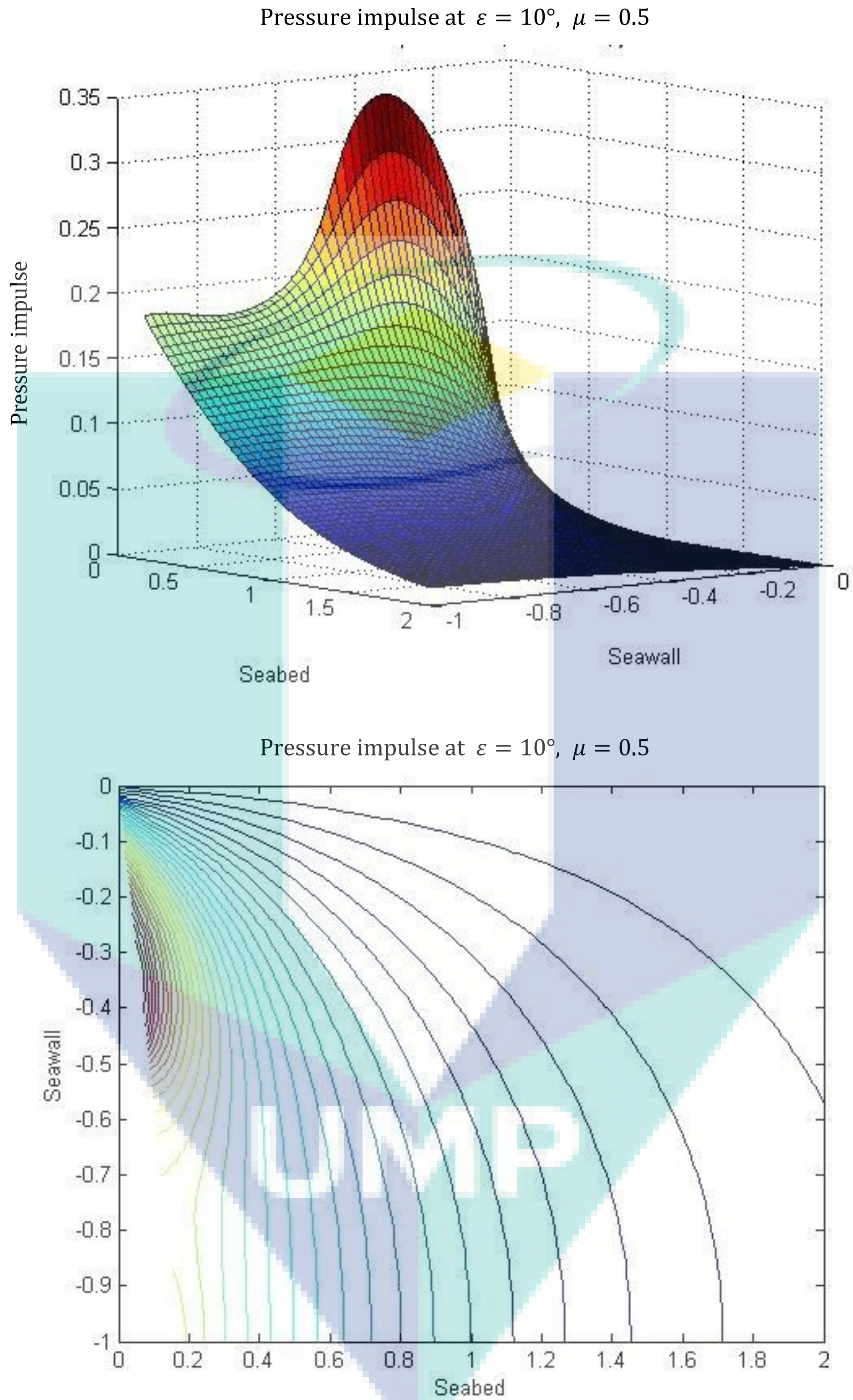

Figure 4.15 The pressure impulse on landward-inclined model at 10° as $\mu = 0.5$

Figure 4.16 and Figure 4.17 illustrate the peak pressure impulse at ε values of 5° and 10° at $\mu = 0.8$. The difference between these two figures is observed.

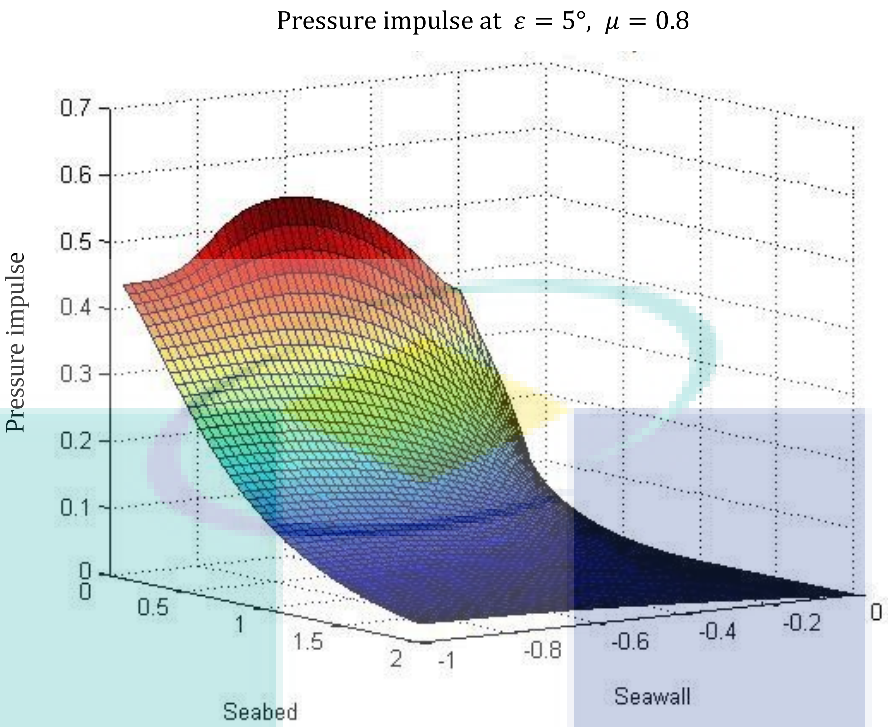

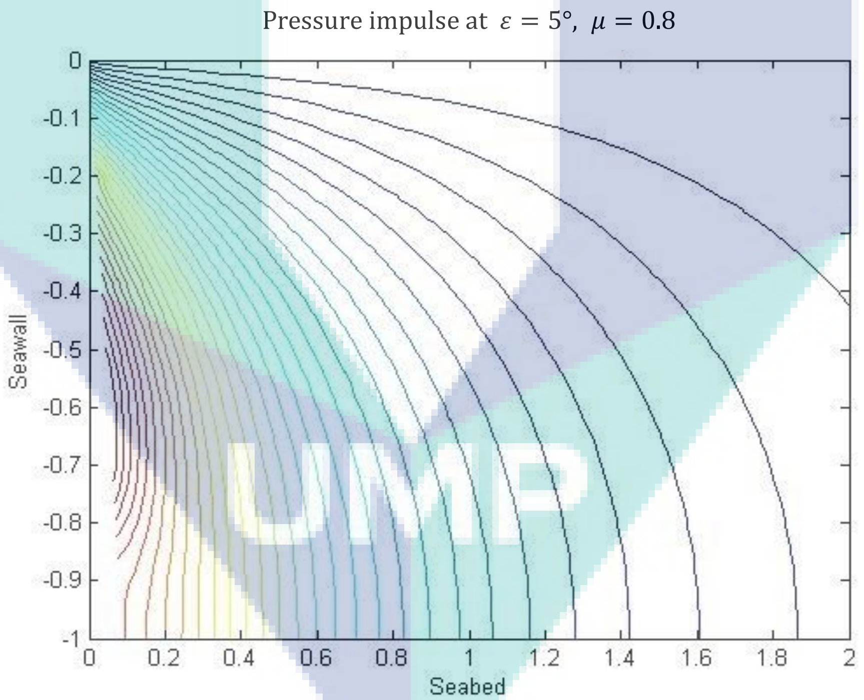

Figure 4.16 The pressure impulse on landward-inclined model at 5° as $\mu = 0.8$

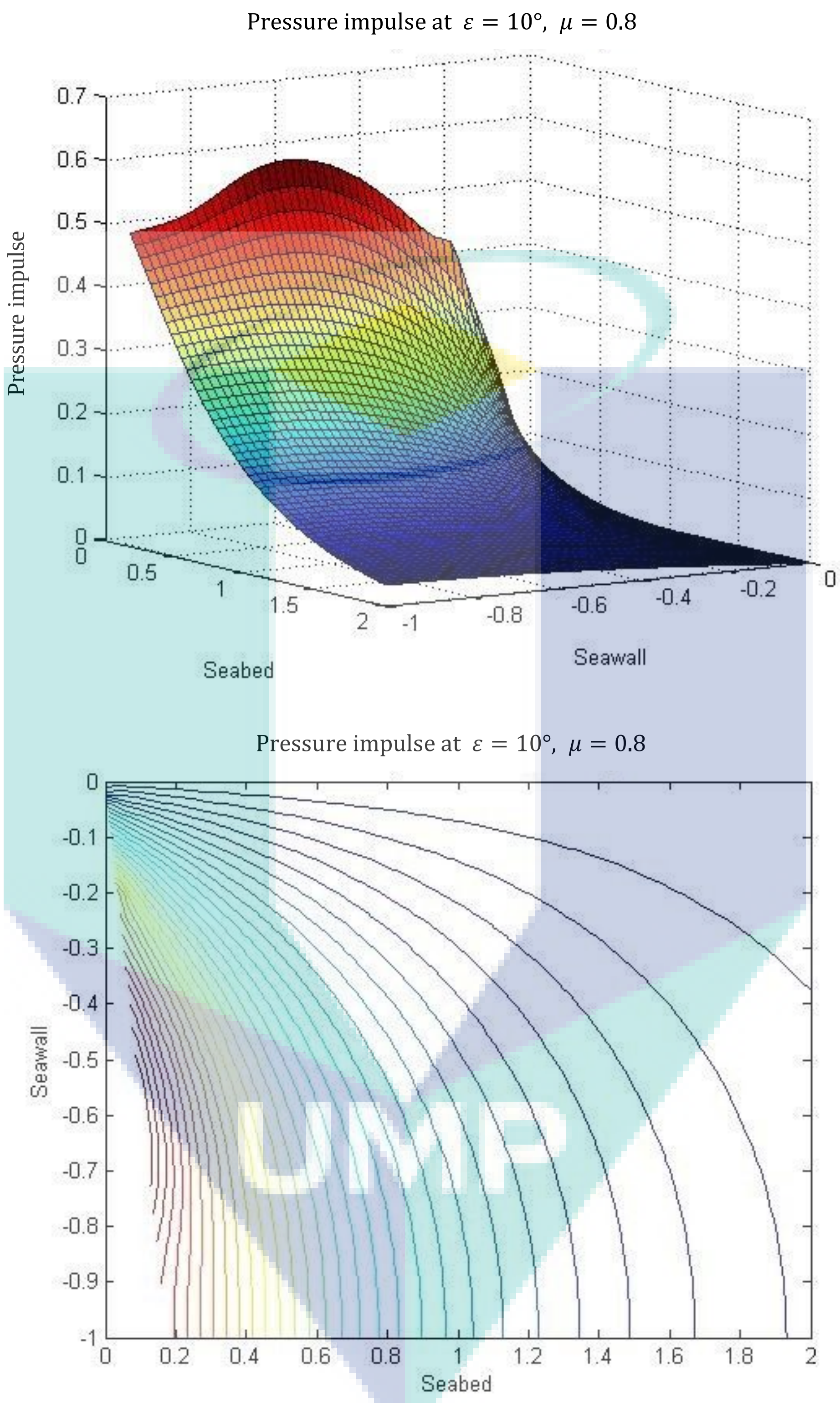

Figure 4.17 The pressure impulse on landward-inclined model at 10° as $\mu = 0.8$

Finally, Figure 4.18 and Figure 4.19 show the peak pressure impulse as the value of ε increases from 5° and 10° at $\mu = 1.0$. The difference between these two figures is recorded.

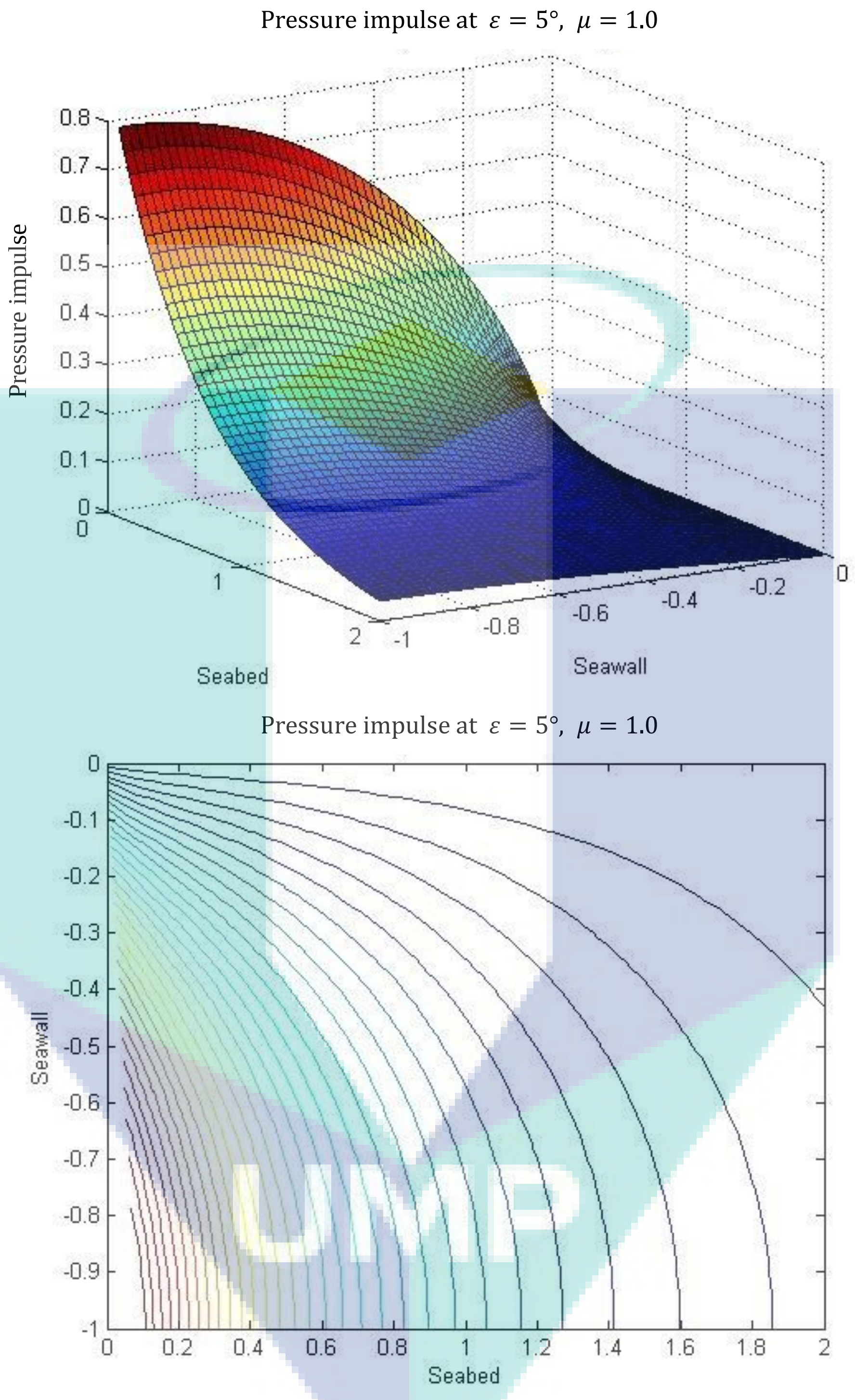

Figure 4.18 The pressure impulse on landward-inclined model at 5° as $\mu = 1.0$

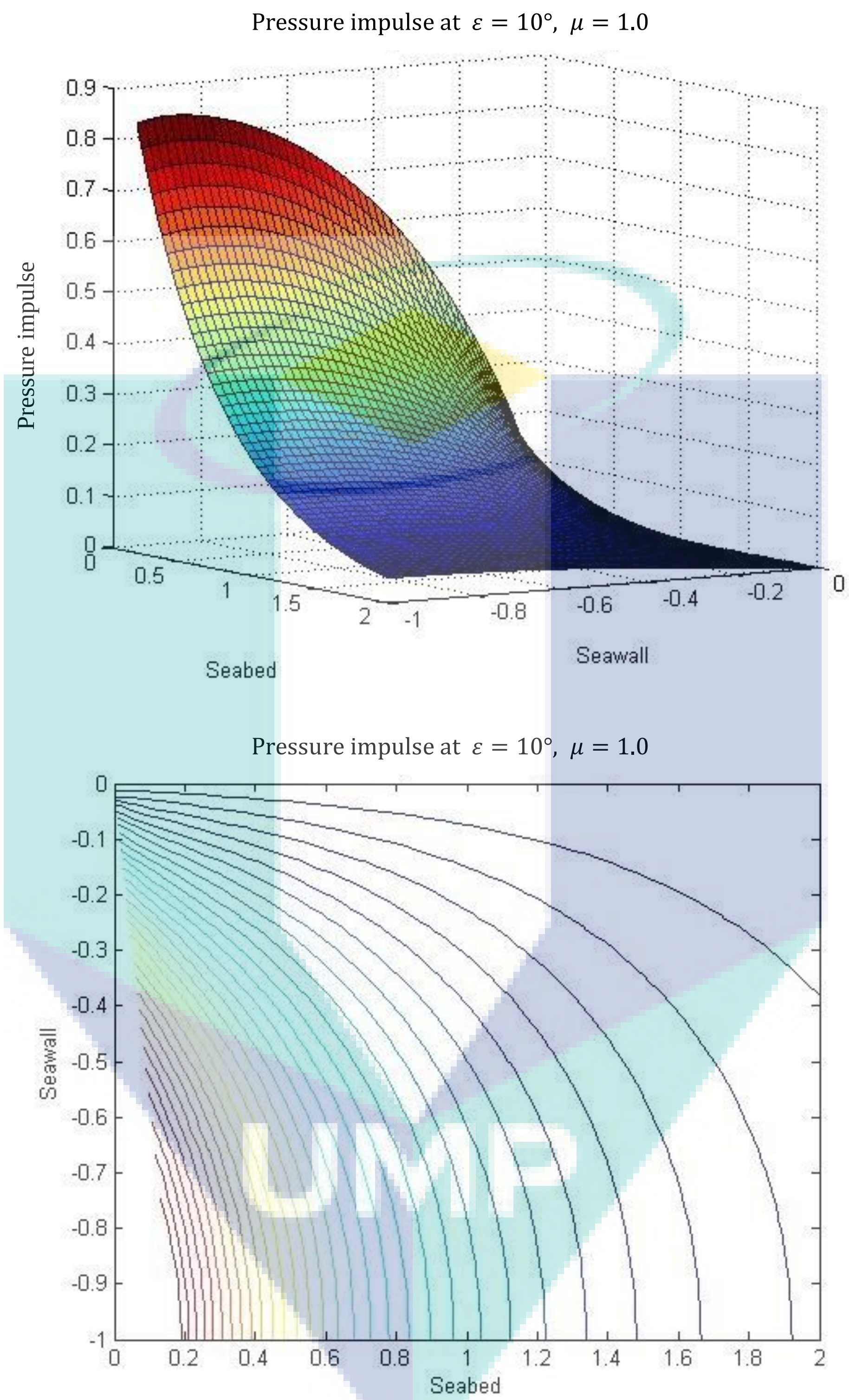

Figure 4.19 The pressure impulse on landward-inclined model at $10°$ as $\mu = 1.0$

The results demonstrate that the pressure impulse increases as the value of angle of inclination of the wall, ε increases. Hence, we can conclude that the pressure impulse will increase as the value of ε increases.

4.8 Previous Study Results

In 1995, Kirkgoz conducted a laboratory experiment on the maximum impact pressure from breaking waves on vertical and landward-inclined coastal structures using a scale model. The results of maximum pressure impulse and bottom pressure impulse from his experiment are illustrated below in Table 4.4.

Table 4.4 Dimensionless Maximum Pressure Impulse on Sloping Wall

Impact Region	0°	5°
99	64.5	88.9
90	33.3	45.6
50	14.9	19.3
10	7.2	7.8

Source: Kirkgoz (1995)

Table 4.4 shows that Kirkgöz (1995) only tested a landward-inclined seawall at an angle of 5°. Comparatively the peak impact pressure at 5° is higher than on a vertical seawall with an angle of 0°.

These results show that the minimum pressure impulse occurs at a vertical seawall. From our model, we notice that the minimum pressure impulse also happens when $\theta = 0°$. Hence, we can validate that our method is correct since we get similar results with Kirkgoz's research.

4.9 Conclusion of Landward-Inclined Seawall

Based on the numerical solution, we have found that the pressure impulse on a landward-inclined seawall increases as impact region, μ is increased. This is proven by previous study by Cooker (1991). Besides, as the angle of the wall increases, the pressure impulse on a landward-inclined seawall also increases. A similar result was found by Kirkgöz (1995) who studied the impact pressure of breaking waves on a landward-inclined seawall via a laboratory experiment. It can be concluded that minimum pressure impulse occurs when the small inclination occurs near the vertical wall.

As impact region, μ and angle of inclination wall, ε increase, the pressure impulse may get trapped at the bottom of the seawall. This can cause the bottom foundation of the seawall become weak and eventually, the seawall may topple over. Hence, if there is a vertical seawall tends to incline landward after several years of construction, it should be fixed as soon as possible in order to prevent seawall from damage. Similarly, if this problem occurred in Tanjung Piai, Kuala Kemaman and Setiu after several years of construction of the seawalls, the government should fix the seawalls as soon as possible in order to prevent seawall from damage and it will affect the cost to build new seawalls.

CHAPTER 5

MATHEMATICAL MODELLING OF A SEAWARD-INCLINED SEAWALL

5.1 Introduction

Kirkgöz (1978) carried out a laboratory experiment of breaking wave impact on a 30° backward sloping wall to investigate the effect of varying the angle of inclination of the wall against the wave impact.

In later studies (Kirkgöz, 1991, 1995) investigated the impact pressure of breaking waves on vertical and backward sloping walls by conducting laboratory experimentation. He conducted experiments on 5°, 10°, 20° and 30° backward sloping walls under breaking wave impact. He found that the impact pressure on backward sloping walls was greater compared to those on vertical walls. A good agreement was found for all experimental results.

Therefore, the aim of the present research is to study how small angles of declination on a vertical structure affect the pressure impulses on the wall. Pressure impulse might increase or decrease when the angle of declination is increased.

5.2 Mathematical Modelling of a Seaward-Inclined Seawall

Similar to the landward-inclined seawall model, the model of a seaward-inclined seawall is illustrated as below. However, there are slight differences.

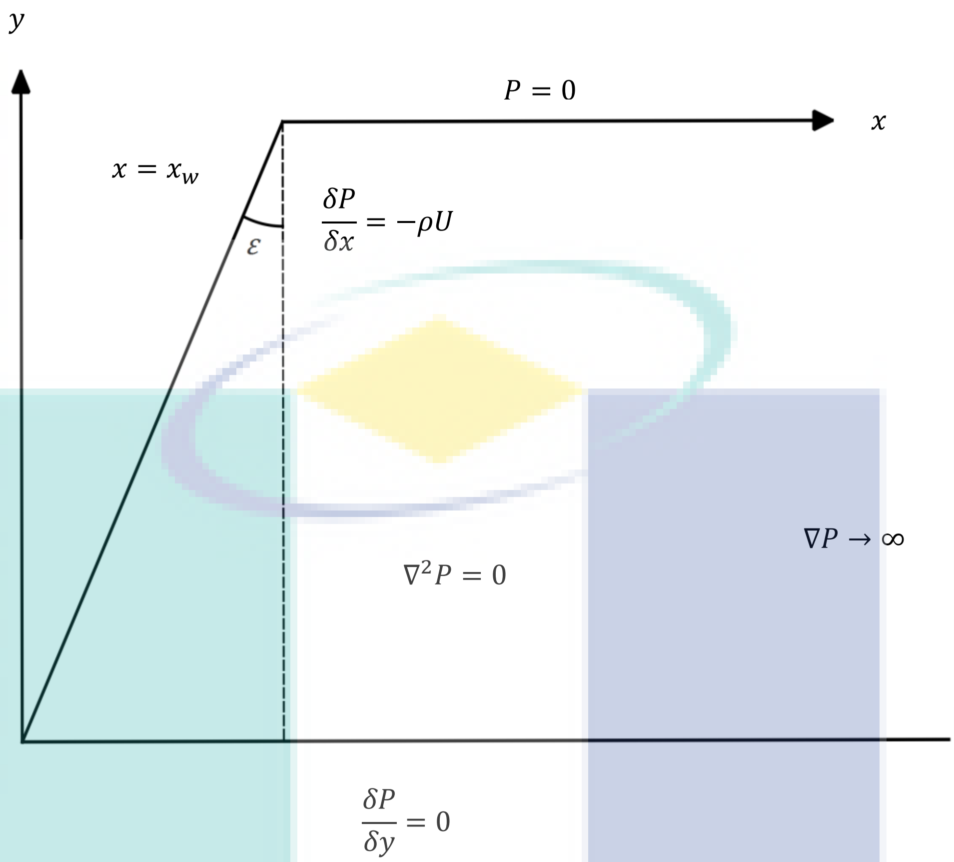

Figure 5.1 Model of a seaward-inclined seawall

The base of the wall is now positioned at $(-H, 0)$ and the top of the wall is at $(x_w, 0)$. An angle, ε is chosen as a parameter, where ε is the angle of the wall from the vertical line in a negative clockwise direction and is greater than zero (positive value) in this case.

5.3 Mathematical Formulation of a Seaward-Inclined Seawall

The equation of pressure impulse on a seaward-inclined seawall is given by

$$P(x, y; \varepsilon) = \sum_{k=0}^{\infty} P^k(x, y)\varepsilon^k \quad 5.1$$

This problem then becomes a series of problems for various types of order of ε, with each new order depending on the previous one. Each of the P^k term is given by:

$$P^k(x, y) = P^k e^{-\lambda_n x} \sin \lambda_n y \quad 5.2$$

We assume the wall is flat and the wall can now be described by:

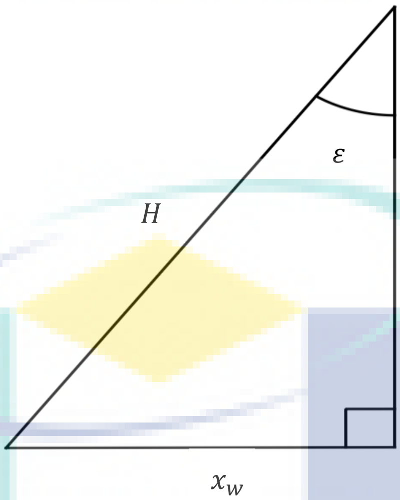

Figure 5.2 Triangle of a seaward-inclined seawall

The value of x can be explained by

$$\tan \varepsilon = \frac{x_w}{H} \tag{5.3}$$

But, in this case, it is slightly different compared to a landward-inclined seawall. It will be

$$x = \frac{x_w}{H} y + x_w = (y + H)\tan \varepsilon, \quad -H < y < 0\,, \tag{5.4}$$

Since the wall is flat, it can be described as in Figure 5.3.

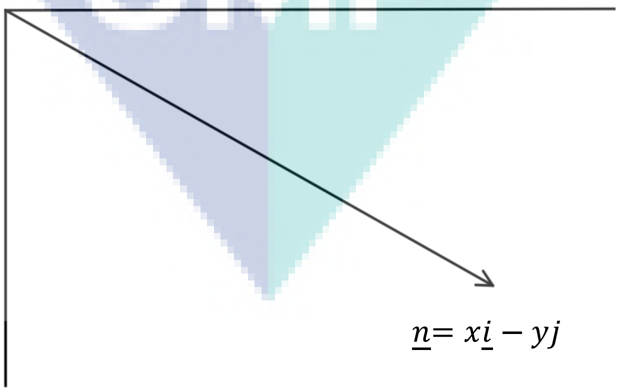

Figure 5.3 Direction of a flat wall

From Figure 5.3, the value of $\underline{n}$ can be defined by

$$\underline{n} = \cos\varepsilon \underline{i} - \sin\varepsilon \underline{j} \qquad 5.5$$

Now, the boundary condition of the wall impacted by the water waves become

$$\frac{\delta P}{\delta n} = \nabla P.n = \cos\varepsilon \frac{\delta P}{\delta x} - \sin\varepsilon \frac{\delta P}{\delta y} = -\rho U_{\circ} \cos\varepsilon \qquad 5.6$$

Equation 5.6 then becomes

$$\frac{\delta P}{\delta n} = -\rho U_{\circ} \cos\varepsilon \qquad 5.7$$

For the region of the seawall in constant contact, the boundary condition is

$$\frac{\delta P}{\delta x} = \tan\varepsilon \frac{\delta P}{\delta y} \qquad 5.8$$

Since $x = (y + H)\tan\varepsilon$ from Equation 4.4 and $\delta P/\delta n = -\rho U_{\circ} \cos\varepsilon = 0$.

The following approximations are given for small ε by using Taylor Series,

$$\tan\varepsilon \approx \varepsilon + \frac{\varepsilon^3}{3} + \cdots \qquad 5.9$$

Now, the perturbation theory will be applied here, and the solution is

$$P = \sum_{k=0}^{\infty} P^k \varepsilon^k = P^0 + \varepsilon P^1 + \varepsilon^2 P^2 + \varepsilon^3 P^3 + \cdots \qquad 5.10$$

Equation 5.10 will be then approximated for small ε, and the perturbation solution to the boundary conditions gives

$$P_x^0 + \varepsilon\left(P_x^1 - P_y^0\right) + \varepsilon^2\left(P_x^2 - P_y^1 - \frac{P_x^0}{2}\right) + \varepsilon^3\left(P_x^3 - P_y^2 - \frac{P_x^1}{2} - \frac{P_y^0}{6}\right) + \cdots$$
$$= -\rho U_\circ \cos\varepsilon = -\,\rho U_\circ\left(1 - \frac{\varepsilon^2}{2}\right) + O(\varepsilon^4) \qquad 5.11$$

Then, by expanding each of the P_x^k and P_y^k terms using Taylor Series at $x = 0$ gives

$$P_x^k = P_x^k(0,y) + xP_{xx}^k(0,y) + \frac{x^2}{2}P_{xxx}^k(0,y) + \frac{x^3}{6}P_{xxxx}^k(0,y) + \cdots \qquad 5.12$$

$$P_y^k = P_y^k(0,y) + xP_{yx}^k(0,y) + \frac{x^2}{2}P_{yxx}^k(0,y) + \frac{x^3}{6}P_{xxx}^k(0,y) + \cdots \qquad 5.13$$

From Equation 5.9 where $x = (y+H)\tan\varepsilon \approx \left(\varepsilon + \frac{1}{3}\varepsilon^3\right)(y+H)$.

Then, the Taylor Series becomes:

$$P_x^k = P_x^k(0,y) + \varepsilon(y+H)P_{xx}^k(0,y) + \frac{\varepsilon^2(y+H)^2}{2}P_{xxx}^k(0,y)$$
$$+ \frac{\varepsilon^3}{3}\left((y+H)P_{xx}^k(0,y) + \frac{(y+H)^3}{2}P_{xxxx}^k(0,y)\right) + \cdots \qquad 5.14$$

While Equation 5.13 becomes

$$P_y^k = P_y^k(0,y) + \varepsilon(y+H)P_{yx}^k(0,y) + \frac{\varepsilon^2(y+H)^2}{2}P_{yxx}^k(0,y)$$
$$+ \frac{\varepsilon^3}{3}\left((y+H)P_{yx}^k(0,y) + \frac{(y+H)^3}{2}P_{yxxx}^k(0,y)\right) + \cdots \qquad 5.15$$

Now, the boundary condition takes the following form as we neglect $0(\varepsilon^4)$ and greater terms, after substituting Equation 5.14 and Equation 5.15 into Equation 5.11:

$$
\begin{aligned}
&P_x^0 + \varepsilon(y+H)P_{xx}^0 + \frac{\varepsilon^2(y+H)^2}{2}P_{xxx}^0 \\
&\qquad + \frac{\varepsilon^3}{3}\left((y+H)P_{xx}^0 + \frac{(y+H)^3}{2}P_{xxxx}^k(0,y)\right) + \cdots \\
&+\varepsilon\left(P_x^1 + \varepsilon(y+H)P_{xx}^1 + \frac{\varepsilon^2(y+H)^2}{2}P_{xxx}^1 - P_y^0 - \varepsilon(y+H)P_{yx}^0\right. \\
&\qquad \left. - \frac{\varepsilon^2(y+H)^2}{2}P_{yxx}^0\right) + \cdots \\
&+\varepsilon^2\left(P_x^2 + \varepsilon(y+H)P_{xx}^2 - P_y^1 - \varepsilon(y+H)P_{yx}^1 - \frac{1}{2}P_x^0 - \frac{1}{2}\varepsilon(y+H)P_{xx}^0\right) \\
&\qquad + \cdots \\
&+\varepsilon^3\left(P_x^3 - P_y^2 - \frac{1}{2}P_x^1 - \frac{1}{6}P_y^0\right) = -\rho U_\circ\left(1 - \frac{\varepsilon^2}{2}\right)
\end{aligned}
\tag{5.16}
$$

There are conditions for the boundary condition of the equation above to remain true. They can be found by equating the coefficients of the powers of ε for both sides of Equation 5.16.

Now, we are going to compare each coefficient of ε^0, ε^1, ε^2 and ε^3.

For ε^0, the solution is

$$
P_x^0 = \begin{cases} 0, & -H < y < -\mu H \\ -\rho U_\circ, & -\mu H < y < 0 \end{cases}
\tag{5.17}
$$

This is still similar to Cooker's solution in Equation 3.15.

For ε^1, the solution is

$$
P_x^1 = P_y^0 - yP_{xx}^0 \quad -H < y < 0
\tag{5.18}
$$

For ε^2, the solution is

$$
P_x^2 = \begin{cases} P_y^1 + \dfrac{P_x^0}{2} - \gamma\left(P_{xx}^1 - \gamma P_{yx}^0\right) - \dfrac{\gamma^2 P_{xxx}^0}{2}, & -H < y < -\mu H \\ P_y^1 + \dfrac{P_x^0}{2} - \gamma\left(P_{xx}^1 - \gamma P_{yx}^0\right) - \dfrac{\gamma^2 P_{xxx}^0}{2} + \rho U_\circ, & -\mu H < y < 0 \end{cases}
\tag{5.19}
$$

Where $\gamma = (y+H)$

For ε^3, the solution is

$$P_x^3 - \frac{P_x^1}{2} - \frac{P_y^0}{6} - (y+H)\left(P_{xx}^2 - P_{yx}^1 - \frac{P_{xx}^0}{6}\right) - \frac{(y+H)^2}{2}\left(P_{xxx}^1 - P_{yxx}^0\right) - \frac{(y+H)^3 P_{xxxx}^0}{6}, \quad -H < y < 0 \qquad 5.20$$

The first order solution, $O(\varepsilon^1)$ is going to be solved. The nth term of P_n^k can be separated on the left hand side by multiplying each condition by $\sin\left(\frac{\lambda_n y}{H}\right)$ and then integrating it over $(-H, 0)$. This can be solved by applying the orthogonality of $\left(\sin\left(\frac{\lambda_n y}{H}\right), n \in N\right)$. But, since the orthogonality does not always apply to the right hand side, we will be left with an infinite sum. Hence, we define each P_n^{k-1} and P_n^{k-2} and so on. These coefficients are determined by the integral of products from the set $\left(\sin\left(\frac{\lambda_n y}{H}\right), \cos\left(\frac{\lambda_n y}{H}\right), y^n, n \in N\right)$. In order to find the first order solution, ε^1, Equation 5.18 will be multiplied by $\sin(\lambda_n y)$ and then integrated over $(-H, 0)$. It gives:

$$\int_{-H}^{0} P_x^1 \sin\left(\frac{\lambda_n y}{H}\right) dy = \int_{-H}^{0} \left(P_y^0 - (y+H)P_{xx}^0\right) \sin\left(\frac{\lambda_n y}{H}\right) dy \qquad 5.21$$

These derivatives will then be displayed as,

$$P_x^1(0, y) = -\sum_{n=0}^{\infty} \lambda_n P_n^1 \sin\left(\frac{\lambda_n y}{H}\right) \qquad 5.22$$

$$P_y^0(0, y) = \sum_{n=0}^{\infty} \lambda_n P_n^1 \cos\left(\frac{\lambda_n y}{H}\right) \qquad 5.23$$

$$P_{xx}^0(0, y) = -\sum_{n=0}^{\infty} \lambda_n^2 P_n^0 \sin\left(\frac{\lambda_n y}{H}\right) \qquad 5.24$$

We substitute Equation 5.22, Equation 5.23 and Equation 5.24 into Equation 5.21 which leads to the following approximation for the first order solution:

$$P(x, y) = P^0(x, y) + \varepsilon P^1(x, y) \qquad 5.25$$

By substituting the equations above, it will be expressed as,

$$P(x,y) = \sum_{n=0}^{\infty} P_n^0 e^{-\lambda_n x} \sin\left(\frac{\lambda_n y}{H}\right) + \varepsilon \sum_{n=0}^{\infty} P_n^1 e^{-\lambda_n x} \sin\left(\frac{\lambda_n y}{H}\right) P^1(x,y) \quad 5.26$$

$$P(x,y) = \sum_{n=0}^{\infty} (P_n^0 + P_n^1) e^{-\lambda_n x}\, sin\left(\frac{\lambda_n y}{H}\right) \quad 5.27$$

$$P(x,y) \approx \sum_{n=0}^{N} (P_n^0 + P_n^1) e^{-\lambda_n x}\, sin\left(\frac{\lambda_n y}{H}\right) \quad 5.28$$

The second order solution, $O(\varepsilon^2)$ is going to be solved. A solution of $P^2(x,y)$ will be found by using a similar method to $P^1(x,y)$. Equation 5.19 will be multiplied by $\sin(\lambda_n y)$ and integrated over $(-H, 0)$. Hence, it will give:

$$\int_{-H}^{0} P_x^2 \sin\left(\frac{\lambda_n y}{H}\right) dy = \int_{-H}^{0} \left(P_y^1 - \gamma\left(P_{xx}^1 - P_{yx}^0\right) - \frac{\gamma^2}{2} P_{xxx}^0\right) \sin\left(\frac{\lambda_n \gamma}{H}\right) dy \quad 5.29$$

Where $\gamma = (y + H)$

Calculating the relevant derivatives and substituting them into Equation 5.19 leads to the following approximation for the second term, $P^2(x,y)$ and therefore the second order solution:

$$P(x,y) = P^0(x,y) + \varepsilon P^1(x,y) + \varepsilon^2 P^1(x,y) \quad 5.30$$

The final solution would be,

$$P(x,y) = \sum_{n=0}^{\infty} (P_n^0 + \varepsilon P_n^1 + \varepsilon^2 P_n^2)\, e^{-\lambda_n x}\, sin\left(\frac{\lambda_n y}{H}\right) \quad 5.31$$

$$P(x,y) \approx \sum_{n=0}^{N} (P_n^0 + \varepsilon P_n^1 + \varepsilon^2 P_n^2)\, e^{-\lambda_n x}\, sin\left(\frac{\lambda_n y}{H}\right) \quad 5.32$$

5.4 Result and Discussion of Seaward-Inclined Seawall

We will discuss the results of our mathematical model in this section. The results of our study will also be confirmed and verified to ensure the result of seaward-inclined seawall's model, method and calculation are accurate and correct. This is done by comparing seaward-inclined seawall's model with Cooker's results from 1991. In addition, the results of previous studies will also be discussed here. The results will be represented by diagrams, figures or tables and will be analysed.

5.5 Validation of Result for a Seaward-Inclined Seawall

Table 5.1 shows a comparison of results of pressure impulse from Cooker's model (1991) and a seaward-inclined seawall's model. From the results, it can be seen that the values of the pressure impulse from Cooker's model (1991) and seaward-inclined seawall's model are equivalent. Although the value of impact region, μ is varied, the similar results are obtained. Here, we can validate our method is correct since we found a good agreement with Cooker's results.

Table 5.1 Comparison of Cooker's model and a seaward-inclined wall model

Impact Region, μ	Cooker's Model	Seaward-Inclined Model
0.1	0.058	0.058
0.5	0.290	0.290
0.8	0.510	0.510
1.0	0.720	0.720

Source: Cooker (1991)

From Figure 5.4, Figure 5.5, Figure 5.6 and Figure 5.7 below, we can see that the values of peak pressure from Cooker's model (1991) and seaward-inclined seawall's model are also equivalent. We are comparing seaward-inclined model at angle $\varepsilon = 0°$ with Cooker's model (1991) at different values of μ as $\mu = 0.1$, $\mu = 0.5$, $\mu = 0.8$, and $\mu = 1.0$. Although we have increased the value of μ, seaward-inclined seawall's model still gives consistent results. When we tested at $\mu = 0.1$ until $\mu = 1.0$, the pressure impulse kept increasing in tandem with Cooker's model (1991). Therefore, the results obtained from seaward-inclined wall model are still similar to Cooker's results. Hence, we can conclude that even though the values of μ varies, the results obtained are comparable. Therefore, seaward-inclined wall model is said to be correctly verified by doing this comparison. As such, our method can also be verified.

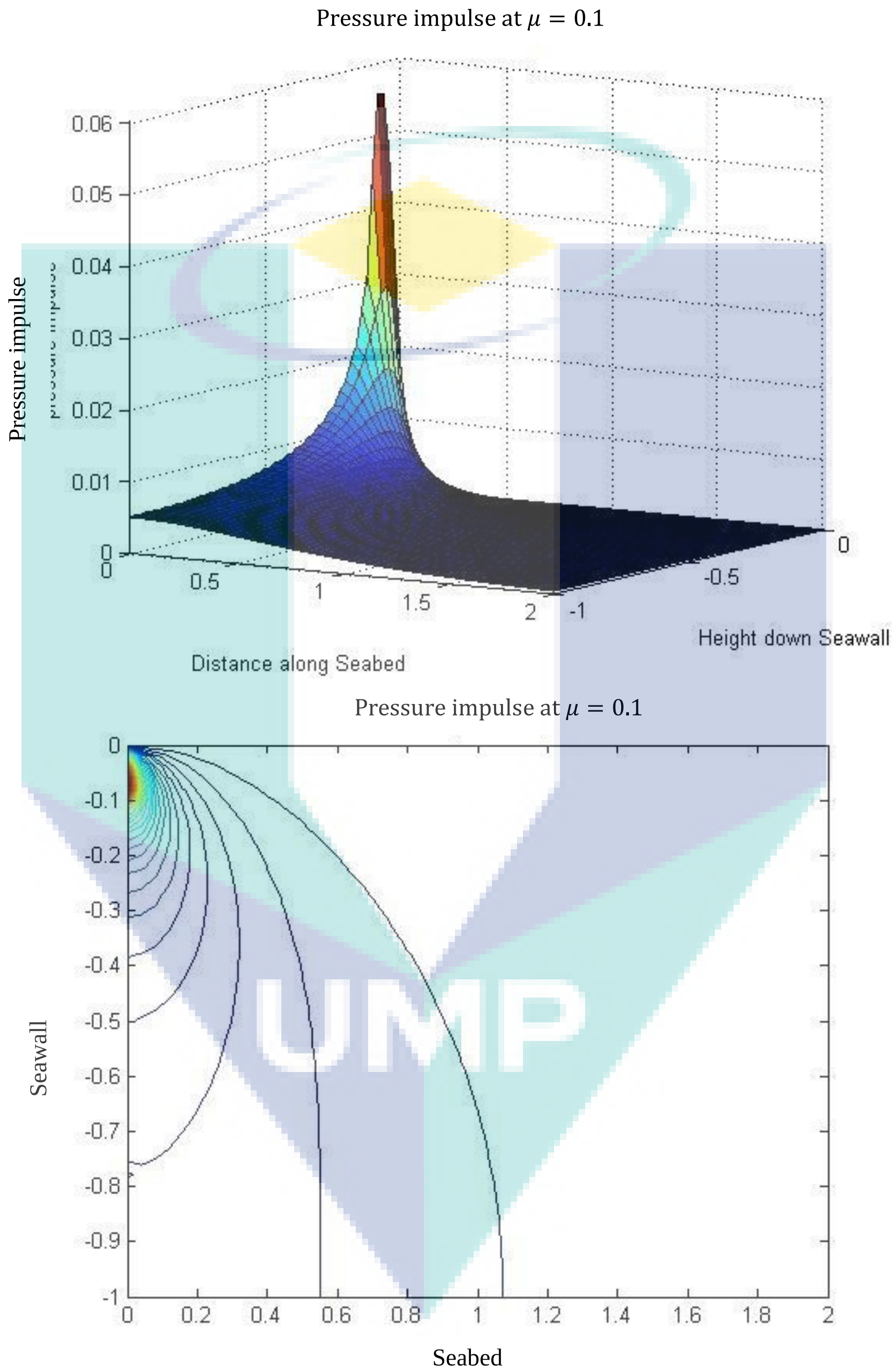

(a)

Figure 5.4 Comparison between Cooker's model, (a) and a seaward-inclined wall model at 0°, (b) when $\mu = 0.1$

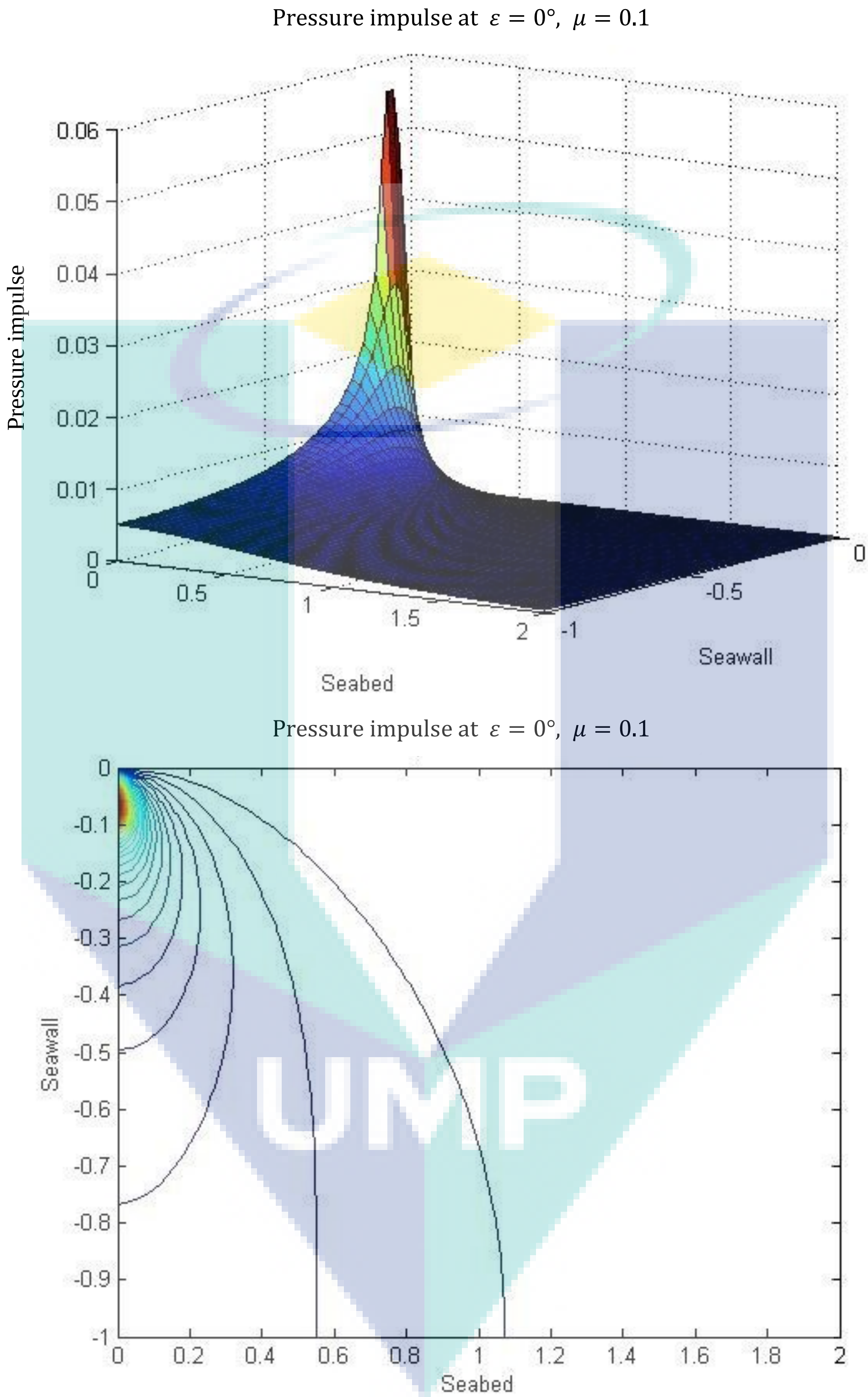

(b)

Figure 5.4 Continued

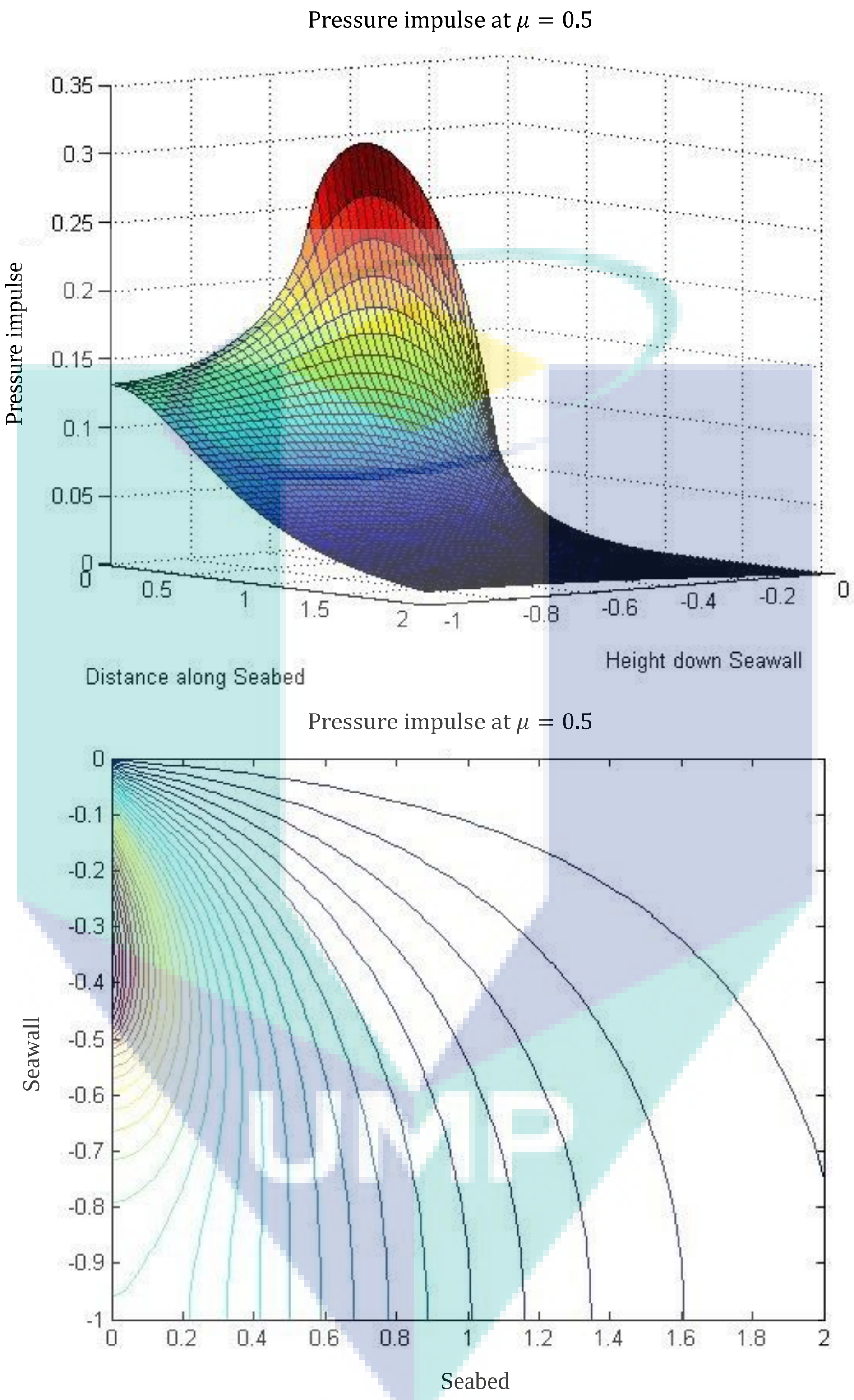

(a)

Figure 5.5 Comparison between Cooker's model, (a) and a seaward-inclined wall model at 0°, (b) when $\mu = 0.5$

Pressure impulse at $\varepsilon = 0°$, $\mu = 0.5$

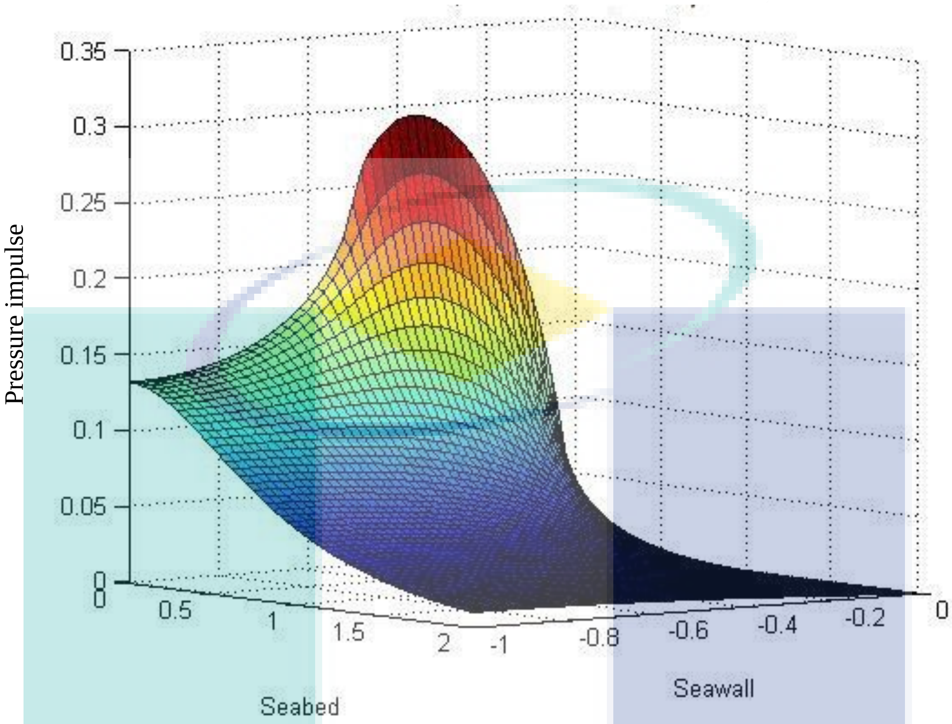

Pressure impulse at $\varepsilon = 0°$, $\mu = 0.5$

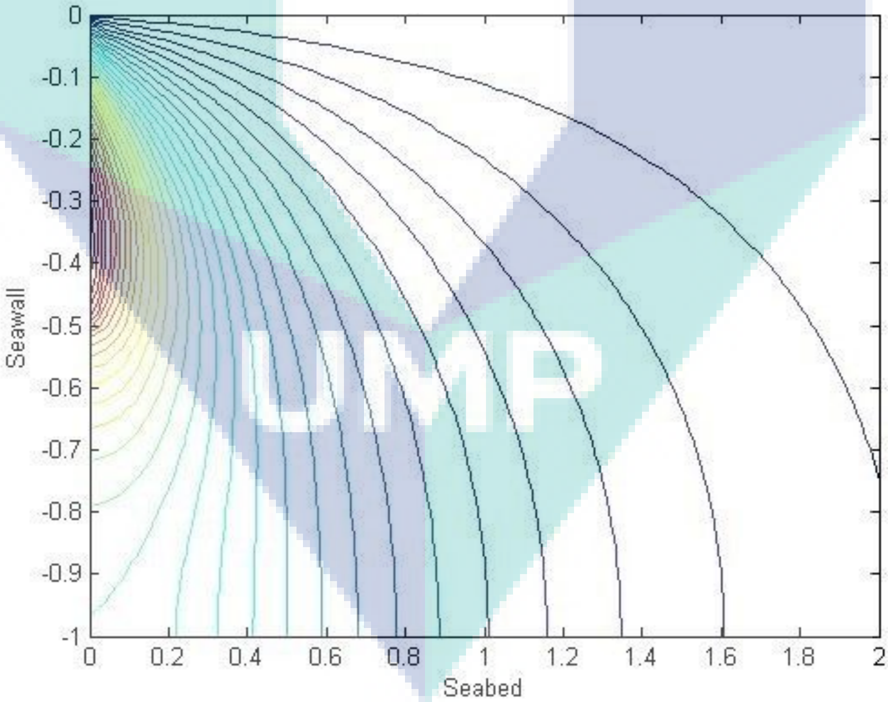

(b)

Figure 5.5 Continued

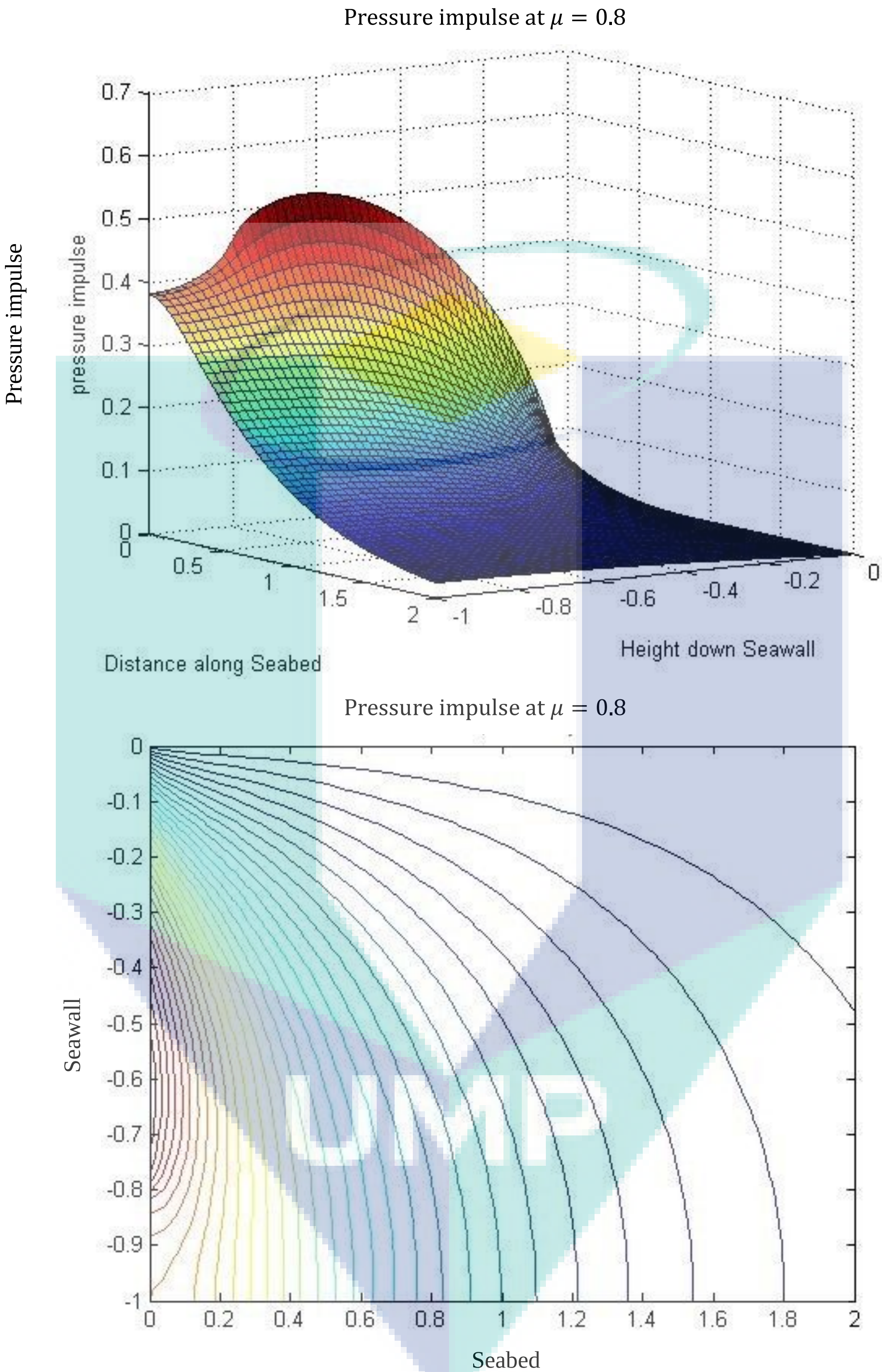

(a)

Figure 5.6 Comparison between Cooker's model, (a) and a seaward-inclined wall model at 0°, (b) when $\mu = 0.8$

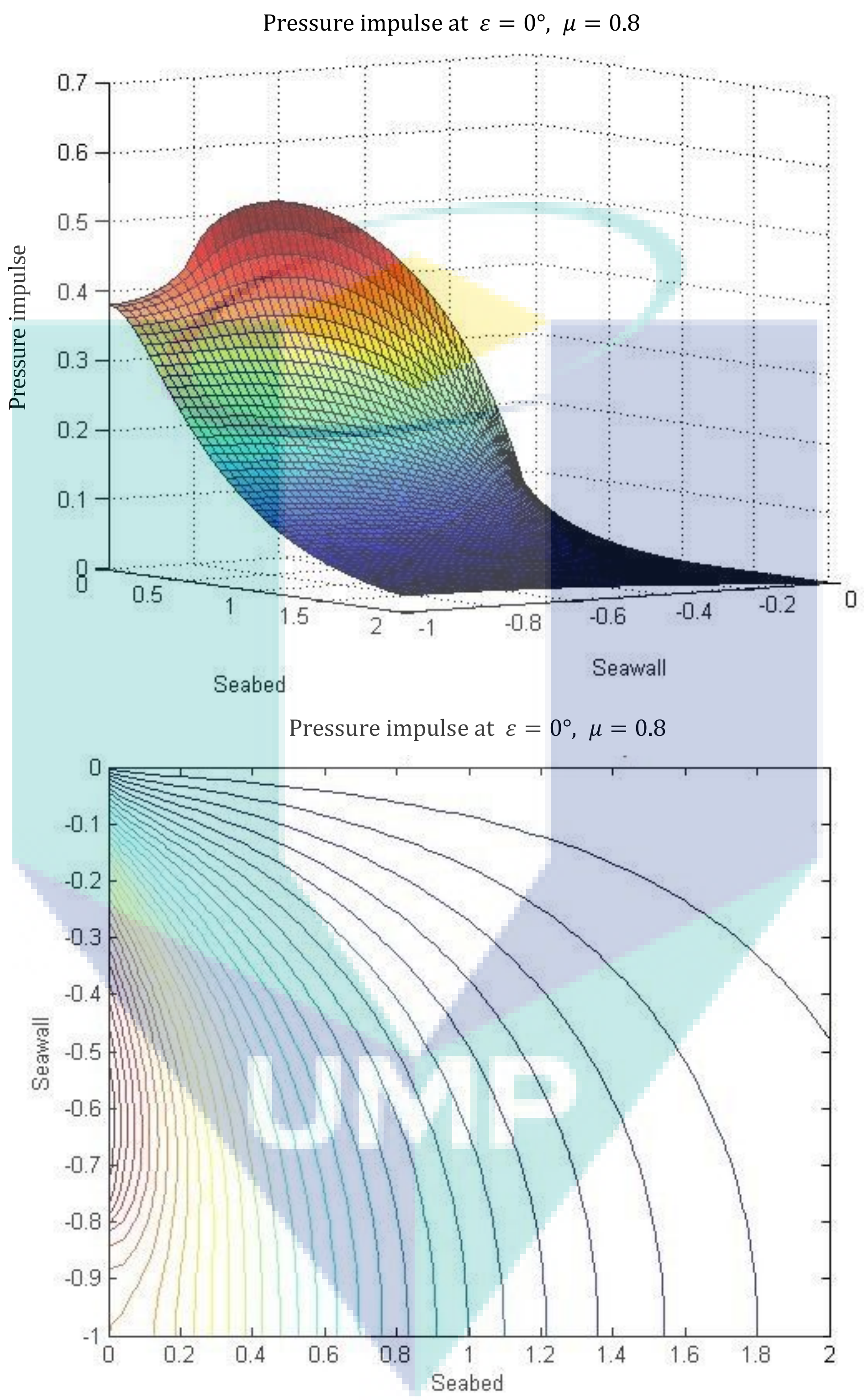

(b)

Figure 5.6 Continued

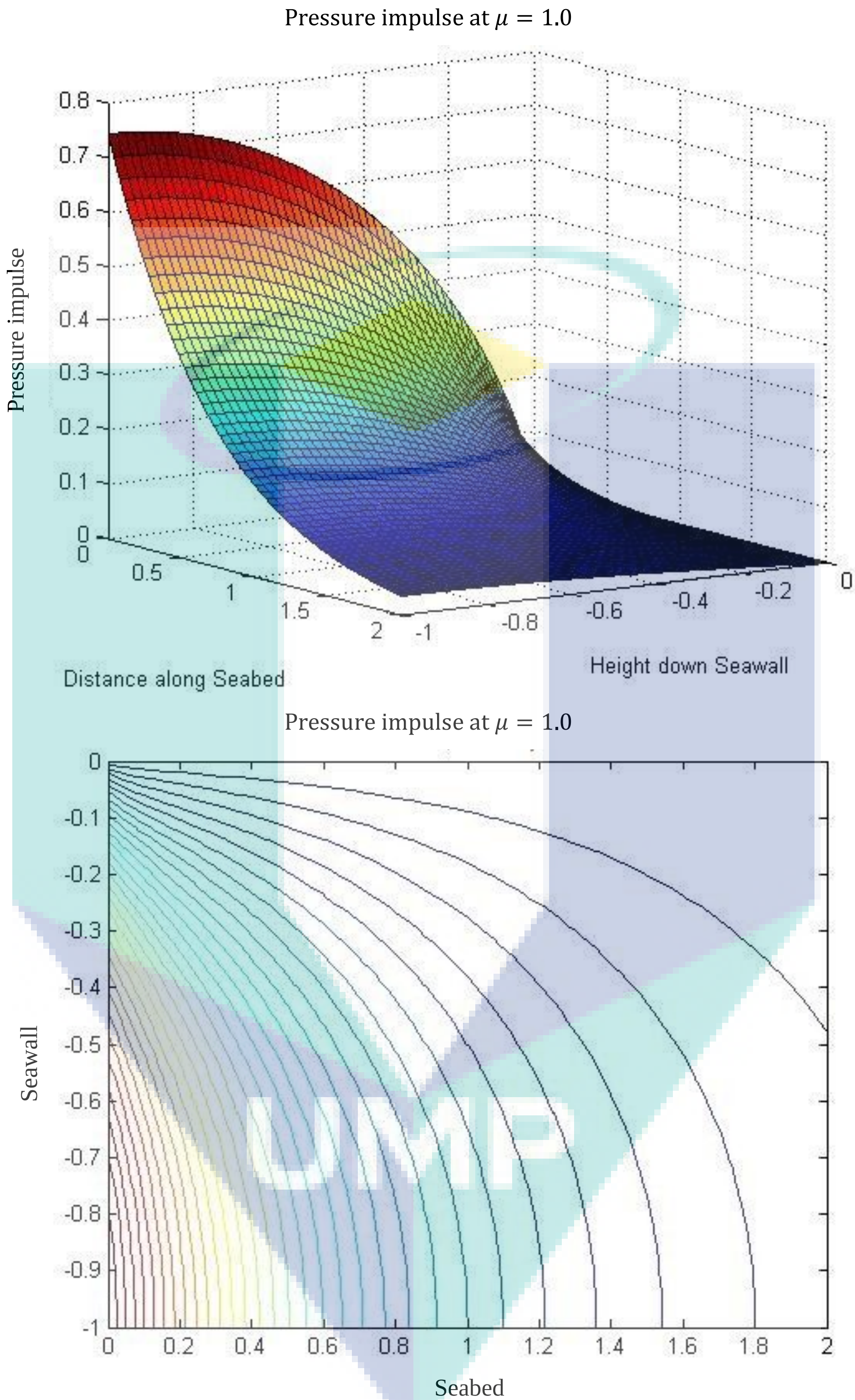

(a)

Figure 5.7 Comparison between Cooker's model, (a) and a seaward-inclined wall model at 0°, (b) when $\mu = 1.0$

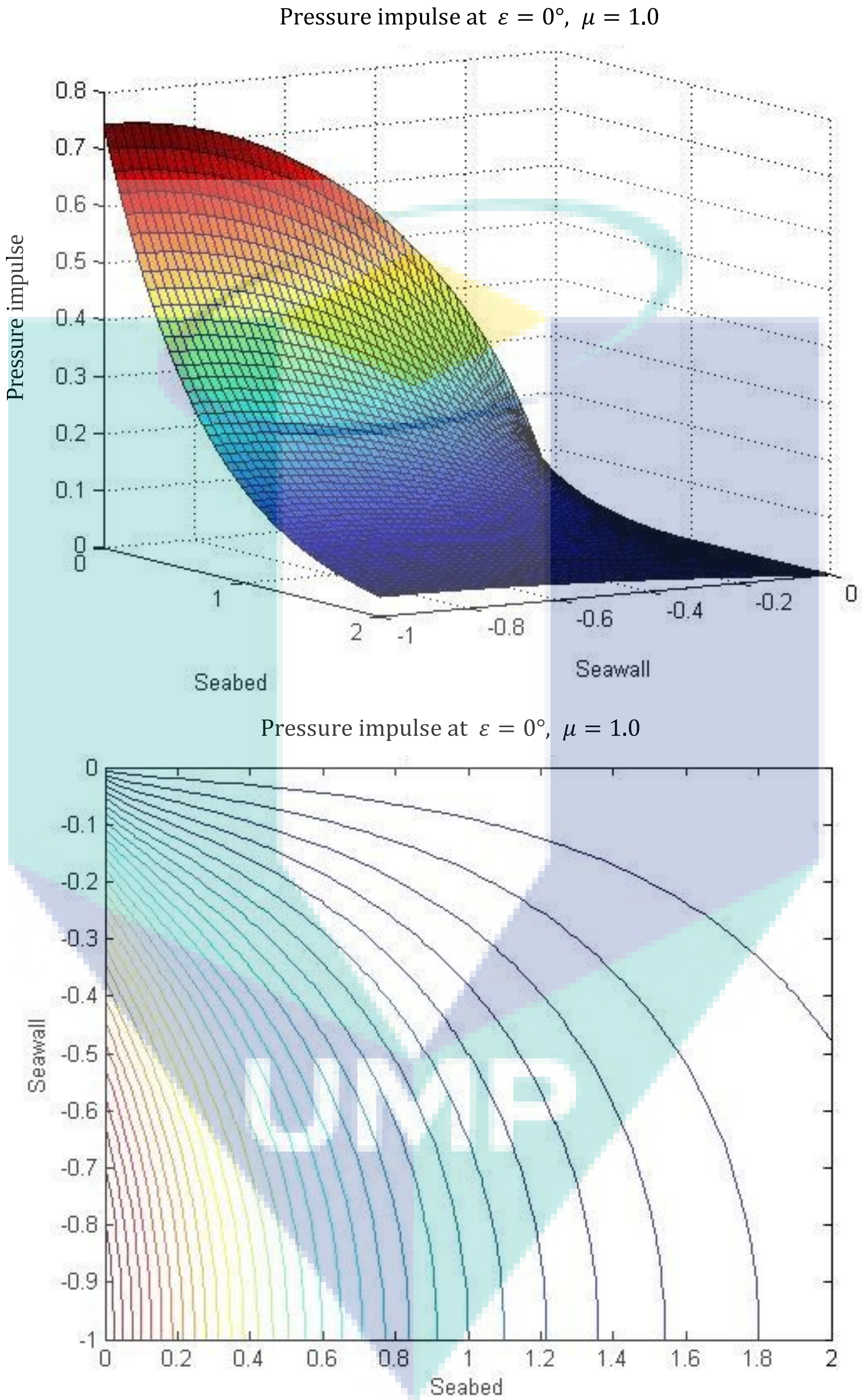

(b)

Figure 5.7 Continued

5.6 The Effect of Varying Impact Zone towards Pressure Impulse

We will discuss in this section how varying the impact zone value, μ affects the pressure impulse. We only tested at angle of inclination of seawall, $\varepsilon = 5°$ at different values of μ. Table 5.2 shows the effect of varying impact region, μ at an angle of $5°$.

Table 5.2 The effect of varying impact region at angle of 5°

Impact Region, μ	**5°**
0.1	0.072
0.5	0.320
0.8	0.550
1.0	0.810

Figure 5.8, Figure 5.9, Figure 5.10 and Figure 5.11 below show that the value of peak pressure will rise as we increase the value of μ. Hence, we can conclude that if the value of μ increases, the value of pressure impulse also increases.

As we can see, pressure impulse increased by 0.248 when we increased the value of impact region, μ from 0.1 to 0.5. When we increased the value of impact region, μ from 0.5 to 0.8, pressure impulse increased by 0.230. The pressure impulse then increased by a further 0.260 when the impact region, μ was raised from 0.8 to 1.0.

Hence, we can conclude that if the value of impact region, μ increases, the value of pressure impulse also increases.

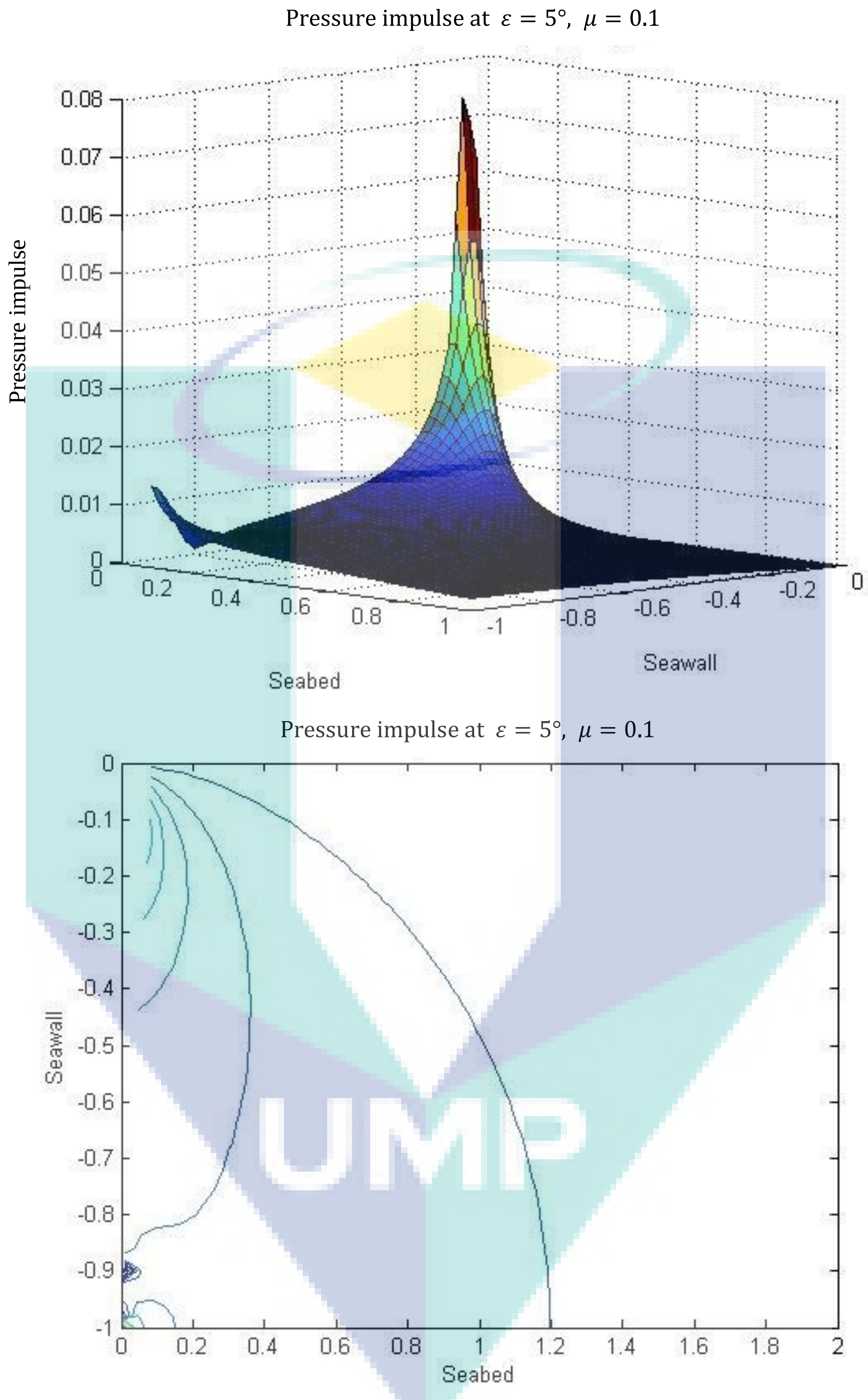

Figure 5.8 The effect of varying impact region, $\mu = 0.1$, at angle of $5°$

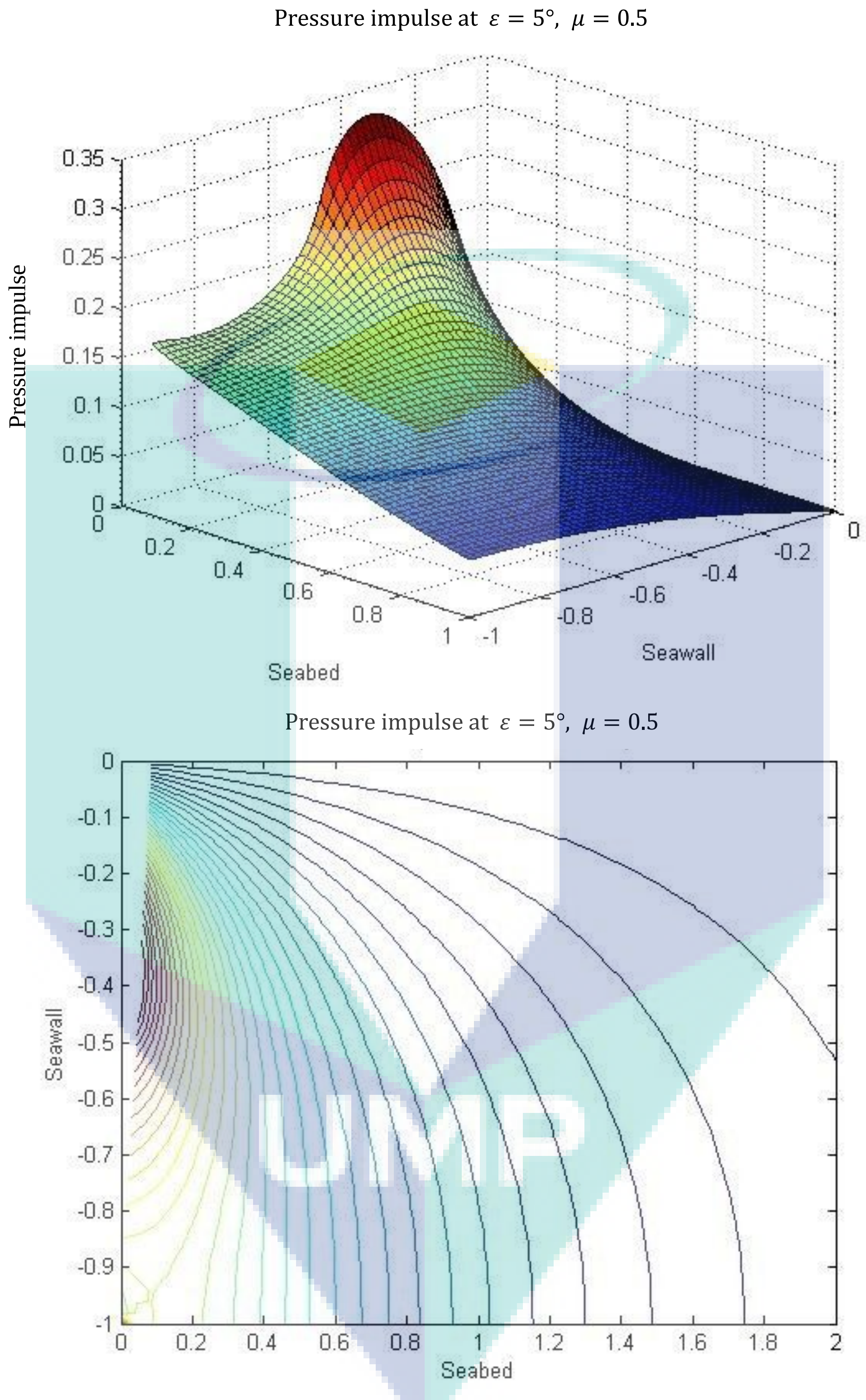

Figure 5.9 The effect of varying impact region, $\mu = 0.5$, at angle of $5°$

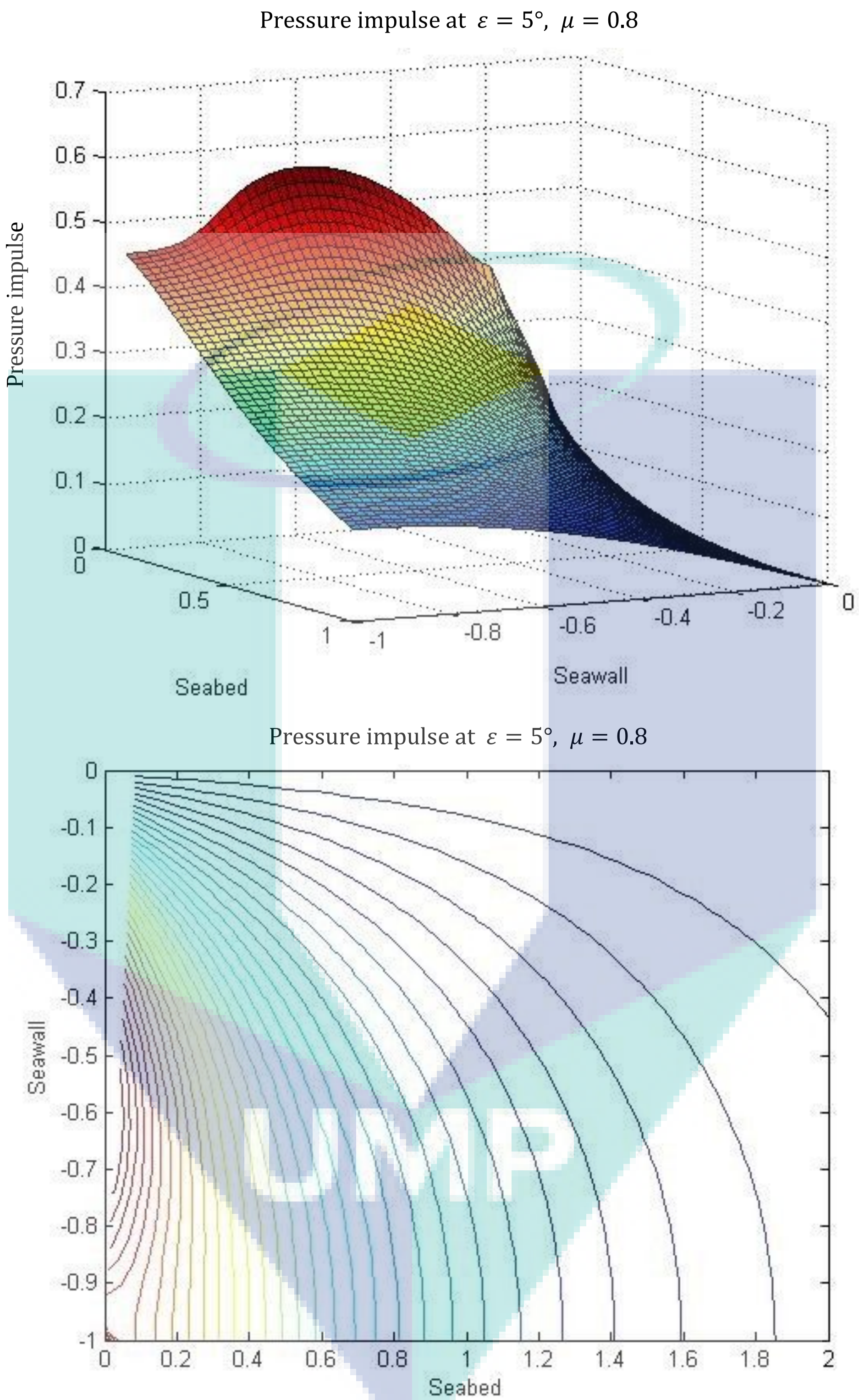

Figure 5.10 The effect of varying impact region, $\mu = 0.8$, at angle of 5°

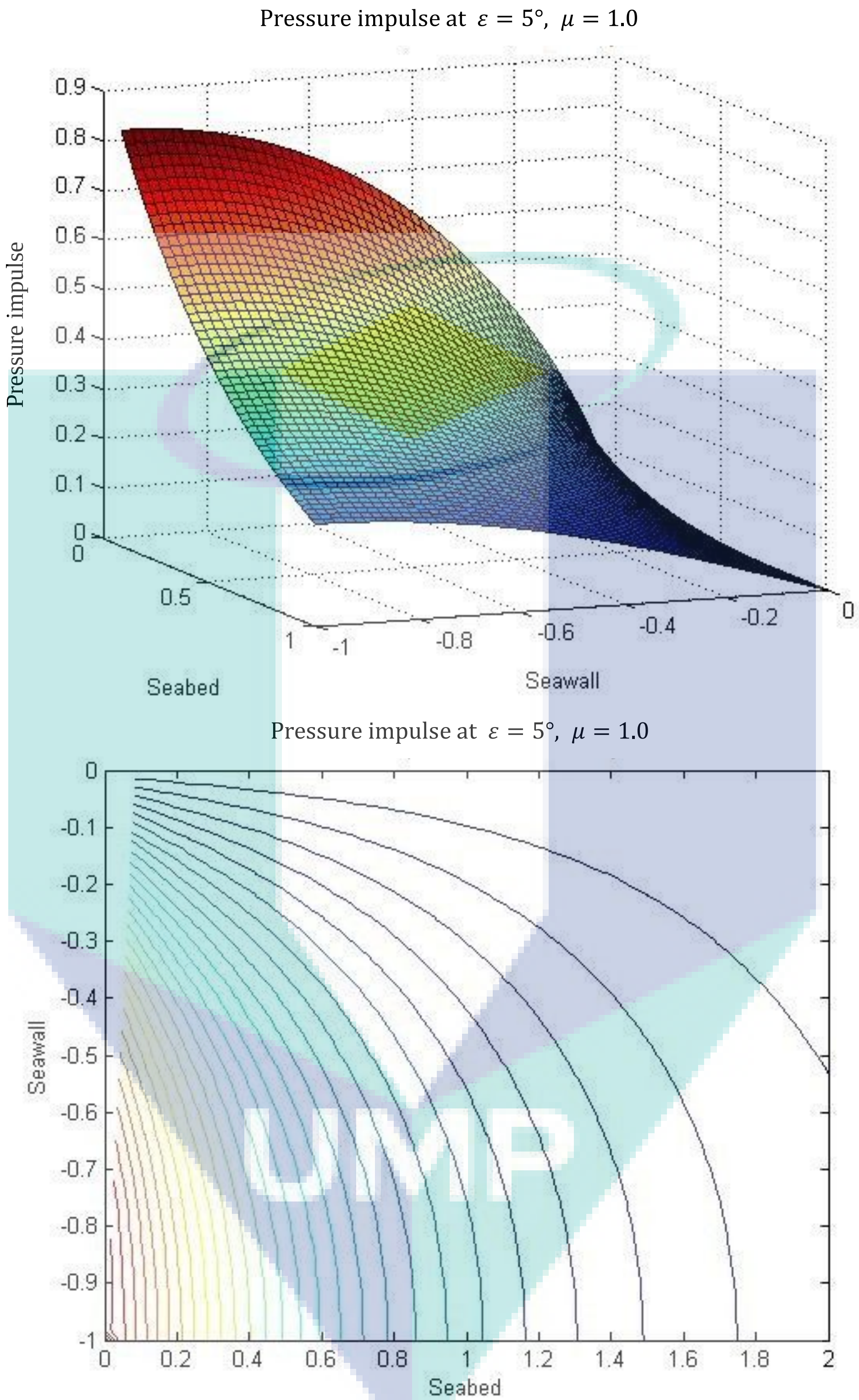

Figure 5.11 The effect of varying impact region, $\mu = 1.0$, at angle of $5°$

5.7 The Effect of Varying Angle of Inclination towards Pressure Impulse

A comparison of pressure impulse values as the angle of a seaward-inclined seawall increases are shown in Table 5.3. We had tested our model at different angles of $\varepsilon = 5°$ and $\varepsilon = 10°$. Here, the values of impact region, μ were varied to get a better result. The results were recorded and compared in the table below.

Table 5.3 Comparison a seaward-inclined seawall model at $\varepsilon = 5°$ and $\varepsilon = 10°$

Impact Region, μ	**5°**	**10°**
0.1	0.072	0.082
0.5	0.320	0.350
0.8	0.550	0.580
1.0	0.810	0.840

From the above table, at impact region of $\mu = 0.1$, the pressure impulse on a seaward-inclined seawall at an angle of $\varepsilon = 10°$ is slightly higher than the pressure impulse on a seaward-inclined seawall at an angle $\varepsilon = 10°$ of by 0.010.

When tested again at impact region of $\mu = 0.5$, the pressure impulse at an angle of 10° is greater than at an angle of 5° by 0.030. The trend of increasing pressure impulse is repeated when μ was increased to 0.8 and 1.0.

Therefore, we can conclude that the peak pressure impulse on a seaward-inclined seawall increases in tandem with an increase in the angle of the seawall.

Figure 5.12 and Figure 5.13 indicate the peak pressure impulse at ε values of 5° and 10° when $\mu = 0.1$. The difference between these two figures are observed.

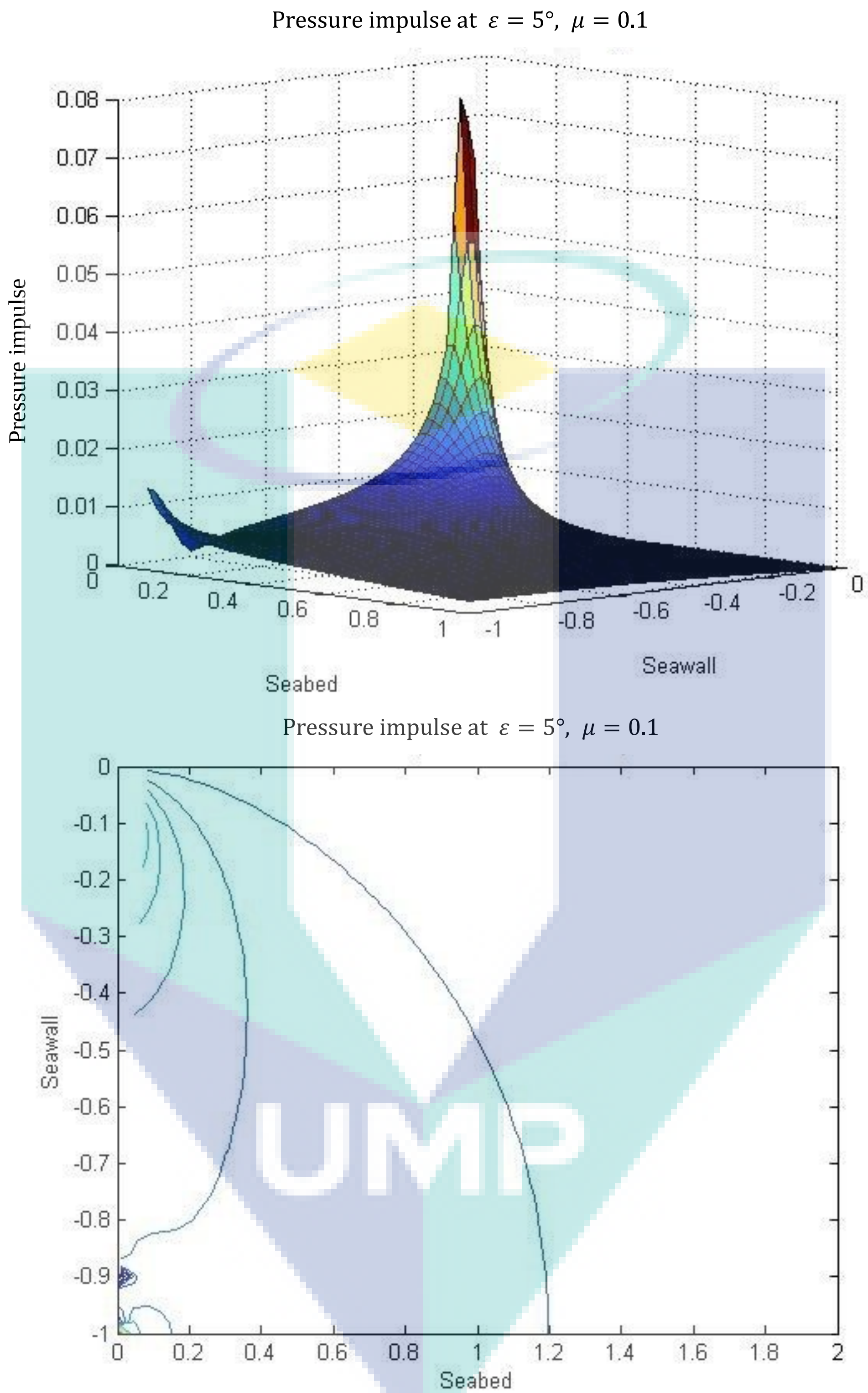

Figure 5.12 The pressure impulse on seaward-inclined model at 5° as $\mu = 0.1$

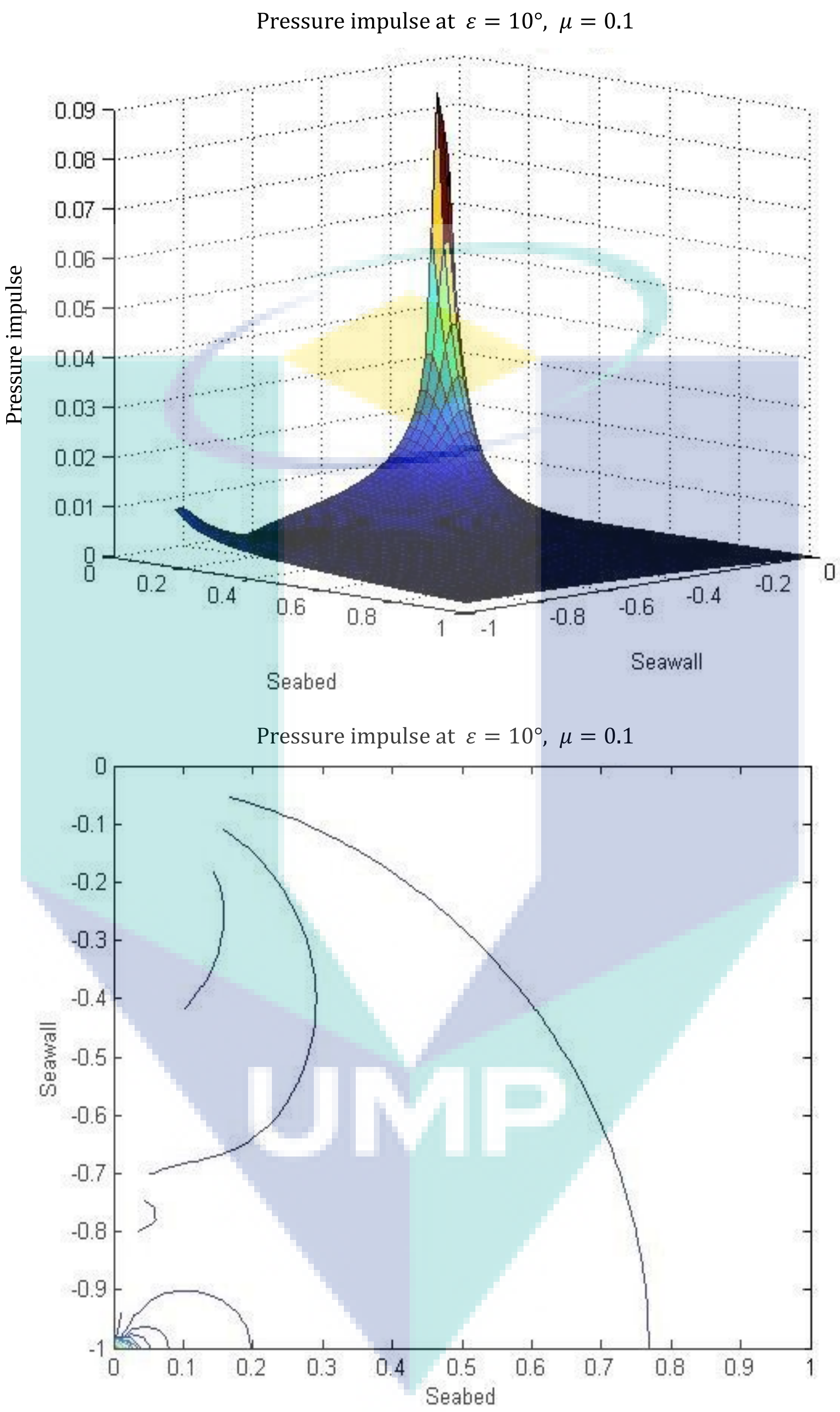

Figure 5.13 The pressure impulse on seaward-inclined model at 10° as $\mu = 0.1$

We are now going to compare the pressure impulse when $\mu = 0.5$ as ε increases from $5°$ to $10°$. Figure 5.14 and Figure 5.15 show the difference between these two figures.

Pressure impulse at $\varepsilon = 5°$, $\mu = 0.5$

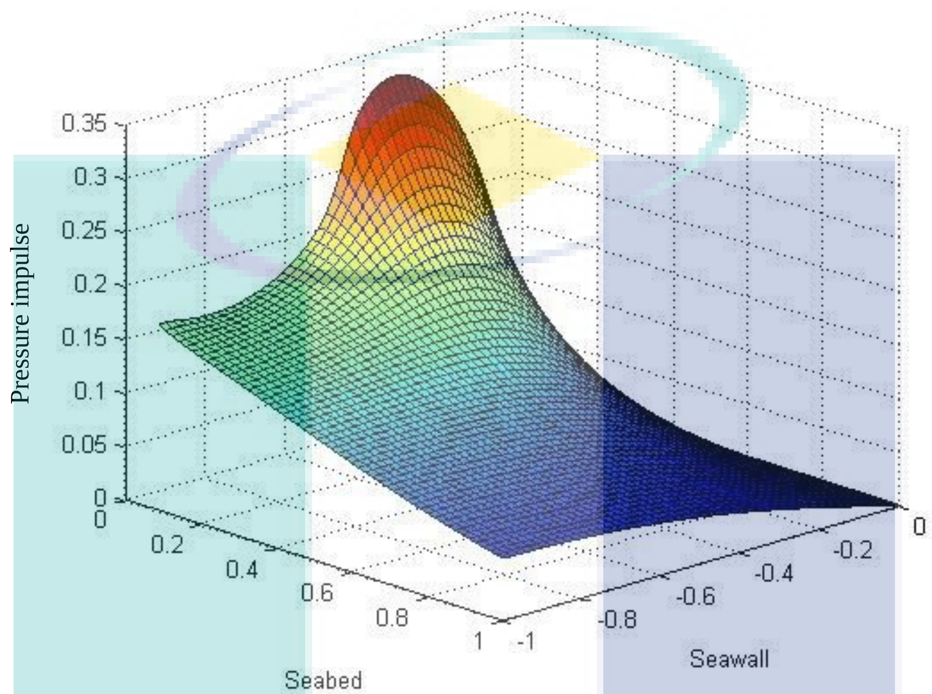

Pressure impulse at $\varepsilon = 5°$, $\mu = 0.5$

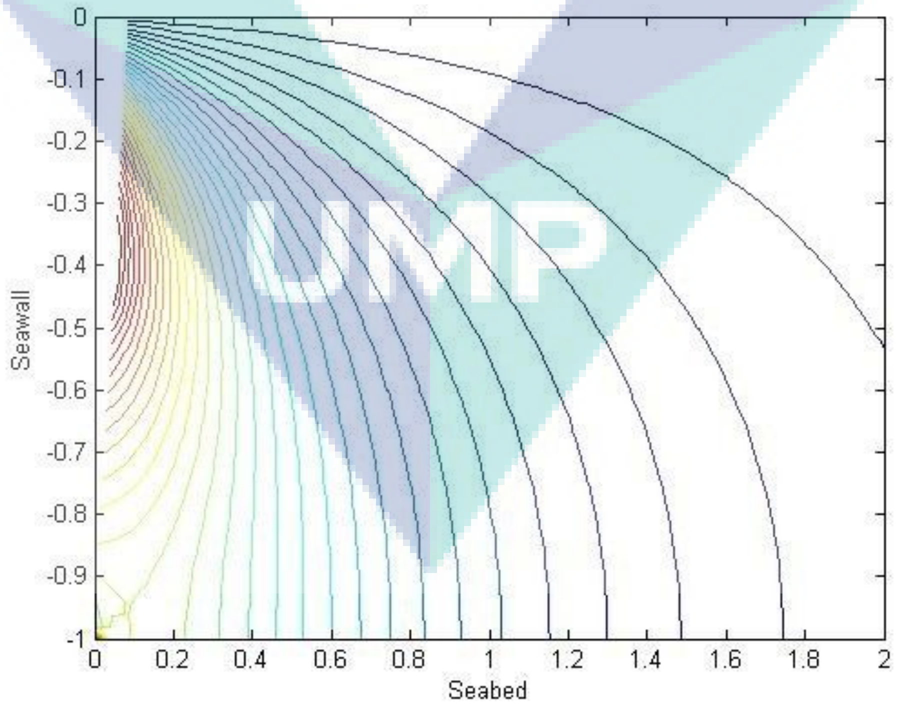

Figure 5.14 The pressure impulse on seaward-inclined model at $5°$ as $\mu = 0.5$

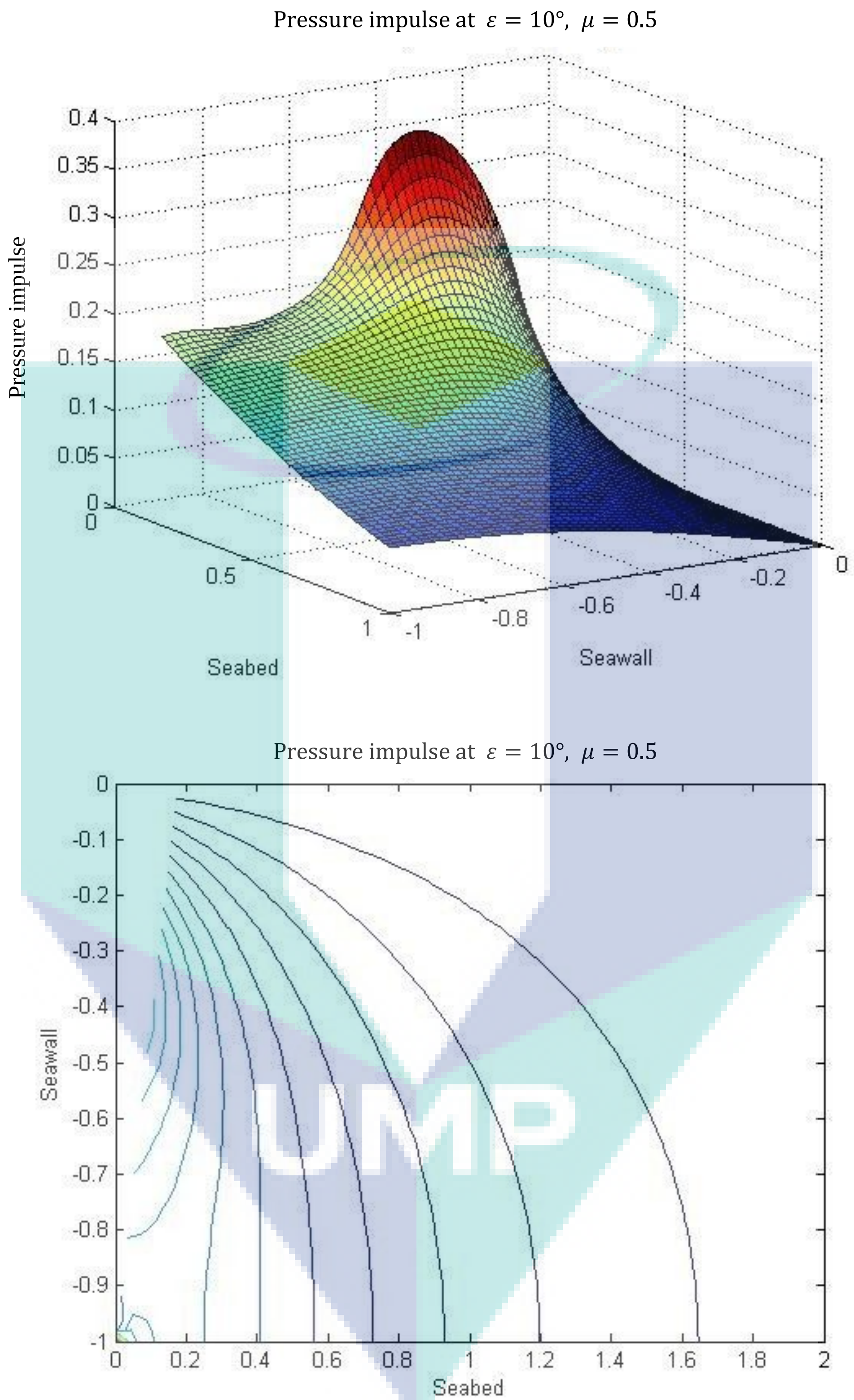

Figure 5.15 The pressure impulse on seaward-inclined model at 10° as $\mu = 0.5$

Figure 5.16 and Figure 5.17 illustrate the peak pressure impulse at ε values of 5° and 10° when $\mu = 0.8$. The difference between these two figures is observed.

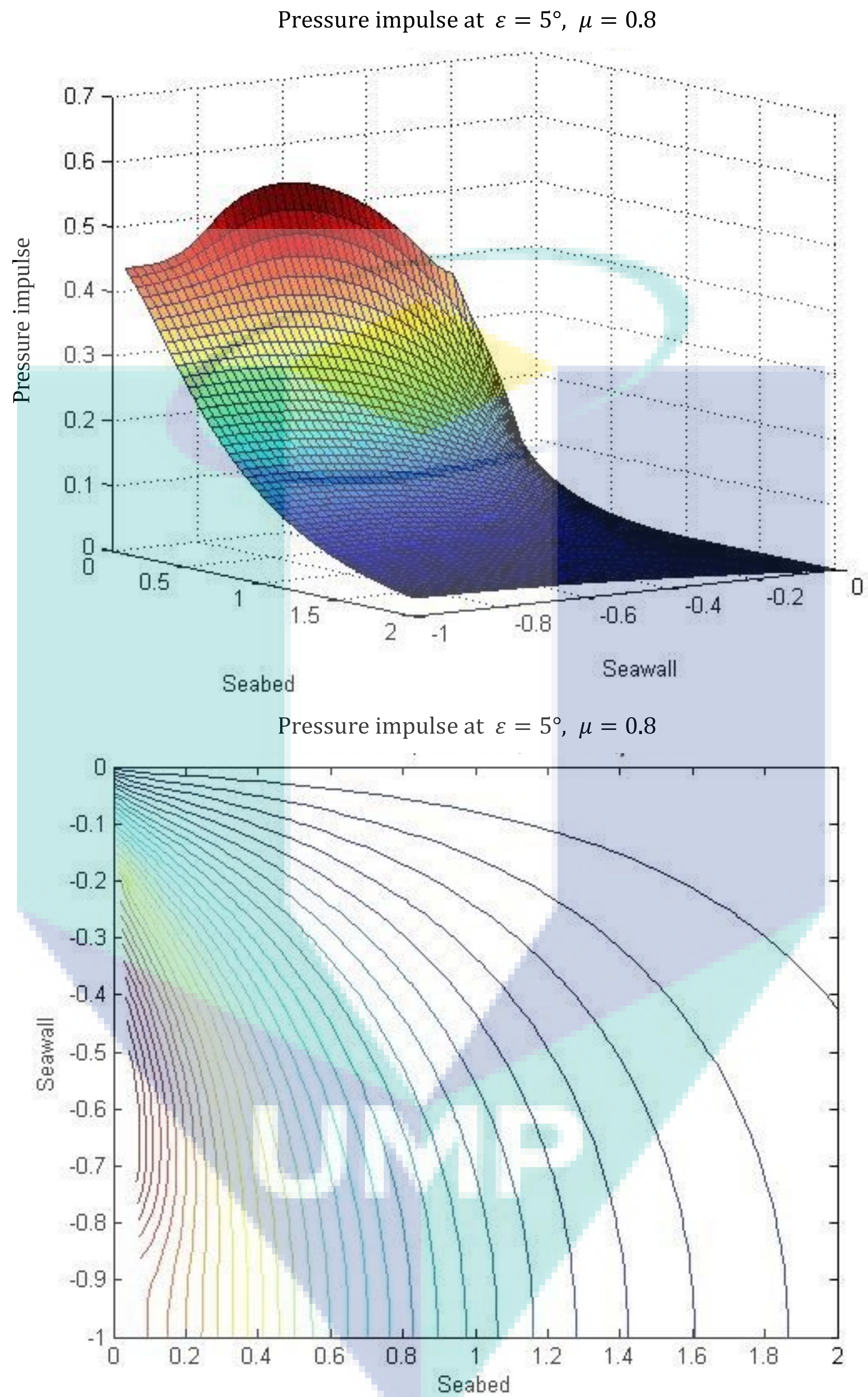

Figure 5.16 The pressure impulse on seaward-inclined model at 5° as $\mu = 0.8$

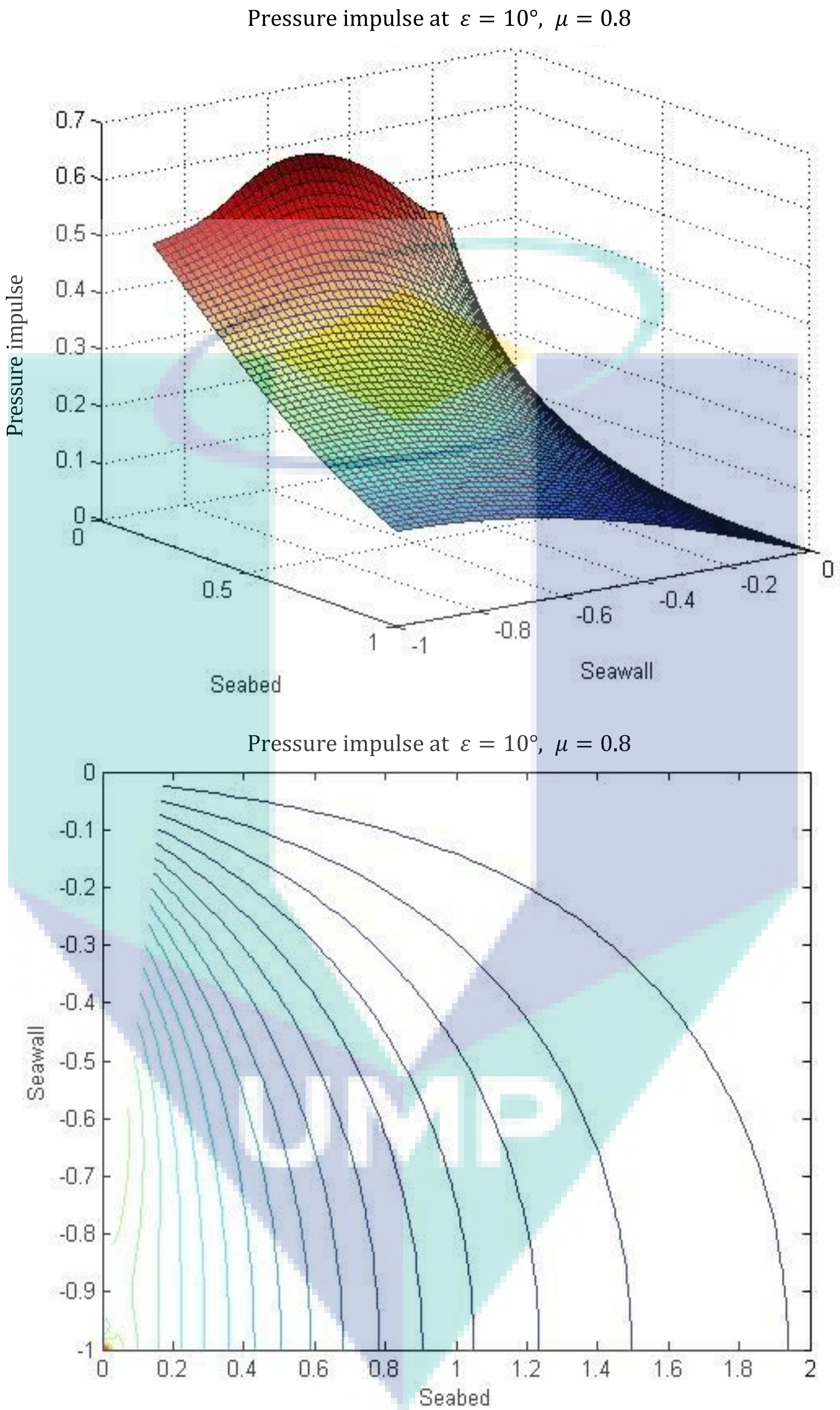

Figure 5.17 The pressure impulse on seaward-inclined model at 10° as $\mu = 0.8$

Finally, Figure 5.18 and Figure 5.19 indicate the peak pressure impulse at ε values of 5° and 10° when $\mu = 1.0$. The difference between these two figures is observed.

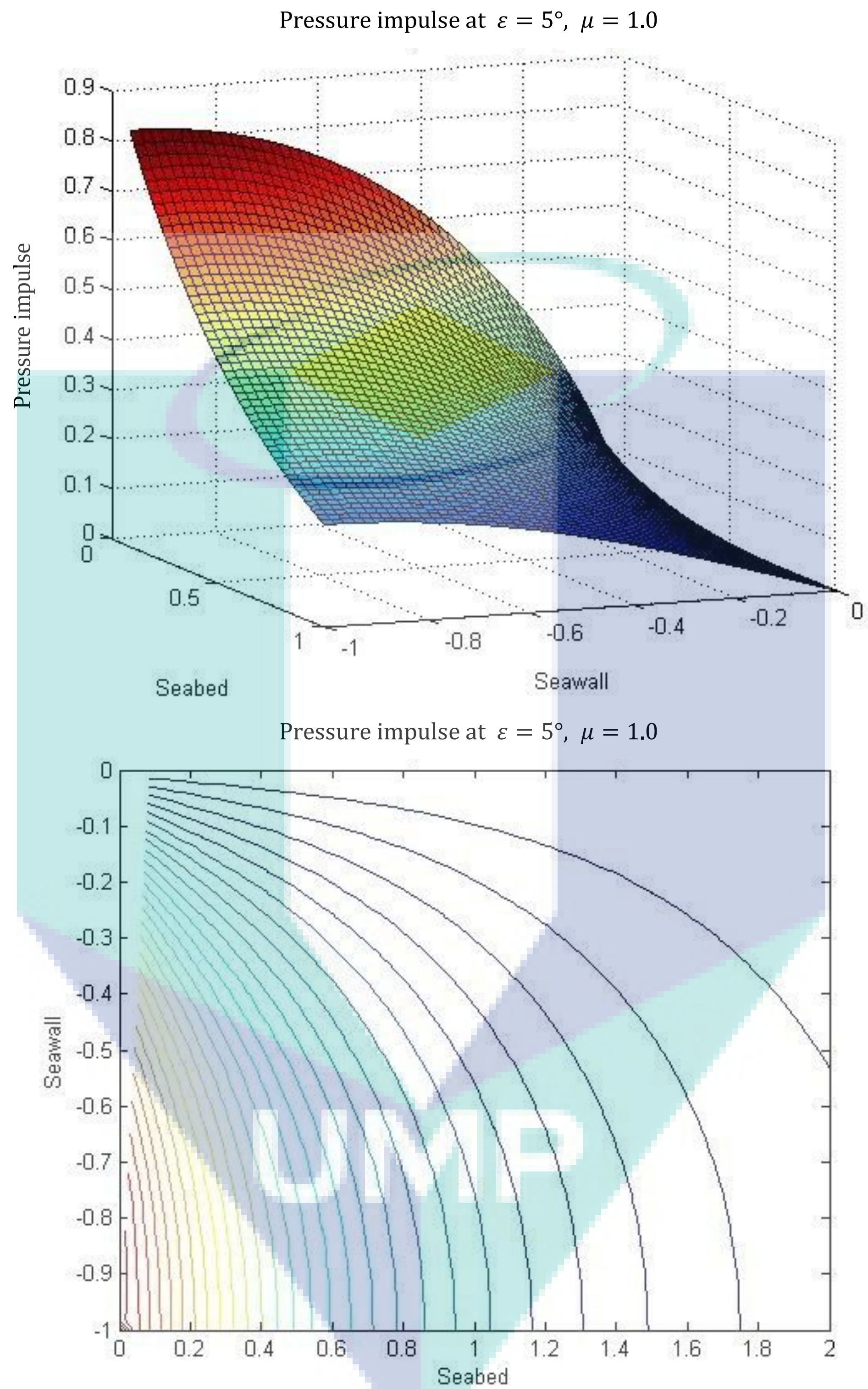

Figure 5.18 The pressure impulse on seaward-inclined model at 5° as $\mu = 1.0$

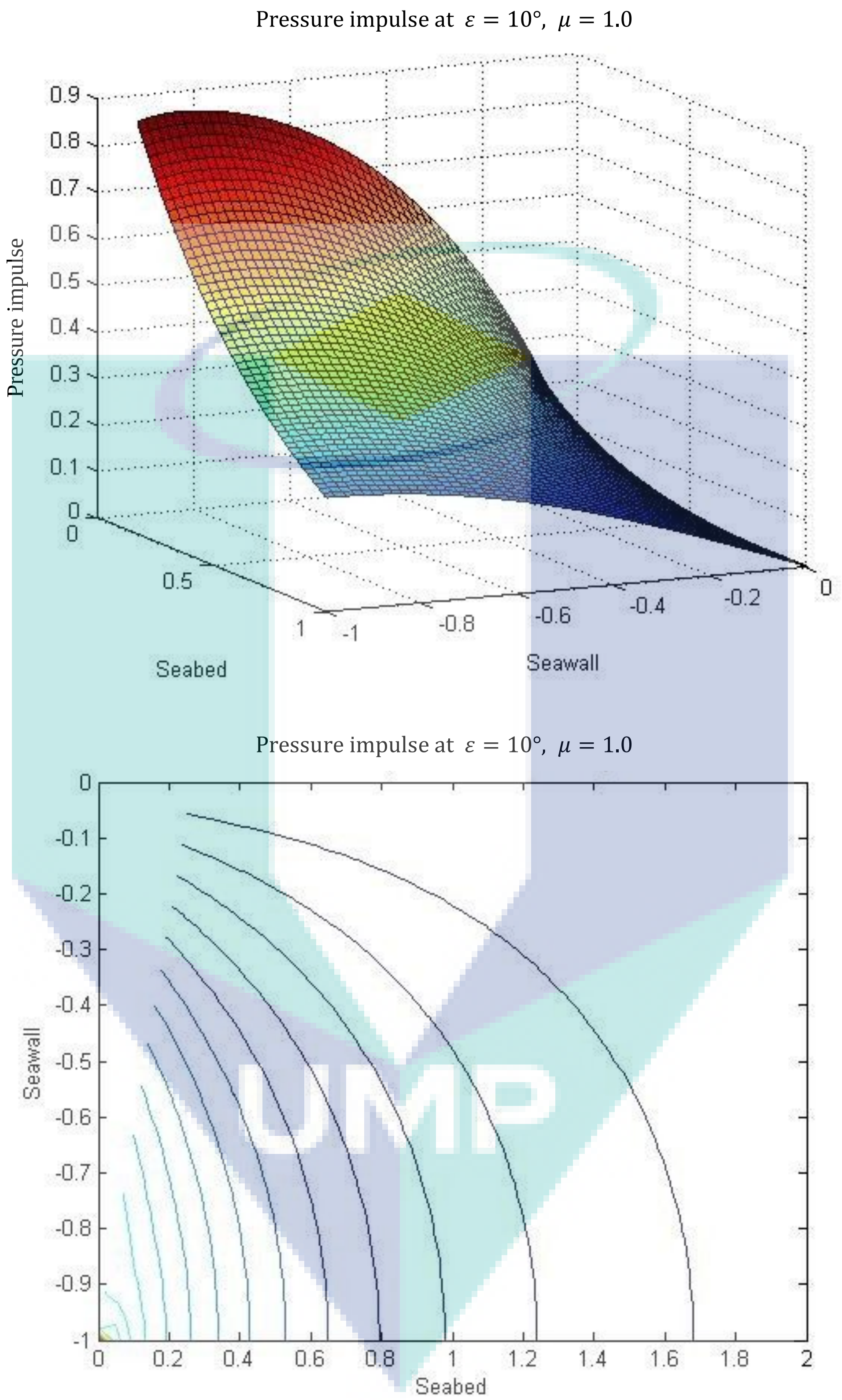

Figure 5.19 The pressure impulse on seaward-inclined model at 10° as $\mu = 1.0$

The results show that the pressure impulse will increase as we increase the value of the angle of seaward-inclined seawall, ε.

5.8 Comparison between Landward-Inclined and Seaward-Inclined Seawall

Table 5.4 shows a comparison of pressure impulse on a landward-inclined and a seaward-inclined seawall. We had tested our model at the angle of $\varepsilon = 5°$. Here, the values of μ are varied to get a better result.

Table 5.4 Comparison between landward-inclined and seaward-inclined wall at 5°

Impact Region, μ	Landward-Inclined Seawall	Seaward-Inclined Seawall
0.1	0.068	0.072
0.5	0.310	0.320
0.8	0.538	0.580
1.0	0.790	0.810

We are now going to compare the pressure impulse when $\mu = 0.5$ at angle of landward-inclined and seaward-inclined seawall of 5°. Figure 5.20 and Figure 5.21 show these values. The difference between these two figures is recorded.

As we can see, at impact region of $\mu = 0.1$ the pressure impulse on a seaward-inclined seawall is higher than on a landward-inclined seawall by 0.004. After the value of impact region was increased to 0.5, the pressure impulse on a seaward-inclined seawall remained higher than on a landward-inclined seawall by 0.010.

Although the value of impact regions increased up to 1.0, the pressure impulse on seaward-inclined seawall was still higher than on a landward seawall by 0.020.

Figure 5.20, Figure 5.21, Figure 5.22, Figure 5.23, Figure 5.24 and Figure 5.25 show the comparison between the pressure impulse on a seaward-inclined seawall and a landward-inclined seawall.

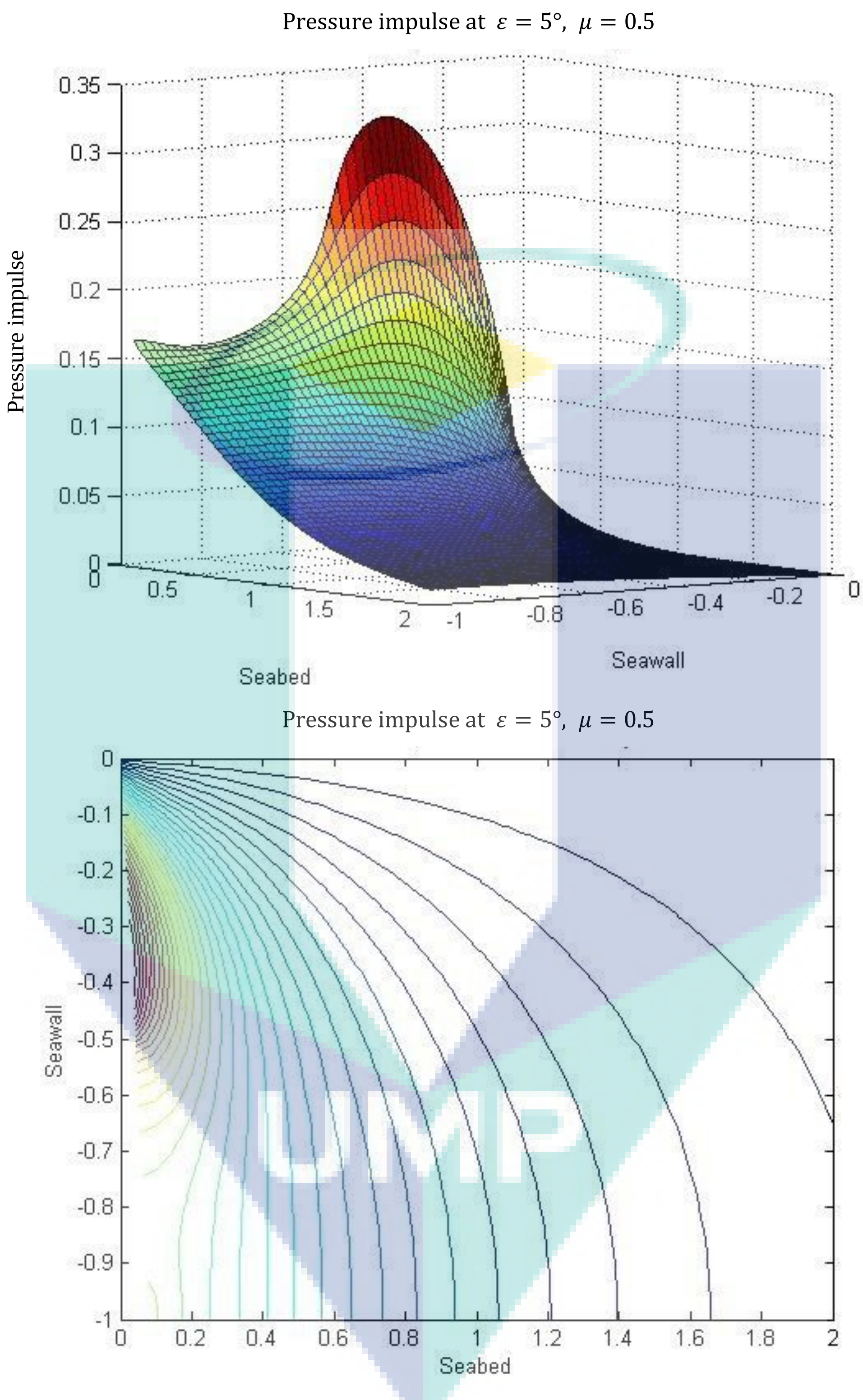

Figure 5.20 The pressure impulse on landward-inclined seawall at 5° as $\mu = 0.5$

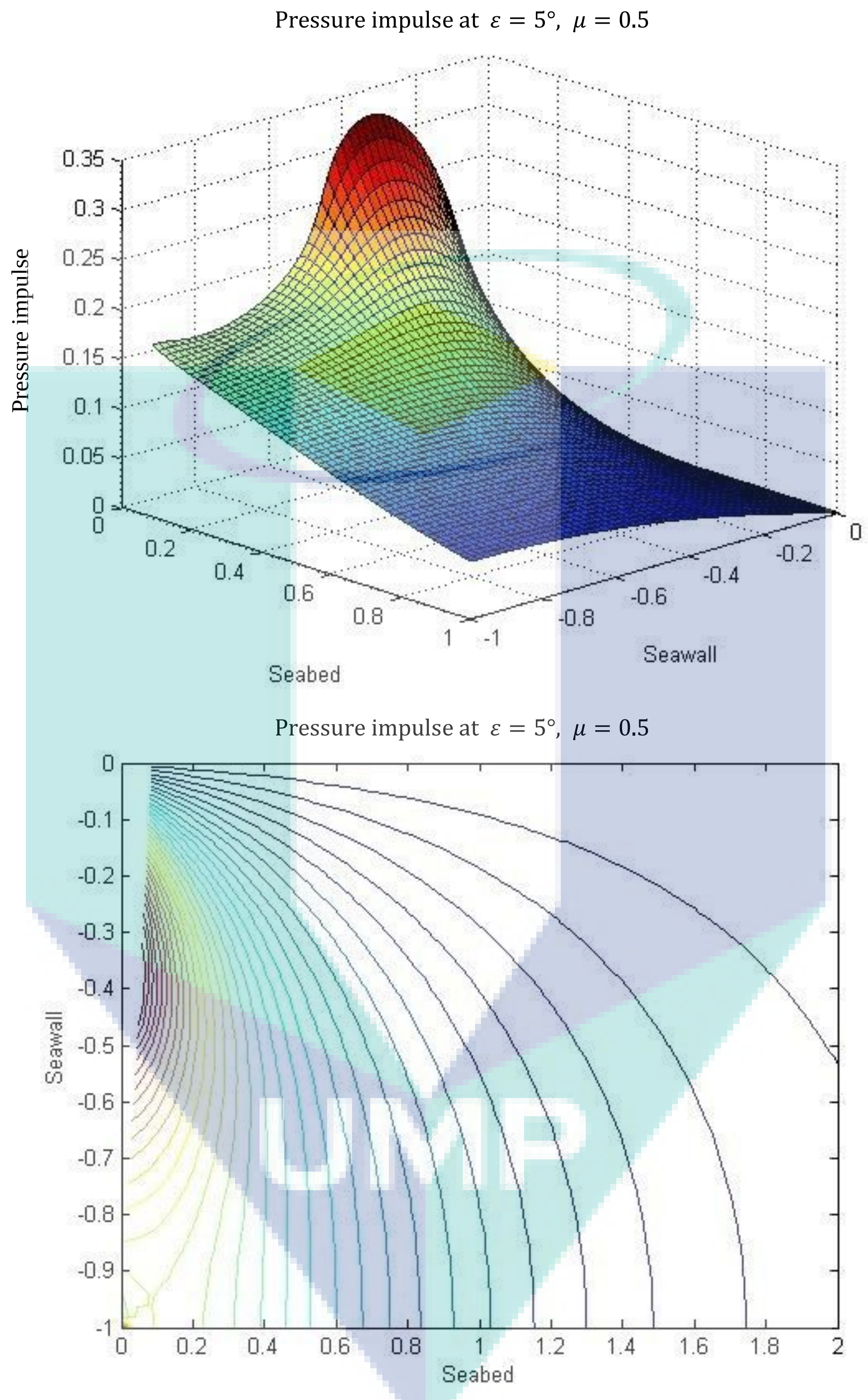

Figure 5.21 The pressure impulse on seaward-inclined seawall at 5° as $\mu = 0.5$

Figure 5.22 and Figure 5.23 illustrate the peak pressure impulse on a landward-inclined and a seaward-inclined seawall at ε values of 5° and 10° when $\mu = 0.8$. The difference between these two figures is observed.

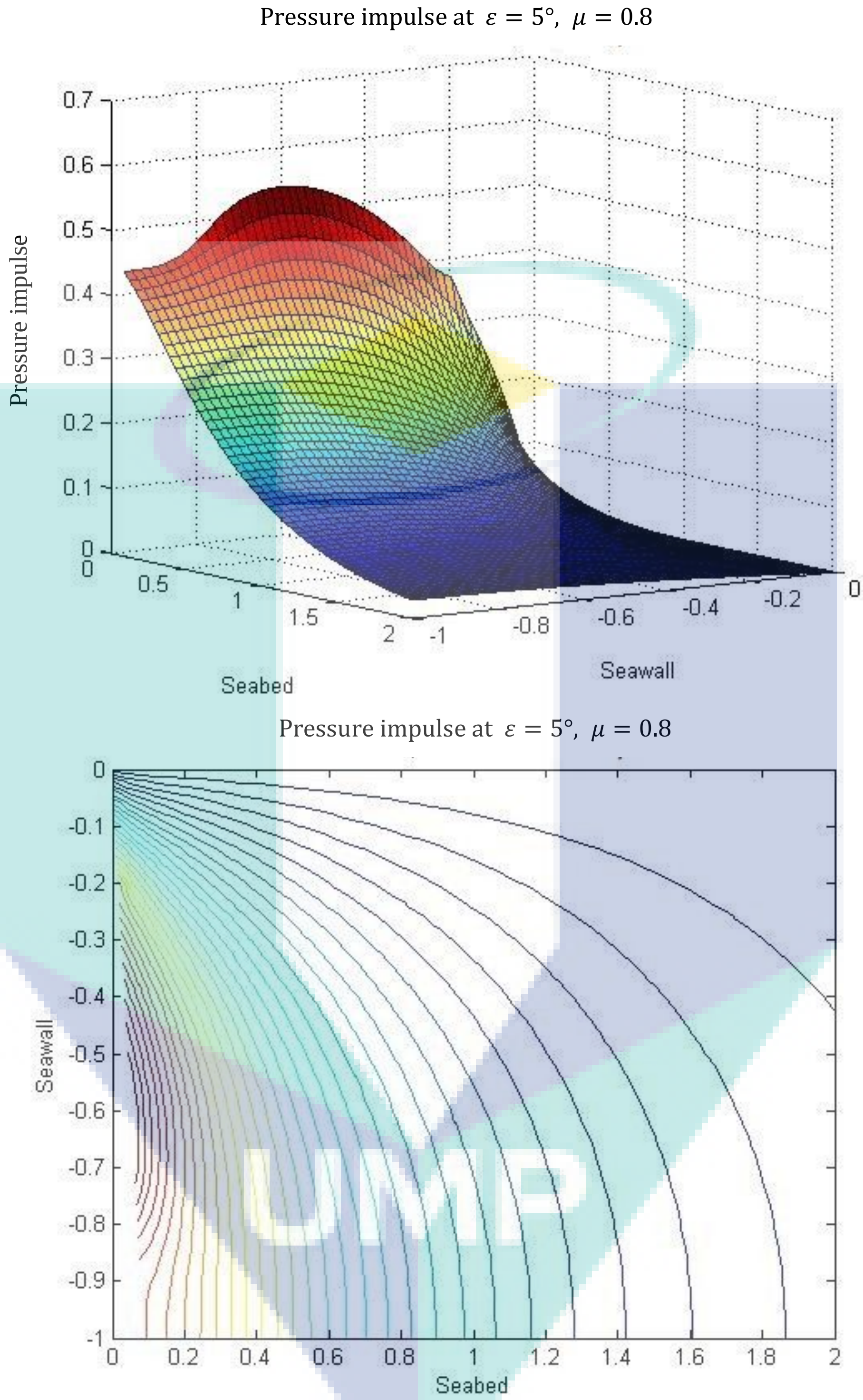

Figure 5.22 The pressure impulse on landward-inclined seawall at 5° as $\mu = 0.8$

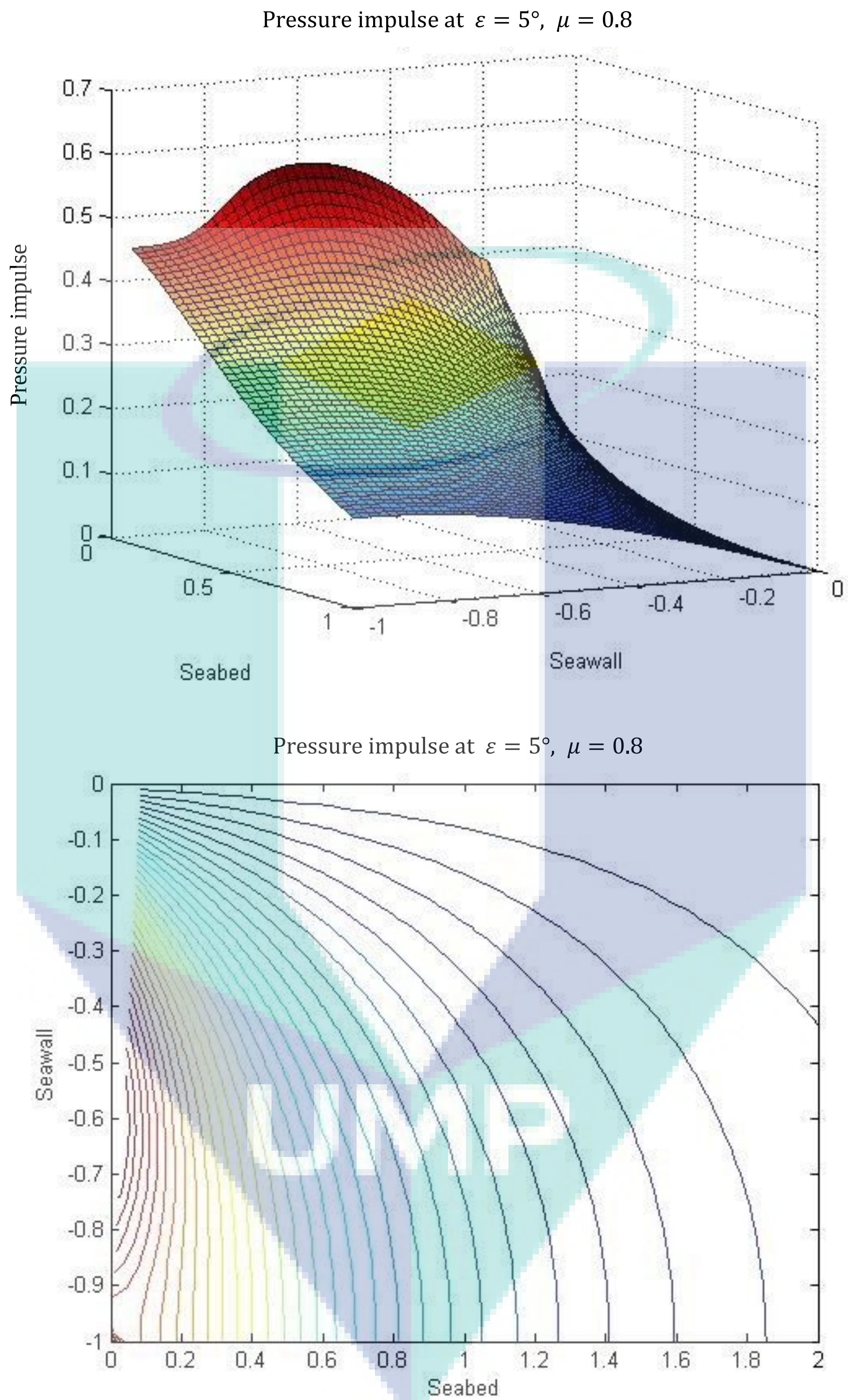

Figure 5.23 The pressure impulse on seaward-inclined seawall at 5° as $\mu = 0.8$

Finally, Figure 5.24 and Figure 5.25 indicate the peak pressure impulse on a landward-inclined and seaward-inclined seawall at the angle ε of 5° when $\mu = 1.0$. The difference between these two figures is observed.

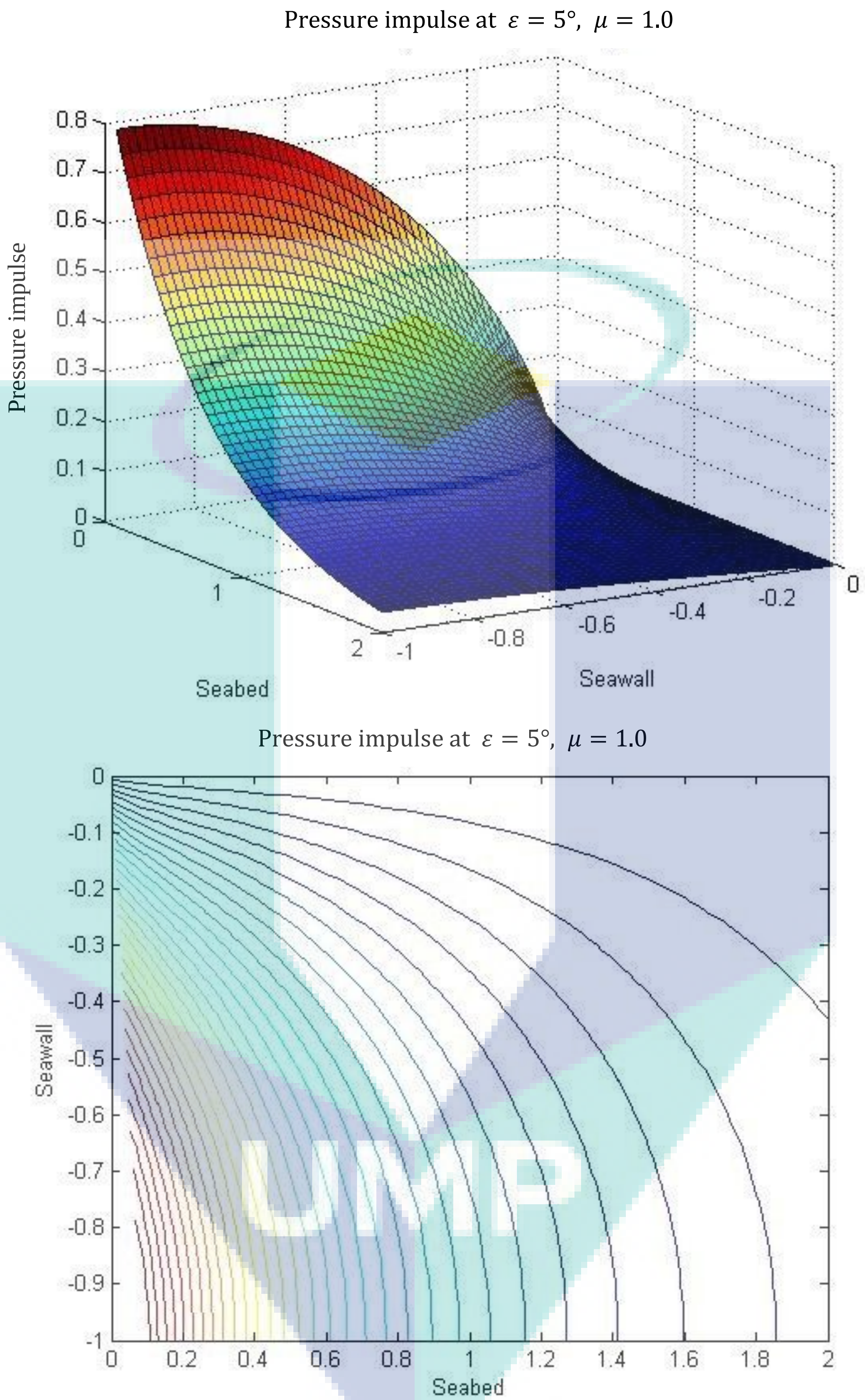

Figure 5.24 The pressure impulse on landward-inclined seawall at at 5° as $\mu = 1.0$

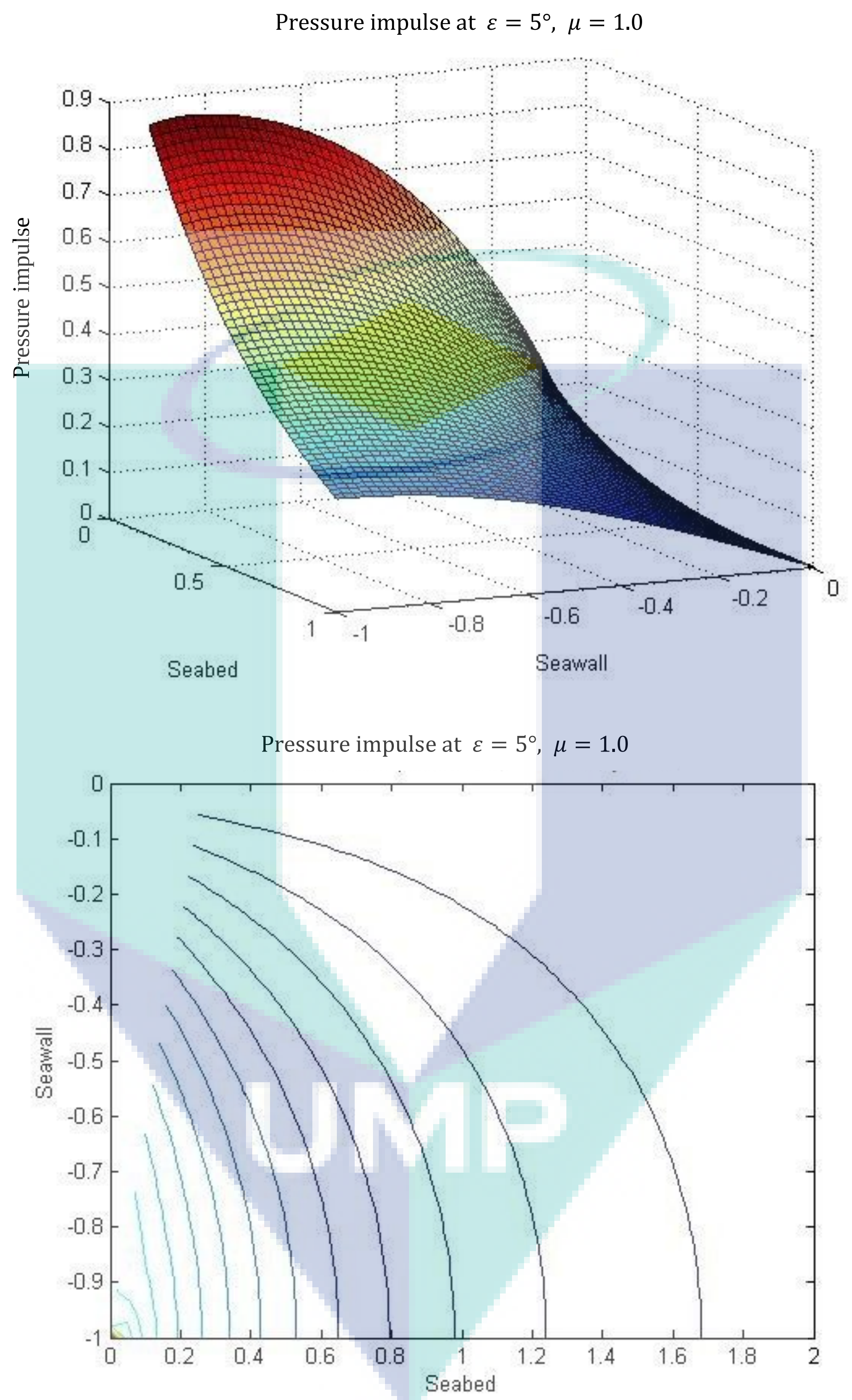

Figure 5.25 The pressure impulse on seaward-inclined seawall at 5° as $\mu = 1.0$

From all the results, we can conclude that a seaward-inclined seawall has a higher pressure impulse on it compared to a landward-inclined seawall. The results were consistent although we varied the value of μ.

5.9 Previous Study Results

Kirkgöz (1991) had conducted an experiment using a model test. He tested for landward-inclined, vertical and seaward-inclined seawalls. A seaward-inclined seawall had been modelled and tested at angles of 5°, 10°, 20° and 30°. The laboratory experiment is illustrated in Figure 5.26.

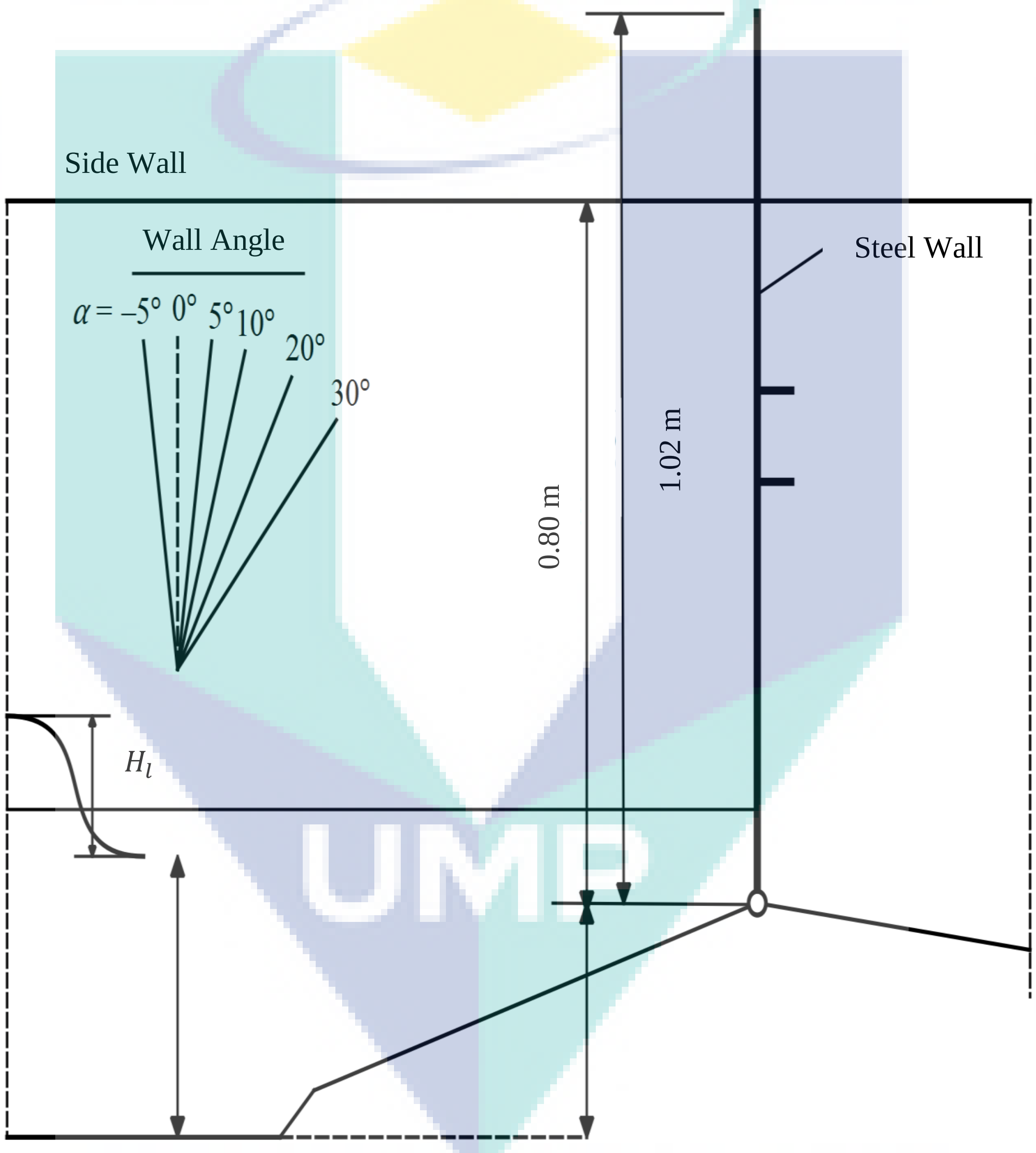

Figure 5.26 An Experimental Model by Kirkgoz

Table 5.5 Dimensionless bottom pressure impulse on a sloping wall

Impact Region	0°	5°	10°	20°	30°
99	64.5	73.7	88.3	97.3	99.4
90	33.3	35.3	42.4	50.3	36.9
50	14.9	16.2	19.4	16.8	13.5
10	7.2	7.9	6.7	5.7	5.2

Source: Kirkgoz (1995)

Based on Table 5.5, it can be said that minimum pressure impulse occurs at a vertical wall during $\varepsilon = 0°$ (Kirkgöz, 1991, 1995). We can also state based on the average and maximum pressure impulse from Kirkgoz's result that as the angle of wall declination increases, the pressure impulse also increases.

5.10 Conclusion of Seaward-Inclined Seawall

We have found in this chapter that based on the numerical solution, as the impact region, μ increases, the pressure impulse increases. This is consistent to Cooker's result (1991). We also noticed that the pressure impulse on a seaward-inclined seawall increases as the angle of the seawall increases. A good agreement was found with the findings of Kirkgöz (1991) who studied the impact pressure of breaking waves on a backward sloping wall via laboratory experiment.

Besides, from our study, we notice a landward-inclined seawall is much better compared to a seaward-inclined seawall since a seaward-inclined seawall produces higher pressure impulse compared to a landward-inclined seawall. Similar to a landward-inclined seawall case, if impact region, μ and angle of inclination wall, ε rise up, the pressure impulse will get trapped at the bottom of the seawall. This can cause the bottom foundation of the seawall become weak and eventually, the seawall may topple over. Hence, if there is a vertical seawall tends to incline seaward after several years of construction, it should be fixed as soon as possible in order to prevent seawall from damage.

From this study, the government should consider to build a proper design of seawall. In addition to reducing costs, a proper seawall can also last a long time from collapse. As in Tanjung Piai, Kuala Kemaman or Setiu, the government should look at the structure of the previous seawall whether it is leaning to incline landward or seaward after several years of construction, it should be fixed as soon as possible. As we know, if the current seawall in Tanjung Piai, Kuala Kemaman or Setiu already inclined, the pressure impulse on the seawall would be greater. The seawall might be collapse soon. Hence, the government should take appropriate action to repair the seawall as soon as possible to prevent it from collapsing in order to prevent seawall from damage and it will affect the cost to build a new seawall. The responsible organisation such as NAHRIM or DID should play a similar role in helping the government to design, build or improve seawall.

CHAPTER 6

CONCLUSION

6.1 Conclusion

This study considered two problems involving the pressure impulse on a landward-inclined and seaward-inclined seawall. This investigation started by analysing and extending the mathematical model of previous researchers.

The pressure impulse theory was discussed and Cooker's model introduced in Chapter Three. The governing equation was also considered in this chapter.

In the next chapter, Cooker's model was extended to design a new mathematical model of a landward-inclined seawall. Chapter Four provided a formulation to obtain the result of pressure impulse. The perturbation method was applied to obtain the numerical solution. Lastly, MATLAB software was run to display the result. The results were then analysed and discussed. Previous studies were also compared to this result.

Chapter 5 covered the extension of Cooker's model into a new mathematical model of a seaward-inclined seawall. The formulation was provided and perturbation method applied to obtain the numerical solution. Finally, MATLAB was used to display the results, which were then analysed and discussed. Previous studies were then compared to the results.

As a conclusion we will relate our result and discussion based on the objectives of this research. Based on the results and discussions, the following conclusions can be derived according to the objectives of this research.

Based on the first research objective, the mathematical model and equation in the fluid motion and its boundary conditions in landward-inclined and seaward-inclined seawalls can be solved by extending and modifying Cooker's model and using the pressure impulse theory.

Next, referring to the second research objective, perturbation method works and can be applied for solving the mathematical formulations of landward-inclined and seaward-inclined seawalls. In these two problems, the results show the perturbation method only works for angles of inclination for a landward-inclined and seaward-inclined seawalls below than 15°.

By going back to the third research objective, MATLAB algorithms can be developed to solve the mathematical formulations of these two problems by solving the formulation and applying the perturbation method in these two problems.

Based on the fourth research objective, the simplified and much more stable results on the model of wave impact on coastal structures by analysing the results can be provided based on this research. As conclusion, when the angle of wall inclination for landward-inclined and seaward-inclined seawalls increase, the pressure impulse also increases. Secondly, as impact region, μ increases, the pressure impulse also increases. Next, the results show a seaward-inclined seawall has a higher pressure impulse on it compared to a landward-inclined seawall. The results are consistent although the value of impact region, μ is varied.

Finally, if there is a vertical seawall tends to incline landward or seaward after several years of construction, it should be fixed immediately in order to prevent seawall from damage.

6.2 Recommendations

Several recommendations are suggested for further work in this field in order to develop a new mathematical model. There are:

a) Investigate the total impulse and moment of seawall and seabed for a landward-inclined and seaward-inclined seawalls.

b) Study the case of overtopping towards a landward-inclined and seaward-inclined seawalls.

c) Apply perturbation method into the berm and ditch for a landward-inclined and seaward-inclined seawalls.

d) Extend the mathematical model of a landward-inclined and seaward-inclined seawalls for missing block problem.

REFERENCES

Abdullah, S. (1992). *Coastal erosion in Malaysia: Problems and challenges*.

Akbari, H. (2017). Simulation of wave overtopping using an improved SPH method. *Coastal Engineering, 126*, 51-68.

Ali, I. A. M. (2018). Penang CM: Project needed to prevent further erosion at popular promenade. from https://www.thestar.com.my/news/nation/2018/08/21/esplanade-seawall-to-get-upgrade-penang-cm-project-needed-to-prevent-further-erosion-at-popular-prom/

Allsop, W., Vicinanza, D., & McKenna, J. (1996). Wave forces on vertical and composite breakwaters.

Aman, D. S. (1970). Department Of Irrigation And Drainage Sri Aman Division Office. from https://did.sarawak.gov.my/page-0-308-178-About-Us.html

Arkib. (2014). Lawatan TrEES ke NAHRIM Pada 3 Julai 2014., from http://www.nahrim.gov.my/ms/lawatan-trees-ke-nahrim-pada-3-julai-2014.html

Awang, N. A., Jusoh, W. H. W., & Hamid, M. R. A. (2014). Coastal Erosion at Tanjong Piai, Johor, Malaysia. *Journal of Coastal Research, 71*(sp1), 122-130.

Azid, A., Hasnam, C. N. C., Juahir, H., Amran, M. A., Toriman, M. E., Kamarudin, M. K. A., . . . Mustafa, A. D. (2015). Coastal erosion measurement along Tanjung Lumpur to Cherok Paloh, Pahang during the northeast monsoon season. *Jurnal Teknologi, 74*(1).

Bagnold, R. (1939). Interim report on wave-pressure research. *Excerpt from the J. of the Institution of Civil Engineers*.

Bullock, G., Crawford, A., Hewson, P., Walkden, M., & Bird, P. (2001). The influence of air and scale on wave impact pressures. *Coastal Engineering, 42*(4), 291-312.

Bullock, G., Obhrai, C., Peregrine, D., & Bredmose, H. (2007). Violent breaking wave impacts. Part 1: Results from large-scale regular wave tests on vertical and sloping walls. *Coastal Engineering, 54*(8), 602-617.

Chan, E. S. (1994). Mechanics of deep water plunging-wave impacts on vertical structures. *Coastal engineering, 22*(1-2), 115-133.

Chan, E. S., & Melville, W. K. (1988). Deep-water plunging wave pressures on a vertical plane wall. *Proceedings of the Royal Society of London. A. Mathematical and Physical Sciences, 417*(1852), 95-131.

Claude, B., Duigou, L., Girault, G., & Cadou, J.-M. (2017). Eigensolutions to a vibroacoustic interior coupled problem with a perturbation method. *Comptes Rendus Mécanique, 345*(2), 130-136.

Cooker, M. (2013). A theory for the impact of a wave breaking onto a permeable barrier with jet generation. *Journal of Engineering Mathematics, 79*(1), 1-12.

Cooker, M., & Peregrine, D. (1991). A model for breaking wave impact pressures *Coastal Engineering 1990* (pp. 1473-1486).

Cooker, M., & Peregrine, D. (1992). Wave impact pressure and its effect upon bodies lying on the sea bed. *Coastal Engineering, 18*(3-4), 205-229.

Cooker, M., & Peregrine, D. (1995). Pressure-impulse theory for liquid impact problems. *Journal of Fluid Mechanics, 297*, 193-214.

Cuomo, G., Allsop, W., Bruce, T., & Pearson, J. (2010). Breaking wave loads at vertical seawalls and breakwaters. *Coastal Engineering, 57*(4), 424-439.

David, A. (2016). Comprehensive study of beach erosion following tidal waves in Terengganu. from https://www.nst.com.my/news/2016/02/126777/comprehensive-study-beach-erosion-following-tidal-waves-terengganu

De Chowdhury, S., Anand, K., Sannasiraj, S., & Sundar, V. (2017). Nonlinear wave interaction with curved front seawalls. *Ocean Engineering, 140*, 84-96.

Faltinsen, O. M., & Timokha, A. N. (2011). Natural sloshing frequencies and modes in a rectangular tank with a slat-type screen. *Journal of Sound and Vibration, 330*(7), 1490-1503.

Hattori, M., Arami, A., & Yui, T. (1994). Wave impact pressure on vertical walls under breaking waves of various types. *Coastal Engineering, 22*(1-2), 79-114.

Hofland, B., Kaminski, M., & Wolters, G. (2011). Large scale wave impacts on a vertical wall. *Coastal Engineering Proceedings, 1*(32), 15.

Holloman, R. L., Deshpande, V., & Wadley, H. N. (2015). Impulse transfer during sand impact with a solid block. *International journal of impact engineering, 76*, 98-117.

Hu, Z. Z., Mai, T., Greaves, D., & Raby, A. (2017). Investigations of offshore breaking wave impacts on a large offshore structure. *Journal of Fluids and Structures, 75*, 99-116.

Husain, M. L., & Yaakob, R. (1988). The beach: our resource and friend. *Nature Malaysiana, 13*(2), 12-15.

Husain, M. L., Yaakob, R., & Saad, S. (1995). Beach erosion variability during a northeast monsoon: the Kuala Setiu coastline, Terengganu, Malaysia. *Pertanika Journal of Science and Technology, 3*(2), 337-348.

Ibrahim, D. I. (2019). Benteng pemecah ombak piramid selamatkan bumi Tanjung Piai. from https://www.bharian.com.my/kolumnis/2017/11/347912/benteng-pemecah-ombak-piramid-selamatkan-bumi-tanjung-piai

Ingram, D. M., Gao, F., Causon, D. M., Mingham, C. G., & Troch, P. (2009). Numerical investigations of wave overtopping at coastal structures. *Coastal Engineering, 56*(2), 190-202.

Jaafar, S. N., Yusoff, M. M., & Ghaffar, F. A. (2017). Ancaman hakisan pantai dan adaptasi komuniti pesisir pantai di Malaysia: Kajian kes Kampung Kemeruk, Kota Bharu, Kelantan. *Geografia-Malaysian Journal of Society and Space, 12*(10).

Jensen, A. (2018). Solitary wave impact on a vertical wall. *European Journal of Mechanics-B/Fluids*.

Kirkgoz, M. S. (1982). Shock pressure of breaking waves on vertical walls. *Journal of the Waterway, Port, Coastal and Ocean Division, 108*(1), 81-95.

Kirkgöz, M. S. (1978). *Breaking waves: their action on slopes and impact on vertical seawalls.* University of Liverpool.

Kirkgöz, M. S. (1991). Impact pressure of breaking waves on vertical and sloping walls. *Ocean Engineering, 18*(1-2), 45-59.

Kirkgöz, M. S. (1995). Breaking wave impact on vertical and sloping coastal structures. *Ocean Engineering, 22*(1), 35-48.

Kisacik, D., Troch, P., Van Bogaert, P., & Caspeele, R. (2014). Investigation of uplift impact forces on a vertical wall with an overhanging horizontal cantilever slab. *Coastal Engineering, 90*, 12-22.

Kocaman, S., & Ozmen-Cagatay, H. (2015). Investigation of dam-break induced shock waves impact on a vertical wall. *Journal of Hydrology, 525*, 1-12.

Mamak, M., & Guzel, H. (2013). Theoretical and Experimental Analysis of Wave Impact Pressures on Curved Seawalls. *Arabian Journal for Science and Engineering, 38*(4), 817-828.

Mangor, K. (2019). Seawall. from http://www.coastalwiki.org/wiki/Seawall

Marzeddu, A., Stagonas, D., Gironella, X., & Sánchez-Arcilla, A. (2018). Experimental set-up and calibration errors for mapping wave-breaking pressures on marine structures. *Ocean Engineering, 151*, 115-126.

Mastura, S. (1987). *Coastal geomorphology of Desaru and its implication for coastal zone management* (Vol. 13): Penerbit Universiti Kebangsaan Malaysia.

McAlister, I. J., & Nathan, R. A. (1987). *Malaysian National Coastal Erosion Study*. Paper presented at the Coastal Zone'87.

Md Noar, N. (2012). *Wave impacts on rectangular structures.* Brunel University, School of Information Systems, Computing and Mathematics.

Md Noar, N., & Greenhow, M. (2015a). *Wave impact on a deck or baffle.* Paper presented at the AIP Conference Proceedings.

Md Noar, N., & Greenhow, M. (2015b). Wave impacts on structures with rectangular geometries: Part 1. Seawalls. *Applied Ocean Research, 53*, 132-141.

Midun, Z. (1988). *Coastal erosion: problems and solutions*: Persatuan Sains Lautan Malaysia.

Mirzazadeh, M., & Ayati, Z. (2016). New homotopy perturbation method for system of Burgers equations. *Alexandria Engineering Journal, 55*(2), 1619-1624.

Mitsuyasu, H., Hase, N., & Sibayama, A. (1958). An experimental study of the pressure of breaking waves. *Month/v Rep. Transport. Tech. Rra. Inst, 8*, 24-42.

Mohd, F. A., Maulud, K. N. A., Begum, R. A., Selamat, S. N., & Karim, O. A. (2018). Impact of Shoreline Changes to Pahang Coastal Area by Using Geospatial Technology. *Sains Malaysiana, 47*(5), 991-997.

Moutsinga, C. R. B., Pindza, E., & Mare, E. (2018). Homotopy perturbation transform method for pricing under pure diffusion models with affine coefficients. *Journal of King Saud University-Science, 30*(1), 1-13.

Neelamani, S., & Sandhya, N. (2005). Surface roughness effect of vertical and sloped seawalls in incident random wave fields. *Ocean engineering, 32*(3-4), 395-416.

Ning, D., Wang, R., Chen, L., Li, J., Zang, J., Cheng, L., & Liu, S. (2017). Extreme wave run-up and pressure on a vertical seawall. *Applied Ocean Research, 67*, 188-200.

Okamura, M. (1993). Impulsive pressure due to wave impact on an inclined plane wall. *Fluid Dynamics Research, 12*(4), 215.

Oumeraci, H. (1994). Review and analysis of vertical breakwater failures—lessons learned. *Coastal Engineering, 22*(1-2), 3-29.

Paprota, M., Staroszczyk, R., & Sulisz, W. (2018). Eulerian and Lagrangian modelling of a solitary wave attack on a seawall. *Journal of Hydro-environment Research, 19*, 189-197.

Partenscky, H., & Tounsi, K. (1989). *Theoretical analysis of shock pressures caused by waves breaking at vertical structures.* Paper presented at the Int Assoc for Hydraulic Res XXIII Congress, Ottawa, Canada.

Peregrine, D. (2003). Water-wave impact on walls. *Annual review of fluid mechanics, 35*(1), 23-43.

Pullen, T., Allsop, W., Bruce, T., & Pearson, J. (2009). Field and laboratory measurements of mean overtopping discharges and spatial distributions at vertical seawalls. *Coastal Engineering, 56*(2), 121-140.

Qin, H., Tang, W., Xue, H., Hu, Z., & Guo, J. (2017). Numerical study of wave impact on the deck-house caused by freak waves. *Ocean Engineering, 133*, 151-169.

Rafiee, A., Dutykh, D., & Dias, F. (2015). Numerical simulation of wave impact on a rigid wall using a two–phase compressible sph method. *Procedia IUTAM, 18*, 123-137.

Rameli, N. L. F., & Jaafar, M. (2015). Changes of Coastline: A Study Case of Carey Island-Morib Coast, Selangor, Malaysia *The Malaysia-Japan Model on Technology Partnership* (pp. 301-309): Springer.

Reka, N. (2017). Coastal Erosion Control Project at Pantai Tg. Piai, Pontian, Johor. from https://www.water.gov.my/index.php/pages/view/617

Sahriman, N., Samad, A. M., Zainal, M. Z., Ghazali, N., & Abbas, M. A. (2017). *Appraising effect of environmental parameter toward mangrove area: A review.* Paper presented at the Signal Processing & its Applications (CSPA), 2017 IEEE 13th International Colloquium on.

Shih, R.-S. (2016). Investigation of random wave impact on highly pervious pipe breakwaters. *Applied Ocean Research, 58*, 146-163.

Song, B., & Zhang, C. (2018). Boundary element study of wave impact on a vertical wall with air entrapment. *Engineering Analysis with Boundary Elements, 90*, 26-38.

Stagonas, D., Marzeddu, A., Cobos, F. X. G. I., Conejo, A. S.-A., & Muller, G. (2016). Measuring wave impact induced pressures with a pressure mapping system. *Coastal engineering, 112*, 44-56.

Stewart, R. D., & Bair, W. (2009). Spiking neural network simulation: numerical integration with the Parker-Sochacki method. *Journal of computational neuroscience, 27*(1), 115-133.

Takahashi, S. (1996). *Design of vertical breakwaters. Breakwater design.* Paper presented at the International Conference On Coastal Engineering, Orlando, Short Course.

Toriman, M. E. (2006). Hakisan Muara dan Pantai Kuala Kemaman, Terengganu: Permasalahan Dimensi Fizikal dan Sosial (Erosion in the Estuary and Coastal Area in Kuala Kemaman, Terengganu: A Physical and Social Dimension Setback). *Akademika, 69*(1).

Van Doorslaer, K., Romano, A., De Rouck, J., & Kortenhaus, A. (2017). Impacts on a storm wall caused by non-breaking waves overtopping a smooth dike slope. *Coastal Engineering, 120*, 93-111.

Wdowinski, S., Bray, R., Kirtman, B. P., & Wu, Z. (2016). Increasing flooding hazard in coastal communities due to rising sea level: Case study of Miami Beach, Florida. *Ocean & Coastal Management, 126*, 1-8.

Weggel, J. R., & Maxwell, W. (1970). Numerical model for wave pressure distributions. *Journal of the Waterways, Harbors and Coastal Engineering Division, 96*(3), 623-642.

Whittaker, C. N., Raby, A. C., Fitzgerald, C. J., & Taylor, P. H. (2016). The average shape of large waves in the coastal zone. *Coastal Engineering, 114*, 253-264.

Xu, R. (2010). *An improved incompressible smoothed particle hydrodynamics method and its application in free-surface simulations.* University of Manchester.

APPENDIX A
MATLAB PROGRAM OF COOKER'S MODEL

```
function cooker =cooker_(mu)
format compact
H=1;                    %  The water depth
U=1;                 %  Velocity of Wave
N=50;              %  Number of terms to be summed
gridpoints=50;       %  The number along an axis of the grid
xmax=2;             %  The maximum distance along the seabed.
B=2;

% Interval & Grid Formed
x=linspace(0,xmax,gridpoints+1);
y=linspace(-H,0,gridpoints+1);
[X,Y]=meshgrid(x,y);

% Initialize the solution Matrix
Zn=zeros(gridpoints+1);

% Calculate the Sum
for n=1:N
   ln=(n-1/2)*pi/H;
    Pn=-2/(ln^2)*(-1+cos(ln*mu));
   Zn=Zn+Pn.*sinh(ln*(X-B))/cosh(ln*B).*sin(ln.*Y);
end

z=Zn;

% Plot the graph

surf(X,Y,Zn)
xlabel('Distance along Seabed')
ylabel('Height down Seawall')
zlabel('pressure impulse')
```

APPENDIX B
MATLAB PROGRAM OF LANDWARD-INCLINED SEAWALL

Main

```
% perturbsol.m
function z=perturbsoln
% This programme calculates the first order perturbation solution.
% Program Parameters
format compact
mu=0.8;                  % Still Water level
H=1;                     % Water Depth
U=1;                    % Wave velocity
%angle=0
angle=-pi/36;
%angle=pi/180;
xmax=2;               % B
xw=H*tan(angle);
gridpoints=100;
N=200;                  % Number of terms to sum over

% Generate the Domain grid

[X,Y]=generategrid_neg(xw,xmax,H,gridpoints);

% Initialize Solutions as Matrices over the whole domain

sol=zeros(gridpoints+1);

P0=P0coeff(N,U,mu,H);
P1=P1coeff(N,H,P0);
P2=P2coeff(N,H,P0,P1);

for n=1:N+1
   ln=(n-1/2)*pi/H;
   sol=sol+(P0(n)+angle*P1(n)+angle^2*P2(n)).*exp(-ln.*X).*sin(ln.*Y);
end

z=sol;
surf(X,Y,z)

%pcolor(X,Y,z)
```

For I seven

```
function z=iseven(n)

if isint(n)==1
   if isint(n/2)==1;
      z=1;
   else
      z=0;
   end
else
   error('Must Enter an Integer')
end
```

For generate grid

```
function [X,Y]=generategrid_neg(xw,xmax,H,N)

% (x,y) defines the bottom of the wall and seabed

y=linspace(-H,0,N+1);
Y=y';
for i=1:N
   Y=[Y y'];
end

x=linspace(xw,xmax,N+1);
X=x;

for j=1:N
   x0=xw*y(j+1)/(-H);
   x=linspace(x0,xmax,N+1);
   X=[X; x];
end
```

For isin

```
function z=isint(n)

if n==round(n)
   z=1;
else
   z=0;
end
```

For coefficient 0

```
function z=P0coeff(N,U,mu,H)

for n=1:N+1
   ln=(n-1/2)*pi/H;
   P0(n)=2*U/(ln^2*H)*(cos(ln*mu*H)-1);
end
z=P0;
```

For coefficient 1

```
function z=P1coeff(N,H,P0)

for m=1:N+1
   P1n=0;                                  % Initialise the nth
term P_n^1
    for n=1:N+1
      ln=(n-1/2)*pi/H;                      % eigenvalues
      lm=(m-1/2)*pi/H;                      % eigenvalues
      if n~=m
         if iseven(n)==1
            term=lm*ln/(ln+lm)^2;
         else
            term=lm*ln/(ln-lm)^2;
         end
      else
         term=-((H*ln)^2+3)/4;
      end
      P1n=P1n+P0(n)*term;
   end
   P1(m)=2*P1n/lm/H;
end

z=P1;
```

For coeeficient 2

```
function z=P2coeff(N,H,P0,P1)

for m=1:N+1
   P2n=0;
    for n=1:N+1
      ln=(n-1/2)*pi/H;                      % eigenvalues
      lm=(m-1/2)*pi/H;                      % eigenvalues
      if n~=m
         if iseven(n)==1
            term1=lm*ln/(ln+lm)^2;
         else
```

```
            term1=lm*ln/(ln-lm)^2;
         end
         term2=((-1)^(n+m+1))*2*H*ln^3*lm^2/(ln^2-lm^2)^2;
      else
         term1=-((H*ln)^2+3)/4;
         term2=H*ln*(1-2*((H*ln)^2)/3)/8;
      end
      P2n=P2n+P1(n)*term1+P0(n)*term2;
   end
   P2(m)=2*P2n/lm/H;
end

z=P2;
```

APPENDIX C
MATLAB PROGRAM OF SEAWARD-INCLINED SEAWALL

Main

```
% perturbsol.m
function z=perturbsoln
% This programme calculates the first order perturbation solution.
% Program Parameters
format compact
mu=0.8;                % Still Water level
H=1;                   % Water Depth
U=1;                  % Wave velocity
%angle=0
angle=pi/36;
%angle=pi/180;
xmax=2;              % B
xw=H*tan(angle);
gridpoints=100;
N=200;                % Number of terms to sum over

% Generate the Domain grid

[X,Y]=generategrid_pos(xw,xmax,H,gridpoints);

% Initialize Solutions as Matrices over the whole domain

sol=zeros(gridpoints+1);

P0=P0coeff(N,U,mu,H);
P1=P1coeff(N,H,P0);
P2=P2coeff(N,H,P0,P1);

for n=1:N+1
   ln=(n-1/2)*pi/H;
   sol=sol+(P0(n)+angle*P1(n)+angle^2*P2(n)).*exp(-ln.*X).*sin(ln.*Y);
end

z=sol;
surf(X,Y,z)

%pcolor(X,Y,z)
```

For I seven

```
function z=iseven(n)

if isint(n)==1
   if isint(n/2)==1;
      z=1;
   else
      z=0;
   end
else
   error('Must Enter an Integer')
end
```

For generate grid

```
function [X,Y]=generategrid_pos(xw,xmax,H,N)

% (x,y) defines the bottom of the wall and seabed

y=linspace(-H,0,N+1);
Y=y';
for i=1:N
   Y=[Y y'];
end

x=linspace(0,xmax,N+1);
X=x;

for j=1:N
   x0=xw*y(j+1)/(H)+xw;
   x=linspace(x0,xmax,N+1);
   X=[X; x];
end
```

For isin

```
function z=isint(n)

if n==round(n)
   z=1;
else
   z=0;
end
```

For coefficient 0

```
function z=P0coeff(N,U,mu,H)

for n=1:N+1
   ln=(n-1/2)*pi/H;
   P0(n)=2*U/(ln^2*H)*(cos(ln*mu*H)-1);
end
z=P0;
```

For coefficient 1

```
function z=P1coeff(N,H,P0)

for m=1:N+1
   P1n=0;                                          % Initialise the nth
term P_n^1
    for n=1:N+1
      ln=(n-1/2)*pi/H;                               % eigenvalues
      lm=(m-1/2)*pi/H;                               % eigenvalues
      if n~=m
         if iseven(n)==1
            term=lm*ln/(ln+lm)^2;
         else
            term=lm*ln/(ln-lm)^2;
         end
      else
         term=-((H*ln)^2+3)/4;
      end
      P1n=P1n+P0(n)*term;
   end
   P1(m)=2*P1n/lm/H;
end

z=P1;
```

For coeeficient 2

```
function z=P2coeff(N,H,P0,P1)

for m=1:N+1
   P2n=0;
    for n=1:N+1
      ln=(n-1/2)*pi/H;                               % eigenvalues
      lm=(m-1/2)*pi/H;                               % eigenvalues
      if n~=m
         if iseven(n)==1
            term1=lm*ln/(ln+lm)^2;
         else
            term1=lm*ln/(ln-lm)^2;
         end
         term2=((-1)^(n+m+1))*2*H*ln^3*lm^2/(ln^2-lm^2)^2;
```

```
        else
            term1=-((H*ln)^2+3)/4;
            term2=H*ln*(1-2*((H*ln)^2)/3)/8;
        end
        P2n=P2n+P1(n)*term1+P0(n)*term2;
    end
    P2(m)=2*P2n/lm/H;
end

z=P2;
```

APPENDIX D
LIST OF PUBLICATIONS

A. Proceeding

Ghani, F. A. A., **Ramli, M. S**., Noar, N. A. Z. M., Kasim, A. R. M., & Greenhow, M. (2017). Mathematical modelling of wave impact on floating breakwater. Paper presented at the Journal of Physics: Conference Series.

Ramli, M. S., Ghani, F. A. A., Noar, N. A. Z. M., Salleh, M. Z., & Greenhow, M. (2017a). Mathematical modeling of wave impacts on inclined seawall. Paper presented at the AIP Conference Proceedings.

Ramli, M. S., Ghani, F. A. A., Noar, N. A. Z. M., Salleh, M. Z., & Greenhow, M. (2017b). Mathematical modelling of wave impacts on landward-inclined seawall. Paper presented at the Journal of Physics: Conference Series.